PhD degree in Systems Medicine (curriculum in Human Genetics)

European School of Molecular Medicine (SEMM),

University of Milan and University of Naples "Federico II"

Settore disciplinare: XXX

Development of ARPE19 Cellular Models of Niemann-Pick Disease Type C1 and C2 and their Application to High Content Drug Screening

Raffaele Pastore

Tigem, Pozzuoli (Naples)

Matricola R11144

Supervisor: Prof. Andrea Ballabio
Tigem, Pozzuoli

Internal Supervisor: Prof. Giancarlo Parenti
Tigem, Pozzuoli

External Supervisor: Prof. Frances Platt
University of Oxford

Anno accademico 2017-2018

TABLE OF CONTENTS

2.0 Material and Methods

RESULTS

3.0 GENERATION OF *NPC1*$^{-/-}$ AND *NPC2*$^{-/-}$ ARPE19 CELL LINES

4.0 CHARACTERIZATION OF *NPC1*$^{-/-}$ AND *NPC2*$^{-/-}$ ARPE19

LIST OF ABBREVIATIONS

a.a.: amino acid

AD: Alzheimer's disease

AP-complex: clathrin adaptor protein complex

BBB: Blood-brain barrier

BSA: Bovine Serum Albumin

CGase: Ceramide Glycanase

DAPI: 4′,6-diamidino-2-phenylindole

DMSO: Dimethylsulfoxide

DSB: Double Strand Break

ERAD: Endoplasmic Reticulum Associated Protein Degradation

FACS: Fluorescence Activating Cell Sorting

FDA: Food and Drug Administration

GFP: Green Fluorescent Protein

gRNA: guide RNA

GSL: Glycosphingolipid

HC: High Content

HDL: High Density Lipoprotein

HDR: Homology directed repair

HMG-CoA: 3-hydroxy-3-methyl-glutaryl-coenzyme A

HPR: Horseradish peroxidase

IDL: Intermediate Density Lipoprotein

LAL: Lysosomal Acid Lipase

LAMP1: Lysosomal-associated membrane protein 1

LC3: Microtubule-associated protein 1A/1B-light chain 3

LDL: Low Density Lipoprotein

LE: Late endosome or late endosomal

LLOMe: L-leucyl-L-leucine methyl ester

LY: Lysosome or lysosomal

NHEJ: Non-Homologous End Joining

***NPC1*$^{-/-}$:** *NPC1*$^{-/-}$ ARPE19

***NPC2*$^{-/-}$:** *NPC2*$^{-/-}$ ARPE19

NTD: N-Terminal Domain

OPA: O-Phthaldialdehyde

PAM: Protospacer Adjacent Motif

PD: Parkinson's disease

PFA: Paraformaldehyde

PVDF: Polyvinylidene difluoride

RND: resistance nodulation division

rNPC1-*NPC1*$^{-/-}$: *NPC1*$^{-/-}$ expressing rNPC1

rNPC1: human recombinant NPC1

SDS: Sodium dodecyl sulphate

SM: sphingomyelin

SMase: sphingomyelinase

SPE: Solid Phase Extraction

SREBP: Sterol Regulatory Element Binding Proteins

SSD: Sterol Sensing Domain

VLDL: Very Low Density Lipoprotein

WB: Western Blot

WT: Wild Type

LIST OF FIGURES

Abstract

Niemann-Pick type C (NP-C) is a lysosomal lipid storage disorder caused by autosomal recessive mutations in either the *NPC1* or *NPC2* genes. The majority of the NPC cases, about 95%, results from dysfunction of NPC1, whereas the remaining 5% is due to malfunction of NPC2. These two proteins mediate the transport of free-cholesterol from the inner lumen to the limiting membrane of the lysosome. More specifically, in a "hydrophobic hand-off" model, the soluble protein NPC2 delivers free-cholesterol directly to the transmembrane protein NPC1. At the cellular level, sphingosine, cholesterol, sphingomyelin and glycosphingolipids (GSLs) accumulate within NPC cells. Clinically, NPC is a neurovisceral disorder characterized by a progressive neurodegeneration similar to AD and PD. The mechanisms linking lipid storage and onset of organ dysfunction are still unknown and an effective therapy is also lacking since the only approved drug, miglustat, ameliorates the neurological symptoms but is not curative. In this respect, a major limitation for *in vitro* studies is represented by the lack of appropriate cellular models of NPC. In fact, *in vitro* experiments have been hitherto carried out mainly on patient skin-fibroblasts, even though NPC is a neurodegenerative disorder. Moreover, NPC fibroblasts as well as their derived iPScs present high phenotypic variability and are difficult to work with. Therefore, there is a need for cellular disease models that exhibit the spectrum of the pathological phenotypes of NPC so as to study its basic biology and to set out translational research approaches. To this aim, in this research project, two isogenic ARPE19 cell lines were generated, in which either the *NPC1* or the *NPC2* genes were knocked-out with the use of CRISPR/Cas9 technology. These knockout cells were characterized assessing the classical lipid pattern (free and total cholesterol, sphingoid bases and GSLs) of NPC and the endolysosomal pathway. It turned out that $NPC1^{-/-}$ and $NPC2^{-/-}$ are good disease models that thoroughly recapitulate the pathological features of NPC. In particular, both knockout cell lines showed accumulation of free-cholesterol within LE/LY. On the basis of this finding the microscopy assay filipin-LAMP1 co-staining was used to monitor the effect of potential therapeutic

compounds on the stored LE/LY free-cholesterol. To this end, the *NPC2*$^{-/-}$ ARPE19 were employed in a high content experiment to screen the 1200 FDA-approved drugs of the Prestwick library. As a result, three candidate drugs, desipramine, fendiline and thioproperazine were selected.

1.0 Introduction

1.1 Lysosomal Storage Disorders (LSDs)

Lysosomal storage disorders (LSDs) comprise about 70 monogenic diseases caused by inborn mutations in genes encoding lysosomal enzymes and lysosomal membrane proteins. The majority of LSDs are autosomal recessive disorders with only three diseases being X-linked. Individually, these disorders are considered rare whereas taken all together they have an incidence of 1:5000 births. At the cellular level LSDs are characterized by non-functional lysosomes full of un-degraded substrates (Platt et al. 2018). The development of lysosomal storage disorders is the outcome of pathogenic cascades triggered by the malfunction of lysosomes. In particular, the dysfunctionality of lysosomal proteins results in the build-up of specific primary substrates such as glycosaminoglycans, glycogen or lipids that cannot be degraded (primary storage). As a consequence, lysosomal trafficking is hampered and secondary substrates not directly linked to the dysfunctional protein accumulate within lysosomes and late endosomes (secondary storage). The disproportionate increase of lysosomal storage alters lysosomal function because it causes defects in Ca^{2+} homeostasis, signalling abnormalities and permeabilization of the lysosomal membrane. Besides, defective fusion between lysosomes and autophagosomes leads to dysregulation of the autophagic pathway. The latter, in turn causes accumulation of cytosolic autophagic substrates such as mitochondria (tertiary storage) (Settembre et al. 2013).

Clinically, the age of onset and the symptomatology exhibited by LSDs are heterogeneous and have different degrees of severity. This variation depends on how severely the specific mutations impact the functionality of the lysosomal protein, on the biochemistry of the stored material, and on the cell types where storage primarily occurs. In the majority of LSDs, the Central Nervous System (CNS) is involved and neurodegeneration can affect multiple brain regions (Platt, Boland and Spoel, 2012).

1.2 The Lysosome

Lysosomes are acidic organelles with a pH of 4.5 that have three main functions: digestion and recycling of cellular waste, secretion of material out of cells (exocytosis) and regulation of cellular metabolism.

Extracellular material that has to be degraded is delivered to lysosomes through endocytosis and phagocytosis whereas intracellular components reach lysosomes by autophagy. These pathways converge in the formation of autolysosomes where cellular debris, aggregated substrates or even pathogens are digested by the about 50 lysosomal hydrolases. The resulting breakdown products (lipids, amino acids, carbohydrates and nucleic acids) are then reused in the anabolic processes of the cell (Settembre et al. 2013). Lysosomes move along microtubule tracks by means of the motor proteins dynein and kinesins (Pu et al. 2015-2016) In fact, they are highly dynamic organelles that continually undergo fusion-reformation processes with endosomal and autophagosomal vesicles through the mediation of SNARE and Rab proteins (Jahn et al 2006; Zerial 2001). In particular, it appears that for vesicle-vesicle or vesicle-plasma membrane fusion, release of lysosomal Ca^{2+} from the channel MCOLN1 is a crucial event (Medina et al. 2015). Lysosomes fuse with the plasma membrane in two instances: to secrete their content out of the cell, in a process called exocytosis, and to repair a damaged plasma membrane. Another important feature of the lysosome is its ability to sense variations in the amino acid content of the cell and consequently trigger a response through the transcription factor EB (TFEB) (Sardiello et al. 2009). In fact, in normal feeding conditions, the kinase mTORC1 (mammalian Target of Rapamycin Complex1) is located on the lysosomal surface as part of the lysosomal nutrient sensing (LYNUS) machinery and there it phosphorylates TFEB (Settembre et al. 2012). Once phosphorylated, TFEB binds to the 14-3-3 protein family and remains sequestered in the cytosol (Medina et al. 2015). However, upon amino acid starvation, mTORC1 detaches from LYNUS and thus TFEB is no longer phosphorylated. As a consequence, TFEB translocates to the nucleus where it binds to the promoter motif of the CLEAR (coordinated

lysosomal expression and regulation) network and up-regulates the expression of the lysosomal genes involved in the autophagic pathway, in lysosomal biogenesis, lysosomal exocytosis and endocytosis (Sardiello et al. 2009; Palmieri et al. 2011). TFEB has been identified as a druggable target for treating Lysosomal Storage Disorders since its overexpression enhances cellular clearance through lysosomal exocytosis (Spampanato et al. 2013; Moskot et al. 2014).

1.3 Rationale of the project

Lack of appropriate cellular models for LSDs represents a major limitation for *in vitro* studies of this class of disorders. This is the case for Niemann-Pick C disease, in which cell biology and drug-testing experiments have been carried out mainly on patient skin-fibroblasts, even though NPC is a neurodegenerative disorder and the types of lipids that accumulate in fibroblasts are different from the lipids found in the CNS (Patterson et al. 2012). A major drawback with the use of NPC-fibroblasts is their high degree of phenotypic heterogeneity that appears to be linked to the different mutations of the *NPC1* gene. It has been reported that this genetic variability results in different levels of storage of free-cholesterol within the NPC-cells. In fact, by filipin staining of free-cholesterol, patient-fibroblasts have been categorized as classical, intermediate and variant NPC-phenotypes. These three classes are characterized by high, intermediate and no cholesterol accumulation, respectively (Vanier and Latour 2015). Furthermore, because fibroblasts are primary cells, they grow slowly and need weeks in culture before reaching an amount of material that is sufficient to be used in experimental research. In addition, after a limited number of cultivation passages, fibroblasts can reach replicative senescence which most probably alters the phenotypes under investigation thus undermining the reproducibility of the experiments (Auburger et al. 2012). Another technical drawback is represented by the difficulty of transfecting exogenous DNA into the cytoplasm of primary cells. To overcome this

limitation, the operator has to introduce the exogenous DNA through previous generation of viral vectors, a procedure that is time consuming.

An attempt to improve cell-based *in vitro* studies was done deriving neuronal and hepatic induced Pluripotent Stem Cells (iPSCs) from NPC patient fibroblasts and skin's stem cells. However, iPSCs are not a real alternative to the use of patient-fibroblasts. In fact, as in the case of NPC disease, iPSCs often do not recapitulate consistently the phenotypic spectrum of the disease and might show features that do not resemble the disease at all (Yu et al. 2014; Efthymiou et al. 2015; Trilck et al. 2013; Bergamin et al. 2013; Maetzel et al. 2014). Besides, the characteristic phenotypic heterogeneity of NPC patient's cells is transferred to their derived-iPSCs as emerges from comparison of the data reported in the works of Yu, in 2014 and Efthymiou, in 2015. These two research groups, independently generated iPSCs-derived NPC-neural cells by reprogramming the fibroblasts harvested from NPC patients. The Efthymiou donor was homozygous for the *NPC1* mutation pI1061T whereas the Yu donor was compound heterozygous for pI1061T/P237S. Interestingly, the iPSCs generated by the two groups showed completely different phenotypes. Efthymiou's iPSCs-derived neural cells did not show any accumulation of free-cholesterol. On the contrary, Yu's cells showed massive accumulation of free-cholesterol that was even comparable to the one of the classical NPC-phenotype. Hence, the heterogeneity in the phenotype of patient and in iPSCs-NPC cell lines as well as the difficulty of their manipulation, highlight the need of new cellular models that are easy to handle and that better recapitulate the pathological features of Niemann-Pick disease type C. Furthermore, in order to perform drug repositioning studies these cell-based disease models have to be suitable for high throughput approaches such as the screening of drug libraries. Therefore, to overcome the limitations deriving from the use of primary and iPS cells it was decided to employ ARPE19 cells for the generation of *NPC1*$^{-/-}$ and *NPC2*$^{-/-}$ cell lines as cellular models of NPC type 1 and NPC type 2, respectively. ARPE19 is a human immortalized cell line that spontaneously arose from the primary culture of RPE (Retina Pigment epithelium) cells (Dunn et al. 1996). ARPE19 are diploid epithelial

cells that in comparison to primary cell lines are very easy to handle because they have a high rate of proliferation (approximately doubling every 24 hours) and are easy to transfect. Besides, these cells are suitable for HC studies, are cheap and commonly available on the market. Notably, since the ARPE19 cell line has a genetically defined condition, the *NPC1*$^{-/-}$ and *NPC2*$^{-/-}$ ARPE19 disease cellular models carry the same genetic background. This feature is particularly advantageous for the study of NPC type 1 and type 2 because it allows a precise comparative analysis of the two diseases.

1.4 Aims

First aim of this research project was to develop new cell-based models of the Niemann-Pick disease type-C to overcome the limitations of the existing cellular models and to carry out *in vitro* experiments on small and large (high-throughput) scales.

The second aim was dependent on the good outcome of the first and consisted of employing these NPC cell lines in a high-content screening of the Prestwick FDA-approved drug library. The idea underlying this drug screening was to identify a drug that is commonly used for another illness but that may be a candidate to treat the Niemann-Pick disease type-C.

1.5 Workflow of the project

As a first step, I generated two isogenic ARPE19 cell lines in which either the *NPC1* or the *NPC2* genes were knocked-out with the use of CRISPR/Cas9 technology.

I then characterized these knockout cells to assess whether they recapitulated the pathological features of NPC. To this end, I carried out biochemical and cell biology experiments to measure the levels of the typical NPC stored lipids (free-cholesterol, total cholesterol, sphingoid bases and GSLs) within *NPC1*$^{-/-}$ and *NPC2*$^{-/-}$. These cells turned out to have increased amounts of the aforementioned lipids. In particular, they showed a massive

accumulation of free-cholesterol within LE/LY that was visualized by filipin-LAMP1 fluorescent co-staining. Since *NPC1*$^{-/-}$ and *NPC2*$^{-/-}$ ARPE19 resulted to be good models of NPC, I decided to use the microscopy assay filipin-LAMP1 co-staining as the readout to monitor the effect of potential therapeutic compounds on the stored LE/LY free-cholesterol. To this end, I employed the *NPC2*$^{-/-}$ ARPE19 in a high content experiment to screen the 1200 FDA-approved drugs that compose the Prestwick library. This screening resulted in three candidate drugs, desipramine, fendiline and thioproperazine being selected from the library.

1.6 Niemann-Pick Disease Type C

Niemann-Pick type C (NP-C) is a lysosomal storage disorder caused by autosomal recessive mutations in either the *NPC1* or *NPC2* genes. The majority of the NPC cases, about 95%, results from dysfunction of NPC1, whereas the remaining 5% is due to malfunction of NPC2. At the cellular level, the disease is characterized by late endosomal/ lysosomal accumulation of lipids such as cholesterol, sphingoid bases and glycosphingolipids (Vanier 2010). In fact, due to the nature of the stored substrates, NPC is also considered a lipid storage disorder. Incidence of NPC has been estimated to be 1/100 000 live births. This value has to be regarded as an approximation because of the limitations in the capacity to diagnose the disease, especially for the late-onset phenotype (Wassif et al. 2016).

1.7 Symptomatology of Niemann-Pick Disease

Clinically, NPC has a very broad spectrum of symptoms with both visceral and neurodegenerative involvement. Although the majority of the patients die before their 25th birthday, there are cases of subjects first developing the disease in their sixties. In fact, on the basis of the age of onset, NPC has been classified into four categories: early infantile, late infantile, juvenile and adult (Vanier, 2010). The degree of severity of the disease is also

a variable feature since it differs notably among affected individuals. Niemann-Pick C is mainly a neurodegenerative disorder and shares clinical similarities with Parkinson's and Alzheimer's diseases (Malnar et al. 2014). The only subset of NPC patients not showing any neurological involvement is that of patients affected by the neonatal fatal form of the disease who die within the first six months of life from hepatic or respiratory failure (Vanier et al. 1988). On the contrary, patients of all the other forms of NPC show progressive deterioration of the central nervous system. When present, visceral manifestations consist of hepato-splenomegaly and pulmonary problems that are always followed by neurological symptoms. The latter, range from clumsiness and seizures at an early stage, to severe ataxia and dementia at a late stage of the disease (Patterson et al. 2012). Vertical supranuclear gaze palsy (VSGP) is a feature present in all the different stages of the disease, and is often used as a sign for clinical recognition of NPC (Vanier, 2010).

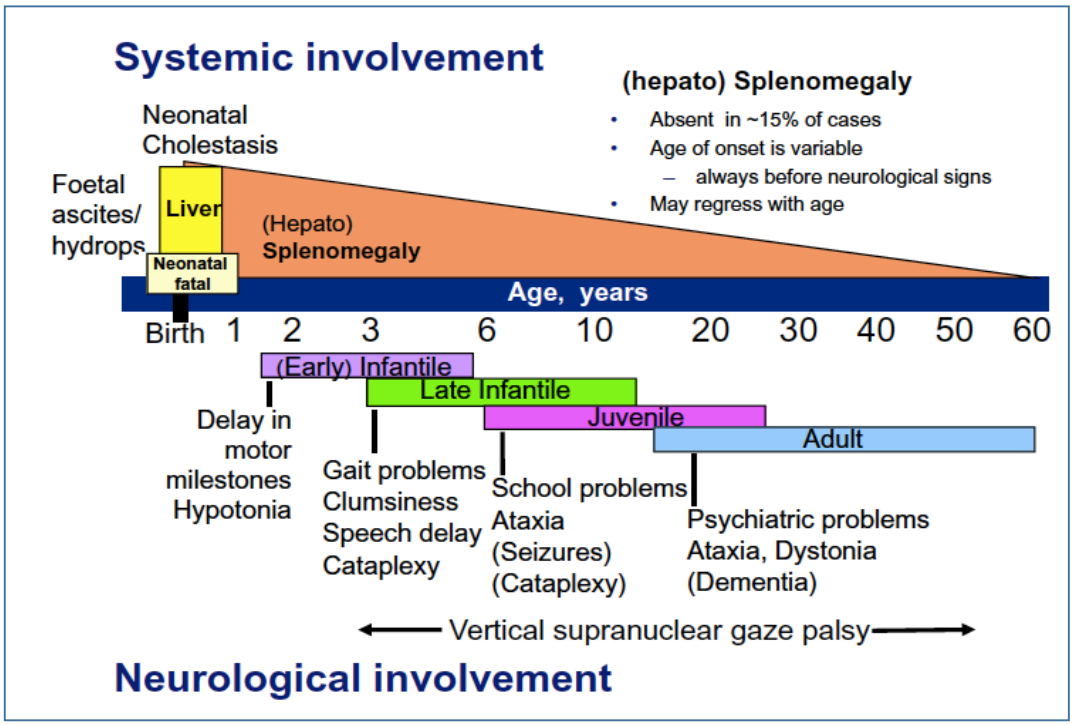

Fig. 1.1 Schematic representation of the visceral and neurological symptoms that characterize the different forms of the Niemann-Pick disease. Image adapted from Vanier 2010.

1.8 Current treatment: miglustat

Miglustat is the only drug that has been approved in for the treatment of Niemann Pick type C. Initially designed for Gaucher's disease, miglustat reversibly inhibits glucosylceramide synthase leading to a reduction in the synthesis of GSLs. The latter are mainly accumulated in the brain of NPC patients and in fact miglustat ameliorates the neurological manifestations of NPC disease (Williamson et al. 2014; EMA 2018). However, miglustat is not curative, therefore there is a need for more effective therapies.

Interestingly, an AAV intracerebroventricular gene therapy pre-clinical study on mice has demonstrated therapeutic potential for the treatment of NPC (Hughes et al. 2018).

1.9 NPC1

The *NPC1* gene is located on chromosome 18q11-q12 and comprises 25 exons. It codifies the 1278 amino acid long NPC1 glycoprotein, an integral protein of the late endosomal/ lysosomal limiting membrane that transiently interacts with the Trans Golgi Network (TGN) (Carstea et al. 1997; Higgins et al. 1999). NPC1 is known to be involved in the transport of free cholesterol to the LE/LY limiting membrane, but its exact function is yet to be elucidated. It has been hypothesised that NPC1 protein may function to transport lipophilic molecules different from cholesterol, out of late endosomes/lysosomes. This efflux pump activity of NPC1 and its homology with the prokaryotic permeases RND (resistance-nodulation-division) has led to consider NPC1 a eukaryotic RND permease (Davies et al. 2000). The NPC1 glycoprotein consists of 13 transmembrane domains, three LE/LY lumenal domains, a sterol sensing domain and a cytoplasmic C-terminal domain (Li, et al. 2016 b) (Fig. 1.2). N-terminal domain (NTD), is the first lumenal domain of NPC1. This site bears the hydrophobic cavity that binds the molecule of free-cholesterol when delivered from NPC2 to NPC1 (Kwon et al. 2009). The second luminal loop of NPC1 is the harbouring site for the NPC2 protein complexed with one molecule of cholesterol. The very first contact

between NPC1 and NPC2 occurs at this site. This step precedes the actual transfer of cholesterol to the sterol-pocket located at the NTD of NPC1 (Deffieu, Pfeffer 2011). The third luminal protrusion is represented by the Cystein-rich domain that, on the basis of its resemblance to a RING-finger motif, has been hypothesized to mediate the interactions with other proteins or lipids (Greer et al. 1999). As for the transmembrane region, five domains spanning from amino acids 616 to 797 form a sterol sensing domain (SSD) that is similar to the ones of SCAP (SREBP Cleavage Activating Protein) and HMG-CoA Reductase (Carstea et al. 1997; Horton and Goldstein 2002). The C-terminal domain of NPC1 (NPC1-C) is cytosolic and its function is still under debate. Some reports claim that the NPC1-C di-leucine motif is critical for the sorting of NPC1 to LE/LY while others have ruled out any involvement of NPC1-C to NPC1 LE/LY targeting (Scott et al 2004). It has also been hypothesized that NPC1 interacts with the AP complex, which in turn mediates the NPC1-targeting to late endosomes /lysosomes (Poirier et al. 2013). Studies on NPC-1 patient skin-fibroblasts have identified mutations throughout the NPC1 protein with the exception of the N-terminal end of the N-terminal domain (Millat et al. 2001). Furthermore, NPC1 plays a key role in the infective process of the filoviruses Ebola and Marburg. Crystal structure experiments show that the NPC1-C interacts with the primed envelope glycoprotein GPcl of the Ebola virus thus allowing the virus to bind NPC1 prior to fusing with the lysosomal membrane and entering the cytoplasm to undergo replication (Wang et al. 2016).

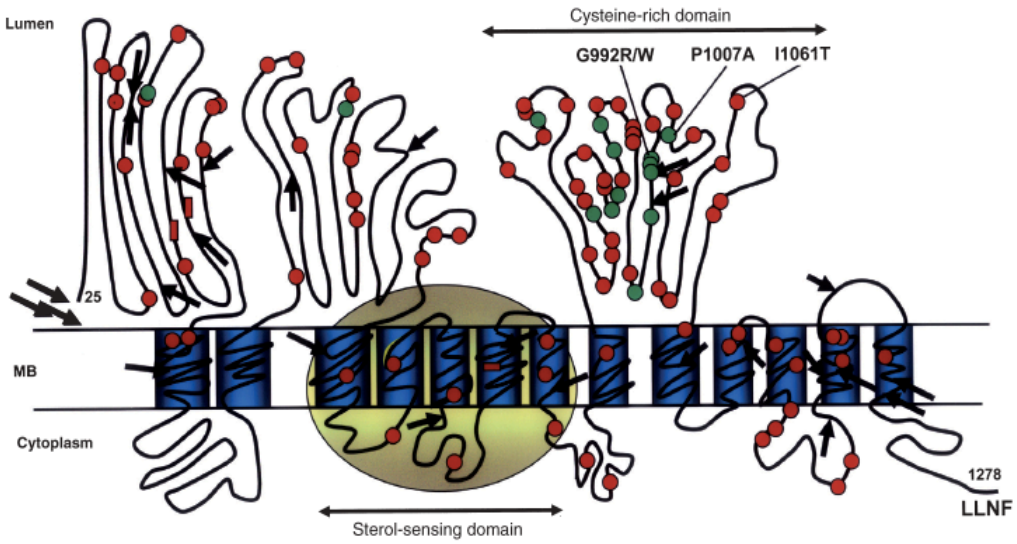

Fig. 1.2 Structure of the NPC1 protein as proposed by David and Iannou 2000. Red and green dots represent the mutations identified in the NPC1 proteins of individuals affected by Niemann Pick-C type1. The image has been adapted from Vanier 2003.

1.10 NPC2

The 5-exon gene *HE1/NPC2* maps to chromosome 14q24.3 and encodes the small soluble glycoprotein NPC2. The latter, composed of 151 amino acids, localizes to late endosomes / lysosomes via a mannose-6-phosphate pathway and is also secreted in the epididymal fluid (Naurekiene et al. 2000; Willingorg et al. 2005; Kirchoff et al. 1996). NPC2 is a cholesterol transporter that within LE/LY binds and conveys free-cholesterol, one molecule at a time, to the NPC1 transmembrane protein (Babalola et al. 2007). NPC2 delivers cholesterol to NPC1 in a two step process. Firstly, NPC2 holds onto the second luminal loop of NPC1 and then it interacts with the NTD-NPC1 to create a tunnel for the exchange of the molecule. The crystal structure of a bovine NPC2-protein bound to cholesterol-3-O-sulfate showed that NPC2 has a hydrophobic pocket that accommodates isooctyl moiety of the sterol in the inner core leaving the sulphate group (the O-R extreme) outside the hydrophobic cavity, exposed to the LE/LY lumen (Xu et al. 2007). For the purpose of our research it is important to highlight that the amino acids located in the segment 101-128 of the primary structure of NPC2 are fundamental components of the sterol hydrophobic pocket (Fig. 3.4 Chapter 3).

1.11 Hypothesis of the NPC2-NPC1 Mechanism of Action

Cholesterol is a lipid with multiple functions in mammalian cells. At the plasma membrane cholesterol is essential for regulating the fluidity of the phospholipid bilayer while in the anabolic processes it is used as the precursor for the synthesis of steroid hormones, bile acids and vitamin D. The amount of intracellular cholesterol is regulated by endogenous and exogenous sources. Endogenously, cholesterol is synthesized in the endoplasmic reticulum via *de novo* synthesis while exogenously it is supplied by the diet through the lipoprotein-delivery system. In the cells of peripheral tissues cholesterol homeostasis is regulated by both endogenous and exogenous supply. The cholesteryl esters that the human organism absorbs through diet are packaged into lipoproteins and transported through the blood vessels to the peripheral tissues. On the contrary, in the central nervous system, the cholesterol requirement is almost exclusively provided by *de novo* synthesis because lipoproteins cannot cross the blood brain barrier (BBB). Four classes of lipoproteins at different densities of cholesterol, LDL, VLDL, IDL and HDL (low, very, intermediate and high, respectively) have been identified. Among them, LDLs (low density lipoproteins) are the most abundant (Fig. 1.3). Cellular uptake of LDLs is mediated by the LDL-receptors that are located on the cell surface. LDLs are internalized in coated vesicles and then delivered to late endosomes/ lysosomes where the esterified cholesterol is hydrolysed into free-cholesterol and fatty acids under the action of the lysosomal acid lipase (LAL) (Fig. 1.4). At this stage free-cholesterol leaves the LE/LY and migrates towards either the endoplasmic reticulum or the plasma membrane (Brown and Goldstein 1986).

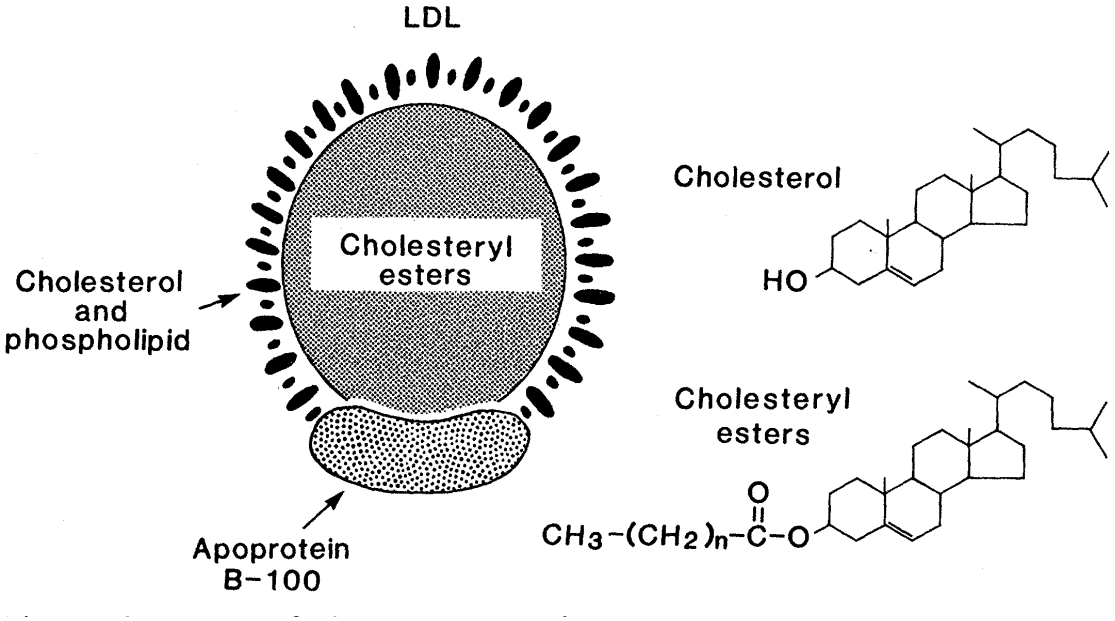

Fig. 1.3 Structure of an LDL (Low Density Lipoproteins) and chemical structure of free-cholesterol and esterified cholesterol. Image adapted from Brown and Gldstein 1986.

Transport of unesterified-cholesterol within LE/LY is thought to be mediated by the concerted activity of the NPC2-NPC1 proteins. To explain the interaction between NPC1 and NPC2, a hypothetical model named "hydrophobic hand-off" transfer, has been developed (Li, et al. 2016 a). This model hypothesises that after the hydrolysis of LDL-esteryl cholesterol by the acid lipase, the resulting free-cholesterol is delivered by NPC2 to NPC1. In particular, at the inner lumen of LE/LY, the sterol binding pocket of NPC2 binds one molecule of free-cholesterol at the isooctyl moiety, and transfers it to the sterol binding pocket of the N-terminal domain (NTD) of NPC1 (Kwon et al. 2009). To further understand this transport mechanism, a recombinant protein-complex composed of three elements: NTD-NPC1, full-length NPC2 and a molecule of cholesteryl sulphate was crystallized and analysed both alone and upon docking onto the NPC1 cryo-EM structure. These crystallization and modelling experiments revealed that the sterol binding pocket of NPC2

binds the sterol binding pocket of NPC1, thus forming a transfer tunnel between the two sterol pockets. In addition, the orientation of these molecules within the sterol pockets is indicative of the fact that the transfer of cholesterol between the NPC proteins actually occurs in the direction NPC2-NPC1 and not the other way round (Li, et al. 2016 a). As for the egress of free-cholesterol from LE/LY to the cytoplasm, the exact mechanism through which cholesterol crosses the lysosomal membrane is still unknown. Besides, whether NPC1 is involved in this exiting process is also an open question.

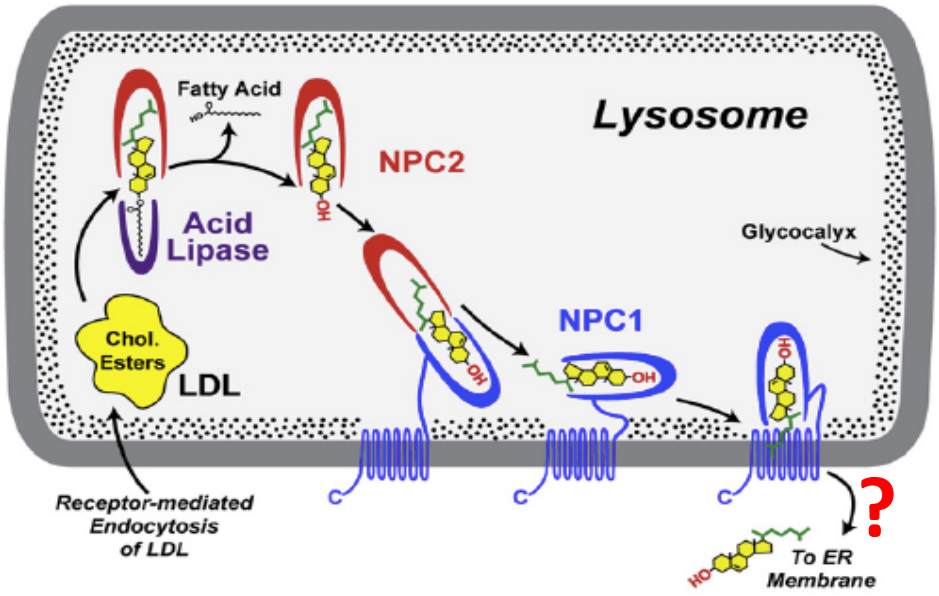

Fig 1.4 Proposed model for the LE/LY pathway of the esterified cholesterol acquired from LDLs. The acid lipase hydrolysis the esterified cholesterol yielding free-cholesterol and fatty acids. Subsequently free-cholesterol is transported by NPC2 to NPC1. How free-cholesterol exits LE/LY is still unknown. Image adapted from Kwon et al. 2009.

1.12 Biochemistry and Tissue Distribution of Lipids in NPC Patients

Biochemically, NPC1 and NPC2 patients show very similar tissue specific lipid accumulation patterns (Vanier and Millat 2003). This lipid storage, consists of various classes of lipids, including cholesterol, sphingomyelin (SM), glycosphingolipids (GSLs) and the sphingoid bases sphingosine and sphinganine. Overall, cholesterol and sphingomyelin are the lipids that mostly accumulate in the peripheral tissues of NPC patients and in fact free-cholesterol is the major diagnostic hallmark of Niemann-Pick C disease (Vanier and Latour 2015). More specifically, the levels of free-cholesterol and sphingomyelin in liver and spleen of NPC individuals appear increased 2-to 5-fold and those of sphingosine and sphinganine 6 to 24-fold in comparison to controls (Rodriguez-Lafrasse 1994). As for GSLs, lactostlceramide, globotriaosylceramide, globotetraosylceramide and GM3 all appeared equally augmented 2 to 4-fold, while glucosylceramide showed a striking 35-fold increase in the spleen and 14-fold increase in the liver. In the central nervous system (CNS) instead, the largest lipid storage was represented by GSLs, with GM3 and GM2 gangliosides showing 10 to 15- fold and 3 to 5-fold rises respectively (Vanier et al. 1983; Rodriguez-Lafrasse 1994). Conversely, no difference in the levels of free-cholesterol was detected between NPC patients and healthy controls. Similar to human symptomatology, animal models of NPC present accumulation of lipids in brain, liver and spleen. In particular, the spontaneous mutant mouse *Npc1*$^{-/-}$ shows an amount of sphingosine in the brain that is double that of controls (Vruchte et al 2004).

1.13 Pathogenesis of NPC

NP-C disease is often associated with pathological accumulation of free-cholesterol. However, there is evidence suggesting that cholesterol storage is not the triggering event underlying NP-C and in fact, among classical NPC patients, there is a percentage of subjects with a variant NPC phenotype that does not present any free-cholesterol storage (Sun et al. 2001). Besides, therapies aiming at lowering the levels of LDLs (and so of esterified

cholesterol) in the plasma were of no clinical benefit (Sturley 2011). Furthermore, the consistent reduction in the level of free-cholesterol that occurs upon overexpression of Rab9 in human NPC-skin fibroblasts indicates that the malfunction of the NPC2-NPC1 transport pathway does not directly hamper cholesterol efflux from LE/LY (Narita et al. 2005). To date, the most accredited cellular model describing the pathogenesis of Niemann-Pick type-C identifies sphingosine as the primary metabolite that accumulates in the cells upon dysfunction of either NPC1 or NPC2. The chronology of the pathogenic cascade was studied in healthy cells in which the functionality of NPC1 was inhibited with the U18666A drug. It was demonstrated that the elevation of sphingosine levels induces a reduction in the concentration of Ca^{2+} within the acidic compartments. This condition results in an insufficient release of Ca^{2+} from LE/LY during fusion between endolysosomal vesicles. As a consequence, the endolysosomal trafficking is altered and the secondary substrates, cholesterol, sphingomyelin and GSLs, accumulate and cause cellular damage (Lloyd-Evans et al. 2008) (Fig. 1.5). In addition, experiments performed with the fluorescent "caged sphingosine" confirmed that NPC-patient fibroblasts have LE/LY with increased levels of sphingosine and lower ability to release Ca^{2+} with respect to healthy controls (Hoeglinger et al., 2015).

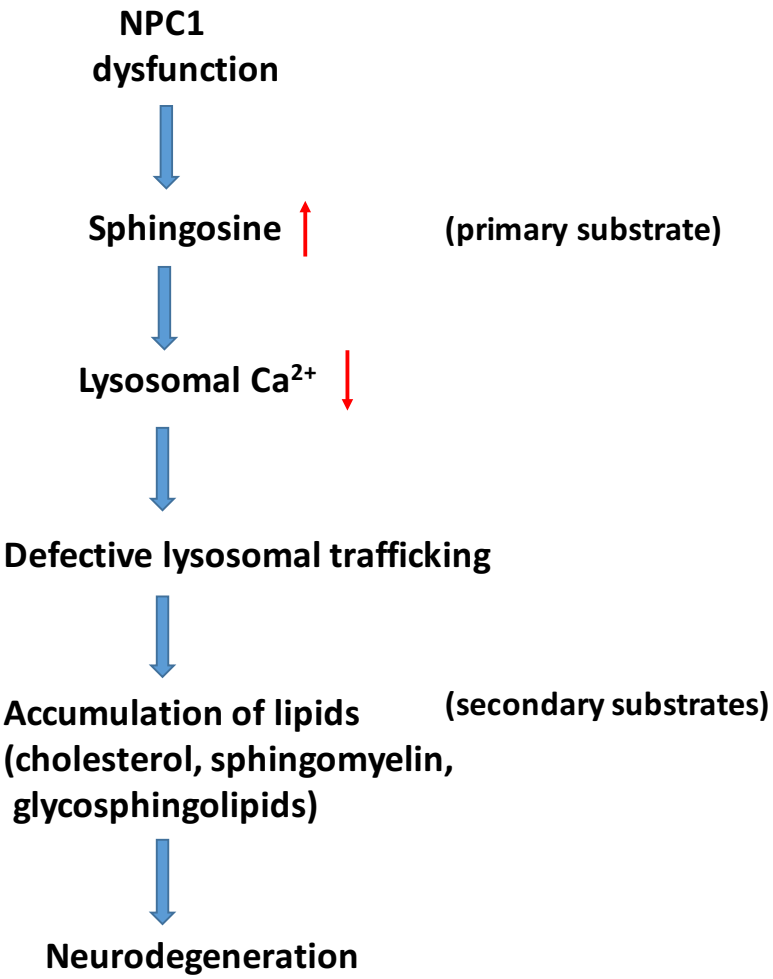

Fig. 1.5 Proposed model for the pathogenic cascade of Niemann-Pick C. The small red arrows indicate increased sphingosine levels and decreased concentration of LE/LY Ca^{2+}. Image adapted from Lloyd-Evans and Platt 2010.

1.14 CRISPR/Cas9 System

The CRISPR/Cas (Clustered Regularly Interspaced Short Palindromic Repeats-CRISPR associated protein) system is a biological mechanism of adaptive immunity found in bacteria and archea (Barrangou et al 2007). Among the six CRISPR systems that have been discovered, the CRISPR/Cas9 type II of the *Streptococcus pyogenes* has been repurposed as a biotechnological tool for genome editing (Jiang and Doudna 2017).

1.15 S. pyogenes CRISPR/Cas9 Type II

CRISPR/Cas9 system type II consists of genes encoding the nuclease enzyme Cas9, the tracrRNA, and CRISPR repeat arrays (Fig. 1.6). Upon bacteriophage infection or plasmid transfer, short fragments of exogenous DNA are integrated within the bacterial chromosome at the DNA loci CRISPR repeat spacer arrays. In this way, bacteria keep memory of a previous infection to counteract a new one. When the same DNA invades the cells again, the DNA fragments previously integrated in the CRISPR arrays and the tracrRNA gene are transcribed into pre-crRNA and tracrRNA, respectively. These two RNA structures anneal to each other and form the pre-crRNA-tracrRNA complex that is then cleaved by the RNase III yielding the mature crRNA-tracrRNA. The latter in turn, recruits the Cas9 and directs it towards a specific site of the invading DNA that is complementary to the 20-nt long crRNA and adjacent in 5' to a 5'-NGG-3'sequence called PAM (protospacer adjacent motive) (Fig. 1.6). At this stage the invading DNA is cleaved by the Cas9 and then degraded. The PAM is a conserved tri-nucleotide NGG, where N can be any nucleotide (Heler et al. 2015).

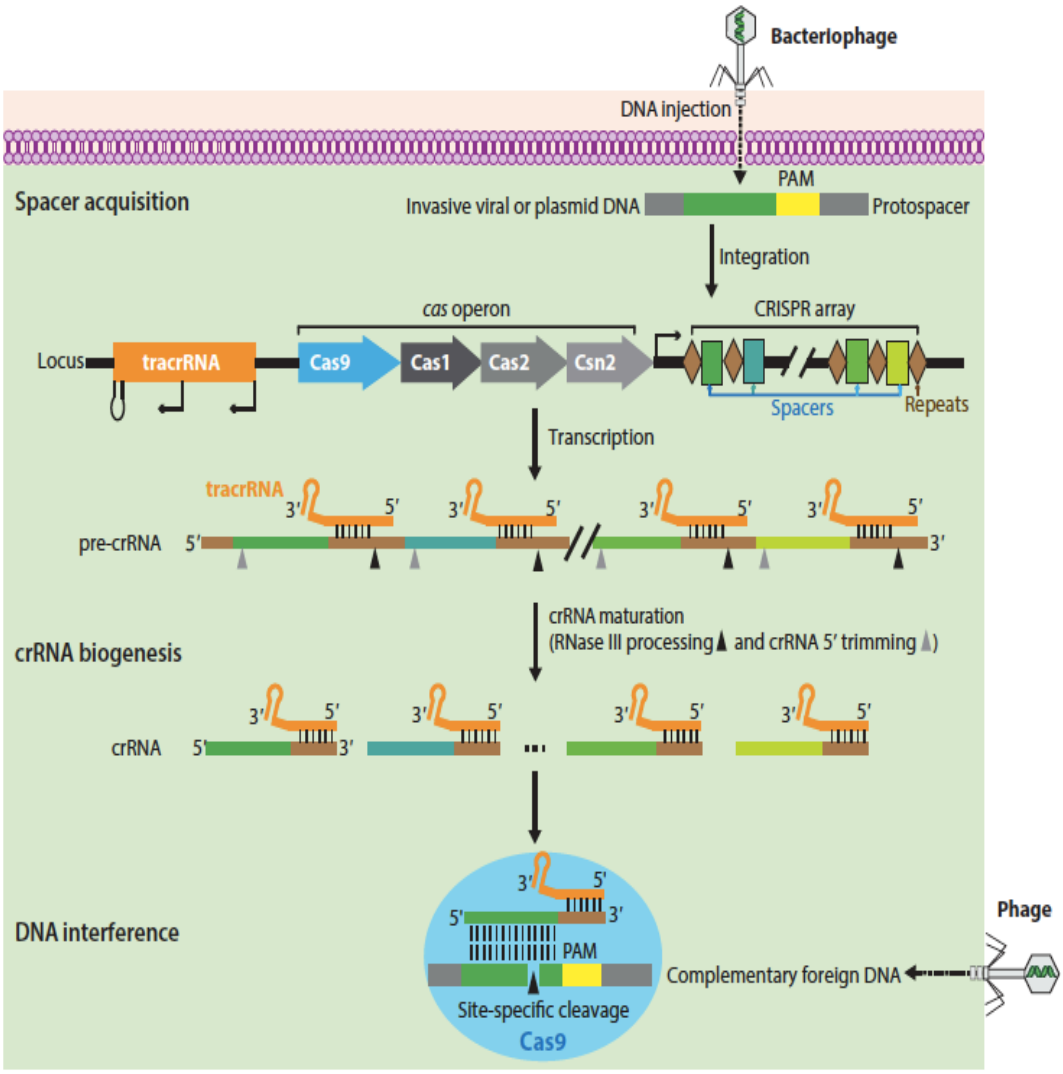

Fig. 1.6. Schematic of the naturally occurring adaptive immune CRISPR/Cas9 system. Upon phage infection of the cell, fragments of the exogenous DNA are integrated in the bacterial DNA at the CRISPR arrays. Subsequently, these DNA sequences are transcribed into pre-crRNA that hybridise with the tracrRNA forming a structure that after RNA III processing binds and leads the Cas9 towards the complementary foreign DNA. Image adapted from Jiang and Doudna 2017.

1.16 Cas9 mediated genome engineering

The *S. pyogenes* CRISPR/Cas9 system has been engineered to be used in mammalian cells by heterologous expression of a human codon-optimized Cas9 and a synthetic crRNA-tracrRNA structure called single-guide RNA (sgRNA). This RNA structure consists of a 20-nt guide sequence (crRNA spacer) that targets the DNA region of interest, and a scaffold (tracrRNA) for the recruitment of the Cas9 nuclease (Fig. 1.6) (Jinek et al. 2012).

The CRISPR/Cas9 technology allows precise targeting and, theoretically, editing of any genome sequence under two conditions: the target-site is complementary to the 20-bp gRNA and to a sequence (protospacer) that is located next to and upstream of a PAM sequence (Fig. 1.7) (Sander and Joung 2014).

1.17 Mechanism of gRNA/Cas9 activity

In this model, the gRNA binds the Cas9 and delivers it to the 20-nt target-site of the gene of interest where the enzyme will carry out a double strand break of the DNA. Cas9 is an endonuclease composed of two domains with nuclease activity, NHN and RuvC, each able to cleave one strand of the DNA within the target-site region, 3bs from the NGG PAM sequence. When the gRNA-Cas9 complex is in proximity of the target-site, the Cas9 enzyme undergoes a conformational variation and switches from an inactive to an active state. However, before starting its nuclease activity, the Cas9 has to recognize the PAM sequence located downstream of the target-site as appropriate for the CRISPR system (Sternberg et al. 2014). Once this crucial step has been overcome, the Cas9 unwinds the target DNA thus enabling the HNH domain to cleave the target-strand (DNA strand complementary to the gRNA) and the RuvC domain to cut the nontarget-strand (DNA strand correspondent to the gRNA). Following cleavage of the double stranded DNA, the Cas9 is displaced from the target site by cellular factors (Jinek et al 2013).

In any organism, upon generation of DNA double-strand breaks, two major mechanisms of repair can be activated to re-establish the phosphodiester bonds: error-free homology

directed repair (HDR) and error-prone non-homologous end joining (NHEJ) repair.

In the presence of a donor segment flanked by arms that are homologous to the ones flanking the DNA broken site, the HDR pathway is triggered. As a result, the donor segment of DNA is inserted at the damaged site. This HDR mechanism is useful when precise insertions need to be carried out. Instead, in the absence of any donor template, the NHEJ pathway is the mechanism activated by the cell to repair a DNA break. However, since NHEJ is error prone, random insertions or deletions (indels) are very likely to occur during the repair process. As a consequence, downstream frameshift mutations or large deletions that lead to disruption of the gene function are originated (Liebers 2011).

In the generation of the *NPC1*$^{-/-}$ and *NPC2*$^{-/-}$ ARPE19 cell lines I took advantage of the NHEJ mechanism to perform the knockout of the *NPC1* and *NPC2* genes.

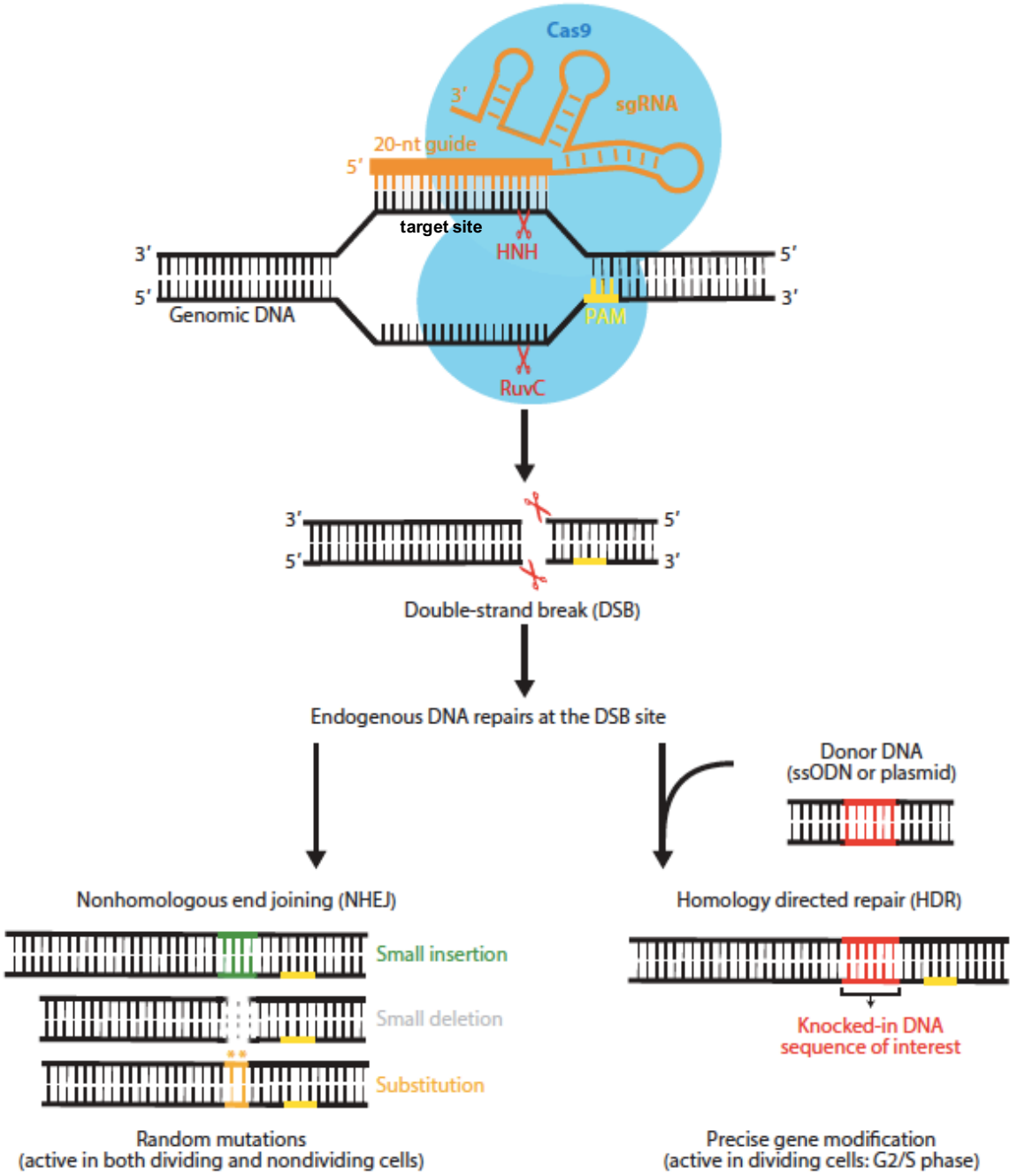

Fig. 1.7. CRISPR-Cas9 genome editing. The sgRNA (crRNA-tracrRNA) delivers the Cas9 to the specific target-site. The two nucleases HNH and RuvC cleave both DNA strands generating a double strand break (DSB). After the cleavage, the DNA-DSB can be repaired by either NHEJ or HDR pathway that are activated in the absence or presence of a repair template, respectively. NHEJ causes random mutations whereas HDR allows precise genetic modifications at the cleaved site inducing the insertion of the repair template. Image adapted from Jiang and Doudna 2017.

2.0 Material and Methods

2.1 CRISPR/Cas9 technology

Cells: ARPE-19 ATCC® CRL-2302

Nucleofection kit: LONZA

Plasmid vector: GFP- All in one Sigma-Aldrich

FACS machine: BD Biosciences FACS-Canto II

A working flowchart to obtain clones with a systematic procedure was set up (Fig. 2.1). ARPE19 cells were grown in Petri dishes ($1*10^6$ cells) and transfected by nucleofection with "all in one" plasmid vectors encoding: the human codon-optimized Streptococcus pyogenes Cas9, a single guide RNA with a 20-nt spacer targeting either exon1 of *NPC1* at (GCTGCTACTGTGTCCAGCGC) or exon 3 of *NPC2* at (CTGATGGTTGTAAGAGTGGA) and a GFP gene reporter. Cas9 and sgRNA genes were under the regulation of CMV and U-6 promoters, respectively. Transfected cells were incubated for three days at 37°C and then singularly sorted by the FACS machine. Only cells expressing GFP were selected by the machine and placed, one cell per well, in 96 well plates. In this way single clones of transfected ARPE19 cells were obtained.

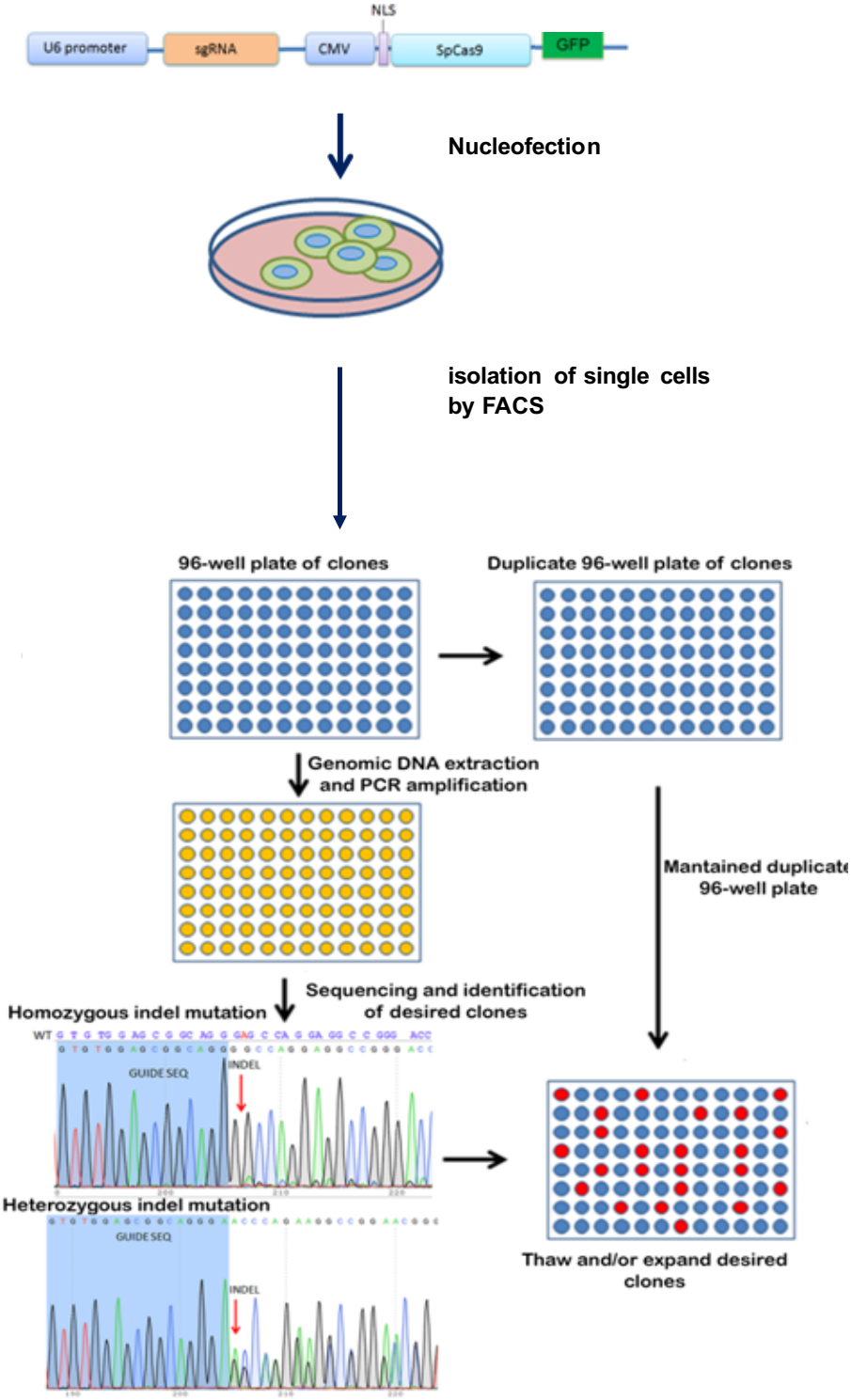

Fig. 2.1. Working flowchart of the procedure to obtain isogenic cell lines. ARPE-19 cells were nucleofected with an "ALL in One" vector expressing Cas9, one specific gRNA for each genes and a fluorescent reporter. After incubation, transfected cells were clonally sorted by FACS into 96-well plates. Each 96-well plate was duplicated, so that one of the duplicate plates was used for genomic DNA extraction and sequencing, whereas the other duplicate was maintained in culture or frozen. Only the clonal populations showing homozygous InDel mutations in the sequence of interest were expanded and analyzed for off-target mutations.

2.2 Filipin staining

The filipin cellular assay was used to visualize the un-esterified cholesterol within WT, *NPC1*$^{-/-}$ and *NPC2*$^{-/-}$ cells. Cells were fixed with PFA (Paraformaldehyde) 4%, washed with PBS 1X and then treated with Glycine 50mM in PBS 1 X for 10 min to quench the PFA. After a second wash with 1X PBS, cells were incubated with filipin III for 1h at room temperature keeping the samples protected from light. Finally, images were acquired with confocal microscopy setting excitation and emission wavelength at 340-380 nm and 385-470 nm.

Filipin III is an antibiotic extracted from Streptomyces filipinensis that is commonly used as a fluorescent biomarker of free-cholesterol. Commercialized as powder, filipin was firstly dissolved in ethanol following the manufacturer's instructions and then diluted 1:100 in the proper Abcam kit solvent.

2.3 Sphingosine and sphinganine HPLC measurement

The following analytical method was applied to perform a qualitative and quantitative measurement of the sphingoid bases contained in WT, *NPC1*$^{-/-}$ and *NPC2*$^{-/-}$ ARPE19 cells. Developed by Merril in 1999, the sphingoid measurement consists of three main steps: solid phase extraction (SPE), OPA-derivatization and HPLC analysis of sphingoid bases (Merrill et al 2000).

Initially, a lipid mixture was obtained from the cell homogenate using organic solvents. Subsequently, the sphingoid bases were extracted from the lipid mixture by SPE on aminopropyl chromatographic cartridges. Once purified, the sphingoid bases were derivatized with O-Phtaladehide and then separated on a reversed phase column by HPLC. The OPA derivatives of the sphingoid bases were analysed fluorometrically by a spectrofluorometer.

Excitation and emission wavelengths of OPA derivatives are 340nm and 455 nm respectively. The concentration of sphingoid bases is reported as pmol of the specific

sphingoid basis /mg protein. This value is calculated using C20 sphingosine as internal standard. In each HPLC analysis C20 sphingosine is run in an amount corresponding to 300 pmol.

Sphingoid bases extraction

Each sample of cell homogenate corresponding to 0.1 mg protein was dissolved in H_2O, added of 500 uL CHCl3/MeOH (1:2), 3uL 0.1mM of the internal standard C20 and sonicated for 10 min at RT. Then, one after another, 500uL NaCl (1M), 500 uL $CHCl_3$ and 100 uL NaOH (3M) were added to the sample tubes that were then incubated for 15 min at RT, vortexing every 5 minutes. Samples were then centrifuged for 10 min at 13000g so as to separate upper and lower phases. Upper phase and protein interphase were removed and the lower phase was applied onto SPE NH_2 columns (Biotage) pre-equilibrated with 2x1 $CHCl_3$. Purified sphingoid bases were then eluted with 3x 300 uL acetone.

OPA derivatization

The elutant was then dried under a stream of N_2, resuspended in 50 uL of pre-warmed EtOH, added of 50 uL of fresh OPA-labelling solution (O-Phtalaldyhyde dissolved in 20X EtOH, 1x 2-mercaptoethanol and diluted in 2000x 3% Boric acid pH 10,5) and incubated for 20 at RT in the dark, vortexing every 10 min.

Once the OPA-labelling reaction was finished, 100 uL MeOH/5mM Tris pH9 (9:1) were added and samples were centrifuged for 2 min at 5000 g.

HPLC analysis

A volume of 150 uL of the supernatant was then transferred to HPLC vials and 50uL were loaded for a reversed phase HPLC analysis.

The mobile phase was constituted of the following solvents: MeOH, H_2O, CH_3CN and CH_3CN/H_2O (1:4). Separation was performed using Hitachi L-2485 FL Detector. OPA has an excitation wavelength of 340nm and emission of 455nm.

2.4 Glycosphingolipids (GSLs) HLPC measurement

Measurement of the the GSLs was carried out applying the method optimized by Neville in 2004 (Neville et al. 2004).

GSLs are analysed indirectly through their oligosaccharides. In fact, once extracted from the lipid mixture, glycans are firstly released from the ceramide by glycanase digestion and then labelled with anthranilic acid (2-amino-benzoic acid; 2AA). Derivatized saccharides, monomers and oligomers are then separated by HPLC and their fluorescence is detected with a spectrofluorometer.

GSLs extraction

On day one, samples of cell homogenates corresponding to 0.1mg protein were added of 2 mL CHCl3/MeOH (1:2 v/v) and left overnight at 4^{o}C.

On day two, samples were centrifuged for 10min at 1500g. The supernatant was transferred to new tubes, added of 0.5 mL CHCl3 and 0.5 mL PBS and then centrifuged for 10min at 1500g so as to separate lower and upper phases. The lower phase was removed from this suspension, placed into new tubes, dried under a stream of N_2, resuspended in 50uL CHCl3/MeOH (1:3) and and then recombined with the upper phase.

The extraction of GSLs from the lipid mixture was performed using the C_{18} Isolute columns (100mg, Biotage) pre-equilibrated with 4x1 mL MeOH and 2x1 mL H_2O. The samples (lower/upper phases mix) obtained from the previous passage were loaded onto the columns. The latter were washed with 2x1 mL H_2O and eluted with 1x1 mL CHCl3/MeOH (98:2), 1x2 mL CHCl3/MeOH (1:3) and 1x1 mL MeOH.

Digestion of the glycosidic bonds

The column elutant was dried under a stream of N_2, resuspended in 200 uL CHCl3/MeOH (2:1) and then dried again under a stream of N_2.

At this stage some samples were digested with the enzyme ceramide glycanase (CGase) and others with the enzyme Cerezyme. For the Ceramide glycanase digestion the dried elutant was firstly resuspended in 86uL of ceramide glycanase (CGase) buffer (50mM sodium

acetate pH 5.5, 1mg/mL sodium taurodeoxycholate) and subsequently added of 4uL CGase (50mU, Orphazyme, APS). Samples were then incubated at 37^{o}C for 16h. As for the Cerezyme digestion, the dried elutant was resuspended in CGase buffer, added of 15 uL of Cerezyme enzyme and incubated at 37^{o}C for 72h.

Derivatization of the oligosaccharides with 2AA

Oligosaccharides released in the enzymatic reactions were labelled with anthranilic acid (2AA). In particular, 310 uL and 200 uL of the 2AA labelling mix were added to the products of reaction of CGs and Cerazyme, respectively. Samples were then mixed with 3x1 mL CH_3CN/H_2O (97:3) and applied onto Discovery DPA-6S columns (SUPELCO) that had been pre-equilibrated with 1x1 mL CH_3CN, 2x1 mL H_2O, and 2x1 mL CH_3CN. Columns were washed with 4x1 mL CH_3CN/H_2O (95:5) and then the purified 2AA-saccharides were eluted with H_2O (600 uL for CGase or 1 mL for Cerezyme).

HPLC analysis

Vials with 60 uL sample: 140uL CH_3CN were prepared for normal phase high performance liquid chromatography (HPLC) and 50uL of the mixture were loaded for the HPLC analysis. The mobile phase of was made up of the following solvents, CH_3CN, mQ H_2O, and 100mM NH_4OH (pH 3.85) in mQ H_2O. Separation was performed at 30^{o}C using Waters Alliance 2695 separation module. 2AA was excited at 360 nm and detected at 425 nm using the Waters 2475 Fluorescence Detector.

2.5 LysoTracker Green FACS analysis

The FACS (Fluorescence Activating Cell Sorting) analysis was performed in accordance with the method applied by Platt et al. in 2014 (Te Vrutchte et al. 2014).

Complete Medium: 10% FBS, 1% penicillin/streptomycin, 1% L-glutamine in DMEM.

Cells were grown at 37^{o}C with 5% CO_2

FACS buffer: 0.1% BSA, 0.02M NaN_3 in 1X PBS

LysoTacker: LysoTracker-Green DND-26 200nM in FACS buffer

Propidium Iodide (PI): 1ug/mL in 1X PBS

Propipdium Iodide is a red-fluorescent dye used to detect dead cells. This compound cannot cross the plasma membrane of live cells whereas it easily permeates the damaged membranes of dead cells. Once within the cell, PI intercalates between the base pairs of the DNA. When the PI is bond to the DNA its fluorescence is increased 20 to 30 fold.

PI excitation is 488 nm and emission > 600 nm (Nicoletti and Riccardi 2006).

ARPE19 cells were grown in petri dishes (1*10^{6}, in triplicates), detached with trypsin, added of complete medium to neutralize trypsin, centrifuged at 800g and washed with 1X PBS.

The latter was then aspirated and cells re-suspended in 0.250 mL of one of the following solutions: FACS buffer to get a negative control of the LysoTracker-Green staining, DMSO 20% in 1X PBS for 5 min, to induce cell death and create a positive control for propidium iodide, or LysoTracker-Green 200nM in FACS buffer for 10 min in the dark at RT. Then, cells were centrifuged for 5min at 800 g, resuspended in 0.250 mL of FACS buffer, placed on ice and analysed with the flow cytometer (BD Biosciences FACS-Canto II). PI (1ug/mL in 1X PBS) was added to the samples immediately prior to FACS analysis.

The FACS machine was calibrated with Cytometer Setup and Tracking beads (BD), and compensation was carried out with unstained and Lysotracker stained WT ARPE19 as well as with WT ARPE19 cells previously treated with DMSO 20% and stained with PI.

The average fluorescence for LysoTracker Green (488 nm filter) and PI (647 nm filter) was calculated using the FACS-Diva software (BD) considering a number of 10000 singlet events per sample.

2.6 Western blot analysis

Laemmli buffer: 4% SDS, 20% glycerol, 10% 2-mercaptoethanol, 0.0004% bromophenol blue, 0.125M TrisHCl, pH 6.8.

PVDF (polyvinylidene difluoride) membrane: BioRad Trans-Blot Turbo^{TM} transfer system

Primary antibodies:

Anti-Niemann Pick C1 antibody [EPR5209] (ab134113), Rabbit monoclonal [EPR5209]. Dilution 1:200 overnight incubation at 4^0C.

Anti-LAMP1 antibody (Rat monoclonal 1D4B) to LAMP1 1:500 at 4^0C.

Anti-LC3 1:200 Cell Signaling LC3B (D11) XP® Rabbit mAb #3868

Anti-NPC2 1:200 Atlas (HPA000835) Polyclonal Antibody (rabbit) against Human NPC2

Secondary antibodies:

Anti-ACTIN conjugated with HPR 1:5000 30 min at RT.

Anti-rabbit or Anti-mouse HRP labelled.

Western blots were performed on 30ug of protein extract.

On day one, protein samples were denatured by heat at 95^{o}C for 5min in Laemmli buffer and loaded onto 4-12% polyacrilamide gradient gels (NuPAGE Novex).

Samples were run in the gels keeping the voltage constant at 140V before being transferred onto PVDF membranes. After transfer, membranes were blocked for 2h with a solution of 5% milk in 1X PBS-Tween 0.1% (PBS-T) then washed with PBS-T and incubated with primary antibodies overnight, at 4^{o}C.

On day two, PVDF membranes were washed three times with PBS-T, incubated with secondary antibodies for 1.5h at RT and then washed again three times with PBS-T.

β-actin was quantified by incubation with mouse anti β-actin antibodies conjugated with HRP diluted 1:5000 for 30 min, RT followed by three washes with PBS-T.

Finally, the ECL reagent (RPN2106, Amersham) was applied on the PVDF membranes and images were acquired using the BioRad ChemiDoc XRS+. Images were then analysed with the Fiji software.

2.7 Cholesterol Measurement

Cholesterol was extracted from total cell lysate following the Folch protocol and then quantified by the Amplex Red cholesterol assay (Molecular probes).

Folch extraction

In glass tubes cell lysates were diluted with 100uL H2O to a get a final protein concentration of 0.1mg to which 2mL CH3Cl:MeOH (2:1) were added. Samples were then homogenised by rotation for 2h at RT. The homogenate mixtures were subsequently added of 0.4mL MeOH and centrifuged at 13000g for 10 min at RT. Lower phases were discarded while supernatants were transferred in new glass tubes and added of CH3Cl and 0.73mL ddH2O. After vortexing for 10s, samples were centrifuged at 13000g for 10 min at RT. At this stage the upper phase was discarded and the lower phase was washed three times with CHCl3:MeOH:H2O 3:48:47 (each washing cycle consisted of centrifuging samples and discarding supernatants) and dried under a stream of N_2.

Amplex red detection

Once extracted, total cholesterol (esterified and non-esterified cholesterol) was quantified applying the Amplex Red assay. The latter allows the quantitation of cholesterol indirectly,

through the detection of the fluorescence signal emitted by resorufin, a compound that derives from a cascade of reactions that has cholesterol as first substrate of reaction.

Cholesteryl esters are firstly hydrolized into unesterified-cholesterol and then converted into H_2O_2 and a ketone product by an enzymatic reaction with cholesterol oxidases.

Subsequently, in the presence of horseradish peroxidase, H_2O_2 reacts with the Amplex red reagent to generate the fluorescent compound resorufin.

2.8 Immunofluorescence

Primary antibodies:

Anti-Gal3 1:100 or 1:200 of the 0.5mg/mL mouse

Anti-LAMP1 antibody [H4A3] mouse monoclonal (abcam 25630) 0.1mg/mL

Anti-Niemann-Pick C1 (NPC1) antibody [EPR5209] (ab134113), Rabbit monoclonal [EPR5209]. Dilution 1:200 overnight incubation at 4^0C.

Secondary antibodies:

Secondary Ab, Alexa-fluor goat anti-mouse-594 1:1000, 1h incubation at RT

Alexa-fluor goat anti-rabbit-488 1:1000, 1h incubation at RT

ARPE19 cells were fixed with PFA 4% for 10 min at room temperature. Following fixation, cells were incubated for 30 min at RT with a blocking solution made up of 3% bovine serum albumin (BSA) and saponin 0.02% in 1X PBS.

Fixed cells were then incubated with the primary antibody dissolved in the blocking solution, overnight at 4^oC. After three washes of 5 min each with 1X PBS, cells were incubated for 1h at RT with the secondary antibody carrying the specific fluorofore. Cells were then washed with 1X PBS and mounted with *VECTASHIELD*® mounting medium with *DAPI.*

2.9 ARPE19

ARPE19 cells ARPE-19 ATCC® CRL-2302 were purchased from ATCC and cultured in DMEM or DMEM F12 with 10% FBS, 1% penicillin/streptomycin and 1% $_{L}$-glutamine at 37^{o}C with 5% CO_2.

2.10 Lentiviral vector encoding NPC1-SNAP

Lentiviral vectors carrying the rNPC1-SNAP protein to transduce *NPC1*$^{-/-}$ were generated in Platt lab at the University of Oxford. The plasmid encoding NPC1 was cloned by Dawn Shepperd and the lentiviral particles were produced by Gokhan Yilmaz.

2.11 Electron microscopy

Electron microscopy after immunogold labelling with an antibody to LAMP1 was performed by Tigem Microscopy Core.

RESULTS

3.0 Generation of *NPC1*$^{-/-}$ and *NPC2*$^{-/-}$ ARPE19 cell lines

Using CRISPR/Cas9 technology I generated *NPC1*$^{-/-}$ and *NPC2*$^{-/-}$ isogenic cell lines. Selection and synthesis of the appropriate gRNAs to identify *NPC1*$^{-/-}$ and *NPC2*$^{-/-}$ target sites for Cas9 genome-editing was done by Sigma-Aldrich. Conceptually, gRNAs were chosen on the basis of their specificity towards Cas9 target-sites with the lowest off-target reactivity and with the aim to introduce a premature stop codon in proximity to the early exons of the genes of interest. The latter requirement was important to get either no protein at all or very short truncated non-functional ones. Following these criteria, gRNAs targeting 20bp sequences adjacent to the NGG PAM, were screened over the *NPC1* and *NPC2* exomes.

3.1 Workflow of the genome editing

I transfected a batch of WT ARPE19 cells with a plasmid encoding the gRNA, the Cas9 enzyme and a GFP tag so that, using the FACS machine, the transfected cells could be isolated and singularly sorted, one cell per well, into 96-well plates. Once that each single clone had been expanded, I extracted the genomic DNA and by PCR I selectively amplified the regions flanking the gRNA target-site. Amplicons were then sequenced and the nucleotide sequences of WT and knockout cells were compared in the electropherograms.

3.2 *NPC1*$^{-/-}$ ARPE19

The *NPC1* gene consists of 25 exons of which exon 1 was the target site of the gRNA/Cas9 complex. The Cas9-editing on exon1 triggered the formation of an NHEJ-mediated frameshift mutation consisting of a homozygous deletion of the cytosine in position 55. As a consequence, a premature stop codon in exon 2 was introduced. The bioinformatics program Expasy predicted that this induced frameshift mutation would generate a 57 amino acid truncated NPC1 (Fig. 3.1). Considering that the original NPC1 protein is composed of 1278 aa, it can be claimed that full knockout of *NPC1* has been achieved.

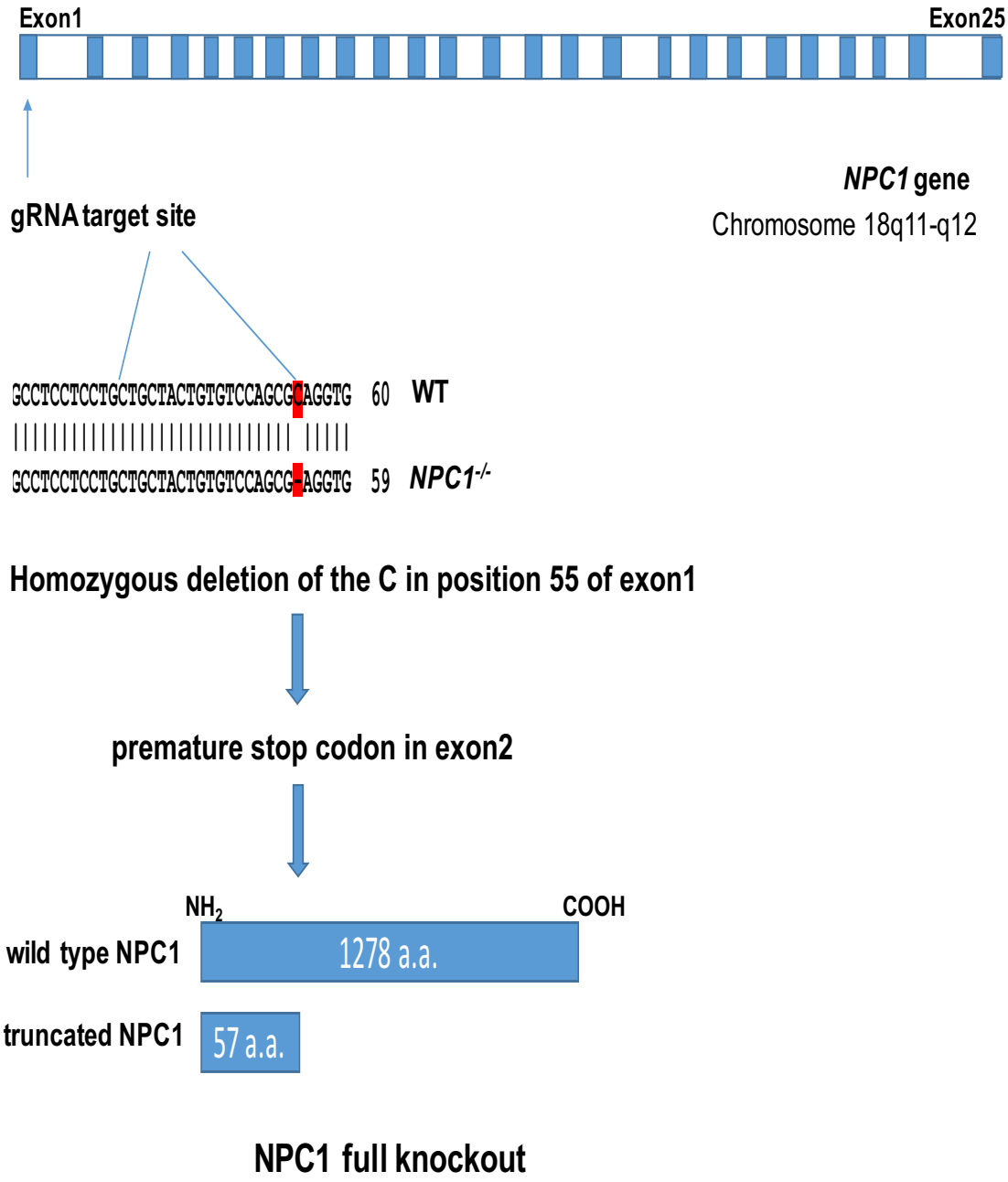

Fig. 3.1. Schematic representation of the CRISPR/Cas9 generation of *NPC1*$^{-/-}$ ARPE19. The upper part of the picture, the comparison between the nucleotide sequences of the exon1 in WT ARPE19 and *NPC1*$^{-/-}$ ARPE19 is illustrated. The homozygous deletion of the cytosine (C) in position 55 is highlighted in red. The deletion occurred within the DNA region targeted by the sgRNA.

By western blotting with an antibody directed against the C-terminal domain of NPC1, I demonstrated the absence of the NPC1 protein in *NPC1*$^{-/-}$ ARPE19 (Fig. 3.2). Confocal microscopy analysis with antibodies to LAMP1 and NPC1 also confirmed that no NPC1 protein was expressed in *NPC1*$^{-/-}$.

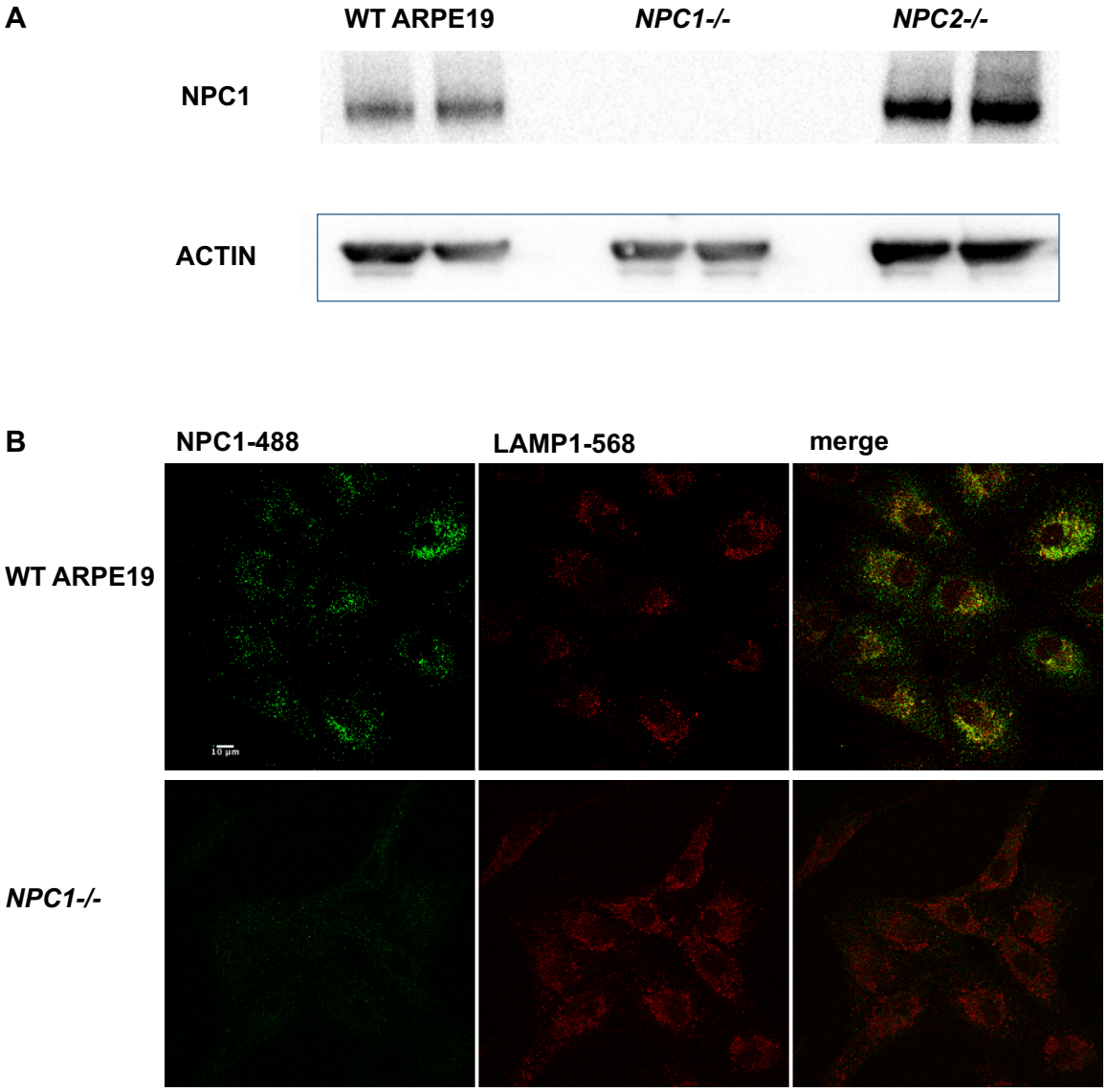

Fig. 3.2. (A) Western blotting analysis using antibodies to NPC1 and ACTIN. (B) Confocal microscopy of WT and *NPC1*$^{-/-}$ cells immunostained with antibodies to NPC1 (Alexa Fluor 488) and to LAMP1 (Alexa Fluor 568).

3.3 *NPC2*$^{-/-}$ ARPE19

NPC2 is a small soluble protein and its gene is composed of only 5 exons. In order to generate an *NPC2*$^{-/-}$ ARPE19 cell line, I employed a gRNA targeting exon 3 of the *NPC2* gene. The resulting Cas9 double-strand-break induced a homozygous deletion of the guanosine (G) in position 226. As a consequence of this frameshift mutation, a stop codon in exon 5 was produced. Expasy predicted that the genetic modification of the NPC2 gene would lead to the expression of a 101 amino acid truncated-NPC2 protein (Fig. 3.3). Knowledge of the crystal structure of NPC2 explains why even such a long truncated NPC2 cannot function (Fig. 3.4). Furthermore, in Chapter-3 I have proven that the NPC2 mutated protein is non-functional.

HE1/NPC2 gene
Chromosome 14q24.3

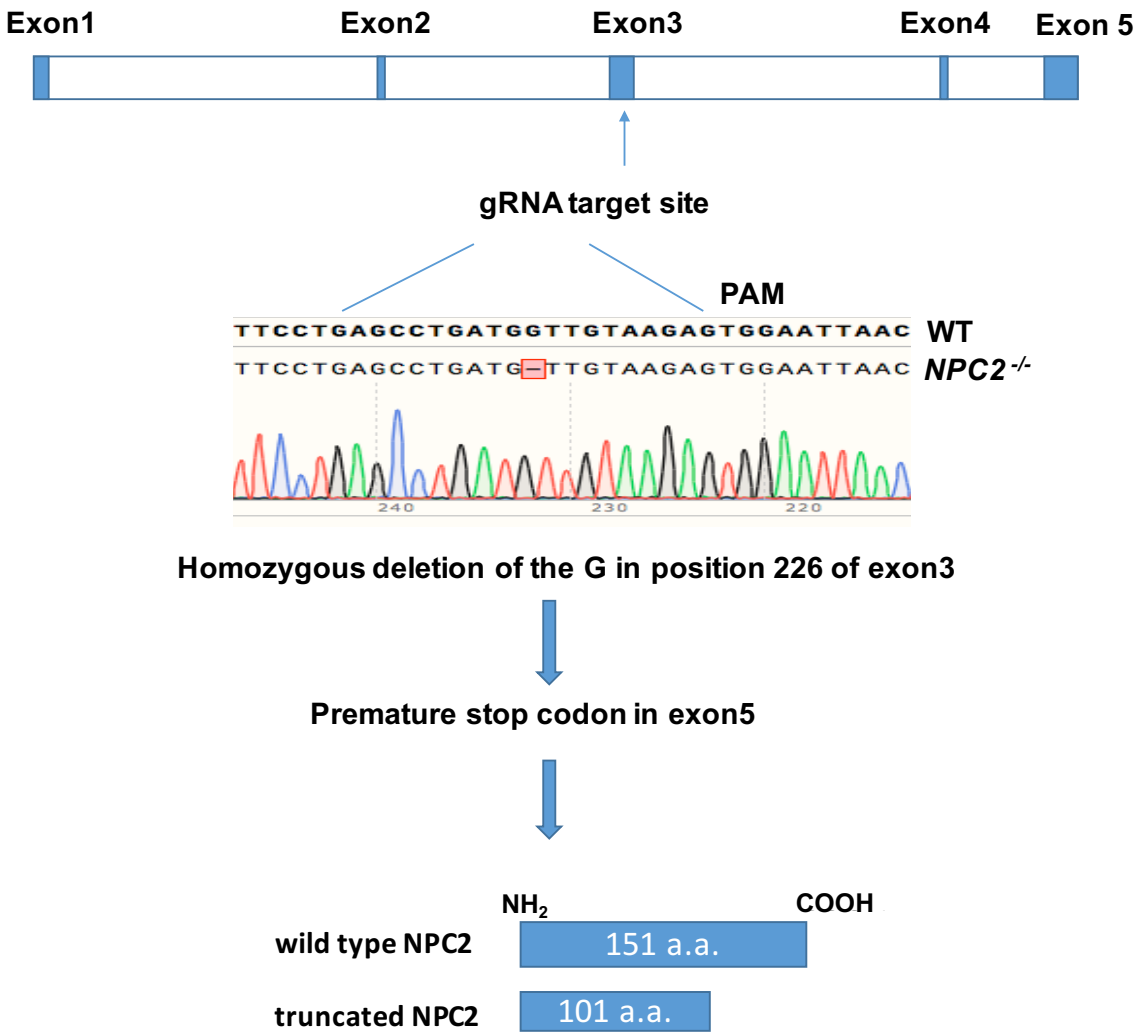

Fig. 3.3 Schematic representation of the CRISPR/Cas9 generation of *NPC2*$^{-/-}$ ARPE19. The electropherogram depicts the homozygous deletion of a guanosin (G) in position 226 of the *NPC2* exon3. Below, the length of wild type and truncated NPC2 proteins are illustrated.

In fact, crystallographic studies of NPC2 show that the amino acids that are missing in the truncated NPC2 protein are fundamental components of the NPC2 hydrophobic sterol binding pocket. The latter, is the key structural element for NPC2 transport of un-esterified cholesterol from the lumen of LE/LY to their limiting membrane (Xu, Stock et al. 2007) (Fig. 3.4)

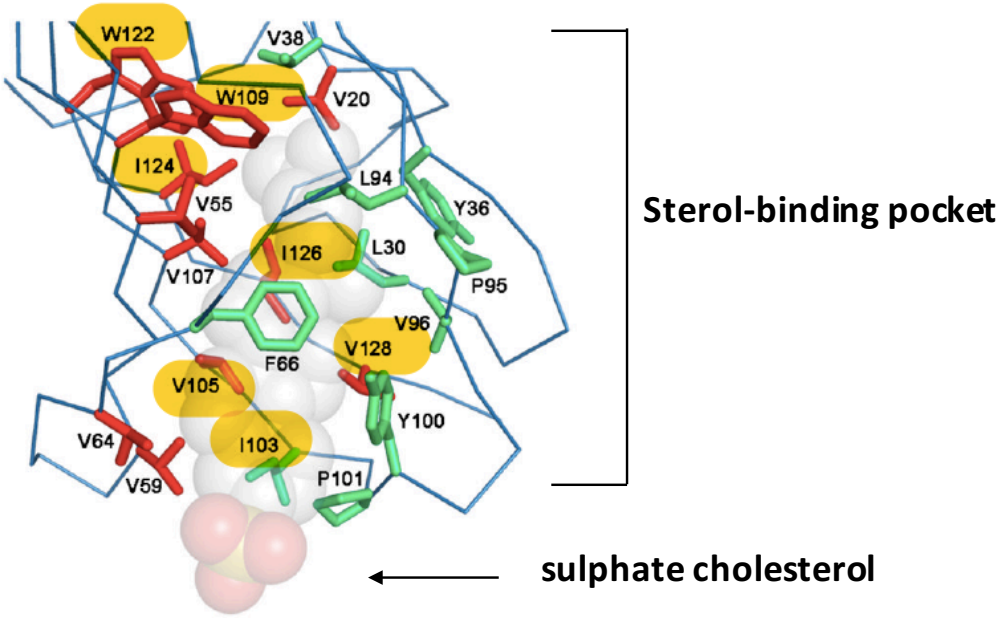

Fig. 3.4. Crystal structure of the sterol-binding tunnel of NPC2 bound to a molecule of sulphate-cholesterol, readapted from Xu, Stock et al. 2007. NPC2 transports cholesterol by binding it to a hydrophobic tunnel formed by the side chains of amino acids depicted in the figure. The positions of the amino acids that are predicted to be missing in the truncated NPC2 protein are highlighted in yellow.

Besides, western blotting against NPC2 shows that its expression was dramatically decreased, almost becoming completely abolished, in *NPC2*$^{-/-}$ with respect to WT. The faint bands of the WB image could be interpreted as the amount of truncated protein that has not been degraded by the ERAD (Endoplasmic Reticulum Associated Protein Degradation). In fact, of the 101 amino acids of the truncated NPC2, 70 amino acids are predicted to overlap with the epitope targeted by the antibody against NPC2.

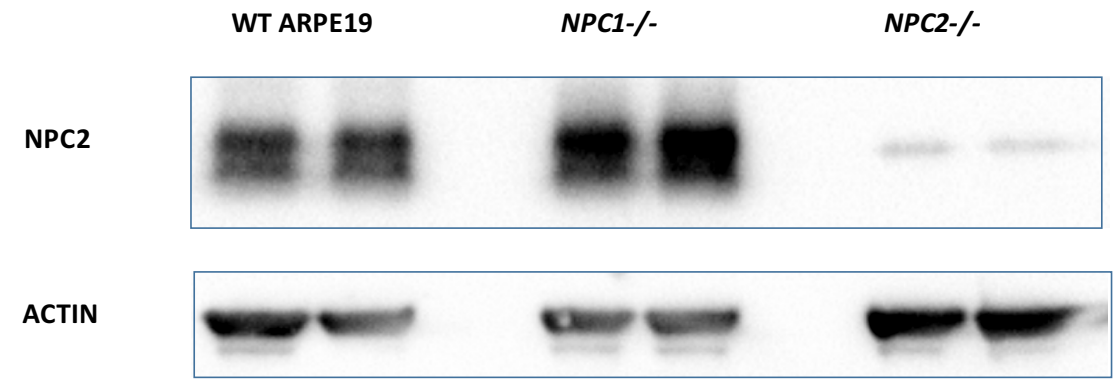

Fig. 3.5 Western blotting analysis with antibodies to NPC1, NPC2 and ACTIN.

4.0 Characterization of *NPC1*$^{-/-}$ and *NPC2*$^{-/-}$ ARPE19

After the generation of the knockout cells lines, I moved onto their characterization to evaluate whether *NPC1*$^{-/-}$ and *NPC2*$^{-/-}$ recapitulate the pathological cellular phenotypes of Niemann-Pick disease type-C that were described in previous studies (Vanier et al. 1983, Rodriguez-Lafrasse et al. 1994).

4.1 Un-esterified cholesterol accumulates within LE/LY of *NPC1*$^{-/-}$ and *NPC2*$^{-/-}$

Firstly, with fluorescence microscopy I assessed the levels of un-esterified cholesterol within the acidic compartments of *NPC1*$^{-/-}$ and *NPC2*$^{-/-}$. For this purpose, WT, *NPC1*$^{-/-}$ and *NPC2*$^{-/-}$ were co-stained with two fluorescent probes: the antibiotic filipin, to specifically target free-cholesterol, and an antibody to LAMP1, to monitor LE/LY (Fig 4.1). Images were acquired from single slides using a normal confocal microscope and from 96-well plates using the Opera high-content machine (Fig 4.1; 4.2). A quantitative analysis carried out on the high-content data showed that the amount of free-cholesterol stored in LE/LY of *NPC1*$^{-/-}$ and *NPC2*$^{-/-}$ was about three times that of WT cells (Fig 4.2). This difference was highly significant with $p < 0.0001$ for both WT vs *NPC1*$^{-/-}$ and WT vs *NPC2*$^{-/-}$ comparisons, assessed by Student's t- test. In collaboration with Medina's lab a script to process the high content data was devised. The script consists of normalizing the fluorescence intensity of filipin-overlapping-LAMP1 (hereafter referred to as filipin-LAMP1) to the fluorescent signal of LAMP1 alone. In this way we make sure that the filipin-LAMP1 fluorescence is independent of the number of cells analysed and is consistent among the cells of the same cell line. This methodological approach is based on the assumption that each cell of a specific cell line has, on average, the same number of LE/LY.

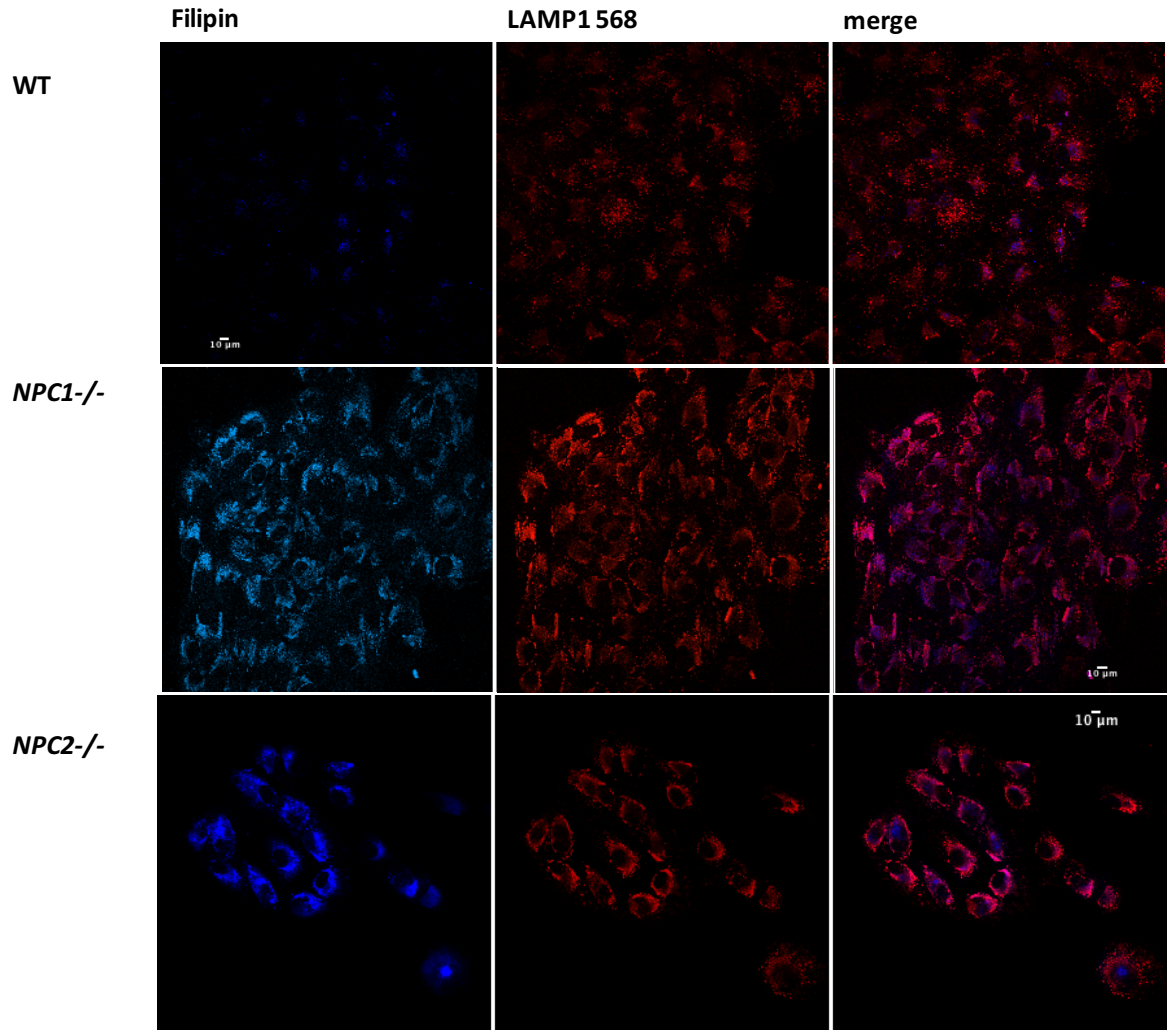

Fig. 4.1. Confocal microscopy images of LE/LY free-cholesterol in WT, *NPC1*$^{-/-}$ and *NPC2*$^{-/-}$. The three cell lines were labelled with Filipin to stain free-cholesterol and an antibody to LAMP1 (Alexa fluor-568 nm) to probe LE/LY (scale bar 10um). Representative images.

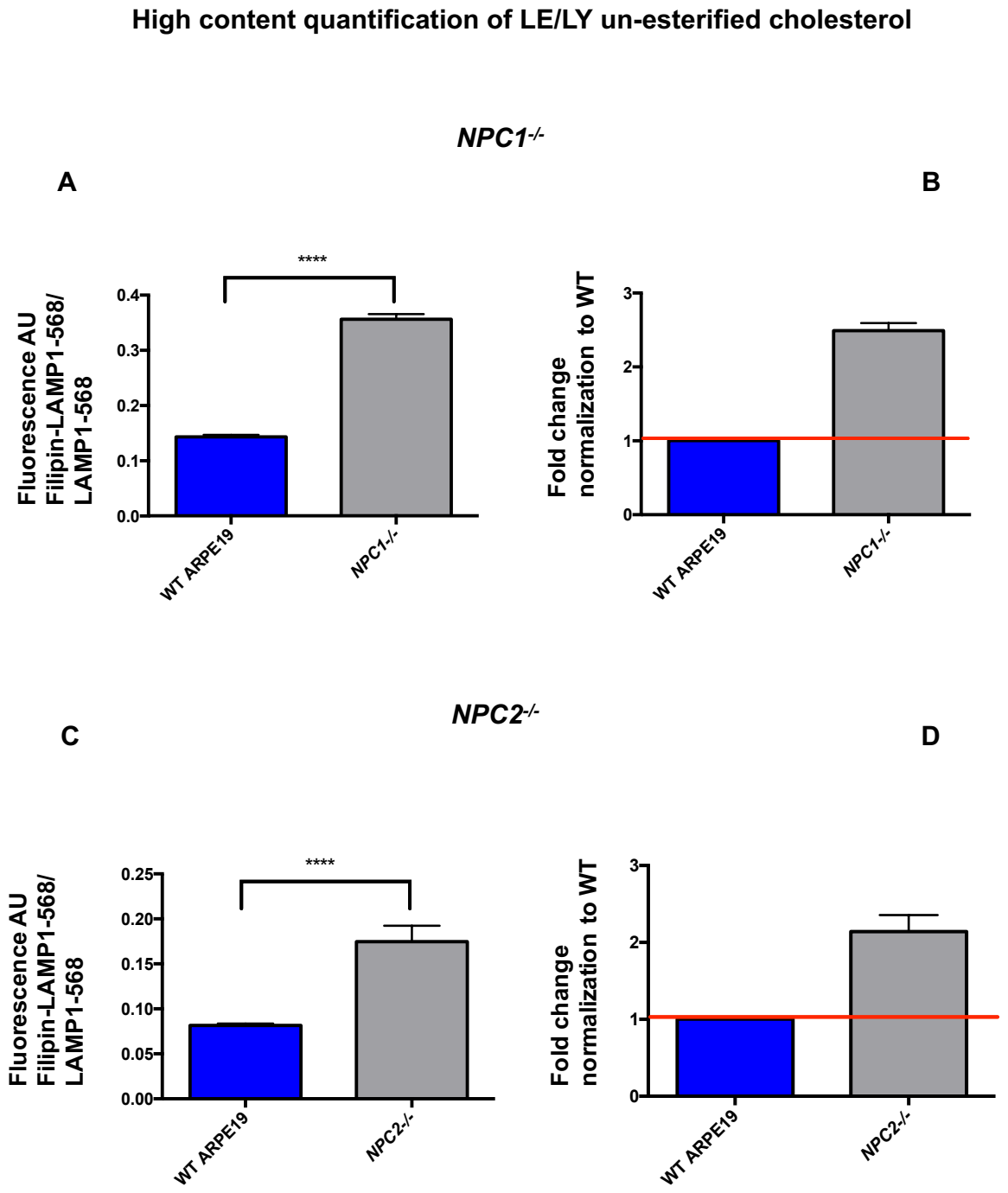

Fig. 4.2. High content quantification of LE/LY free-cholesterol in WT, *NPC1*$^{-/-}$ and *NPC2*$^{-/-}$. Cells were immunostained as reported in Fig. 4.1. Data on the Y axis are expressed as fluorescence of the co-staining filipin-LAMP1-568, normalized to the LAMP1-568 signal alone. AU= Arbitrary units. Error bars indicate standard deviation (SD). ** indicate *p* value < 0.0001 calculated with the Student's t test. Panels B and D report the fold change of filipin-LAMP1/LAMP1 data of panels A and C respectively, normalised to WT.**

4.2 Increased size and altered morphology of LE/LY of *NPC1*$^{-/-}$ and *NPC2*$^{-/-}$ cells

To further understand the impact that the dysfunction of either NPC1 or NPC2 proteins has on morphology and positioning of late endosomes/lysosomes, I performed a fluorescence immunostaining of LAMP1 only. As illustrated in Fig. 4.3, LE/LY of control-cells appear circular, well distinguishable from one another and scattered throughout the cytoplasm. In contrast, LE/LY of mutant cells appear swollen and clustered in the perinuclear region, forming a sort of ring around the nucleus (Fig. 4.3). Furthermore, a quantitative analysis of the LAMP1 expression detected by western blotting experiments showed that the levels of LAMP1 in *NPC1*$^{-/-}$ and *NPC2*$^{-/-}$ were significantly increased in comparison to that of WT with $p < 0.05$ for *NPC1*$^{-/-}$ and $p < 0.01$ for *NPC2*$^{-/-}$ (Fig. 4.4). Expanded LE/LY volume and increased expression of LAMP1 were more pronounced in *NPC2*$^{-/-}$ than in *NPC1*$^{-/-}$ cells.

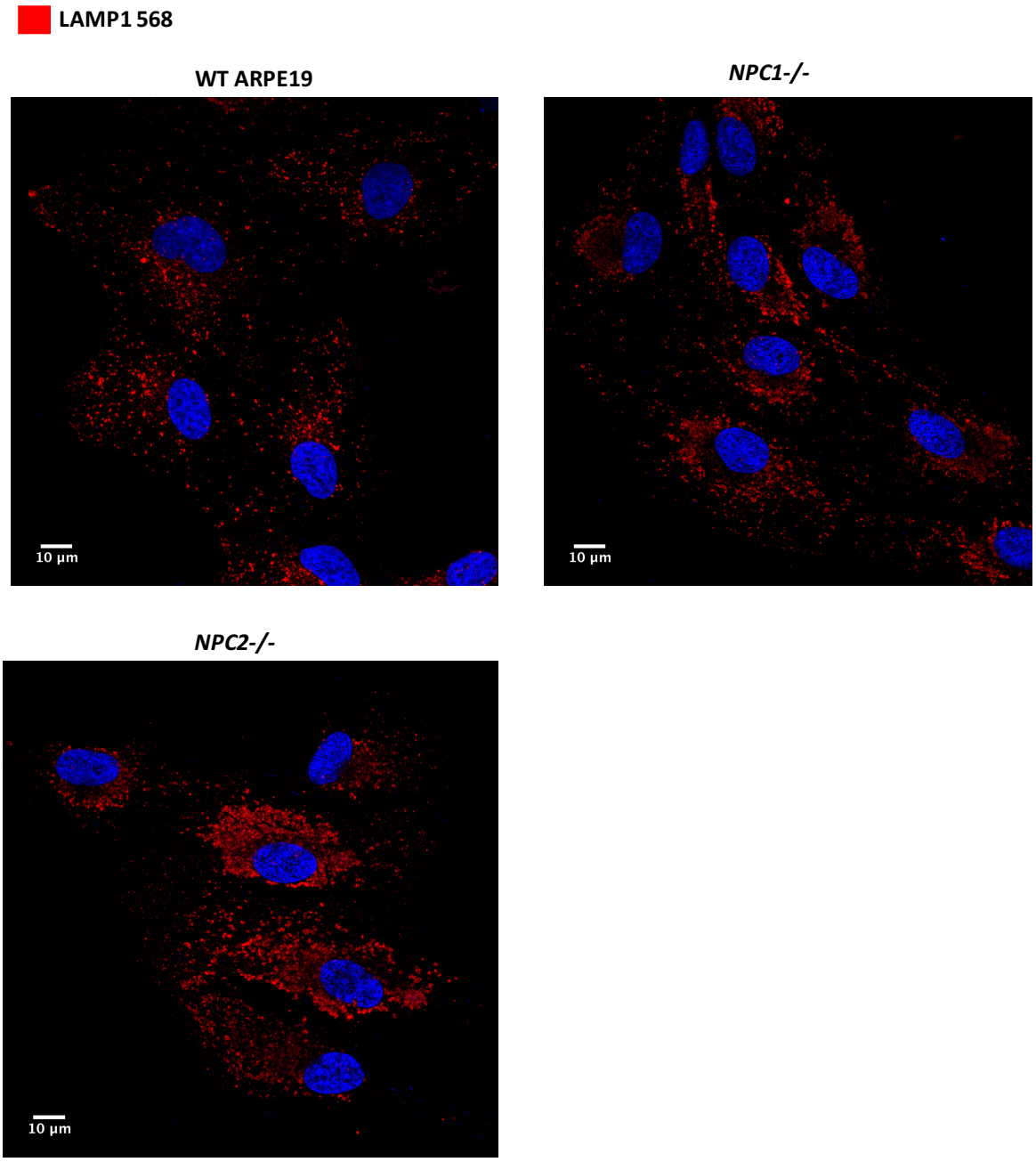

Fig. 4.3. Confocal microscopy images of LE/LY morphology and distribution in WT, *NPC1*$^{-/-}$ and *NPC2*$^{-/-}$. Cells were immunostained with LAMP1 (Alexa Fluor-568) whereas nuclei were stained with DAPI. Representative images (scale bar 10um).

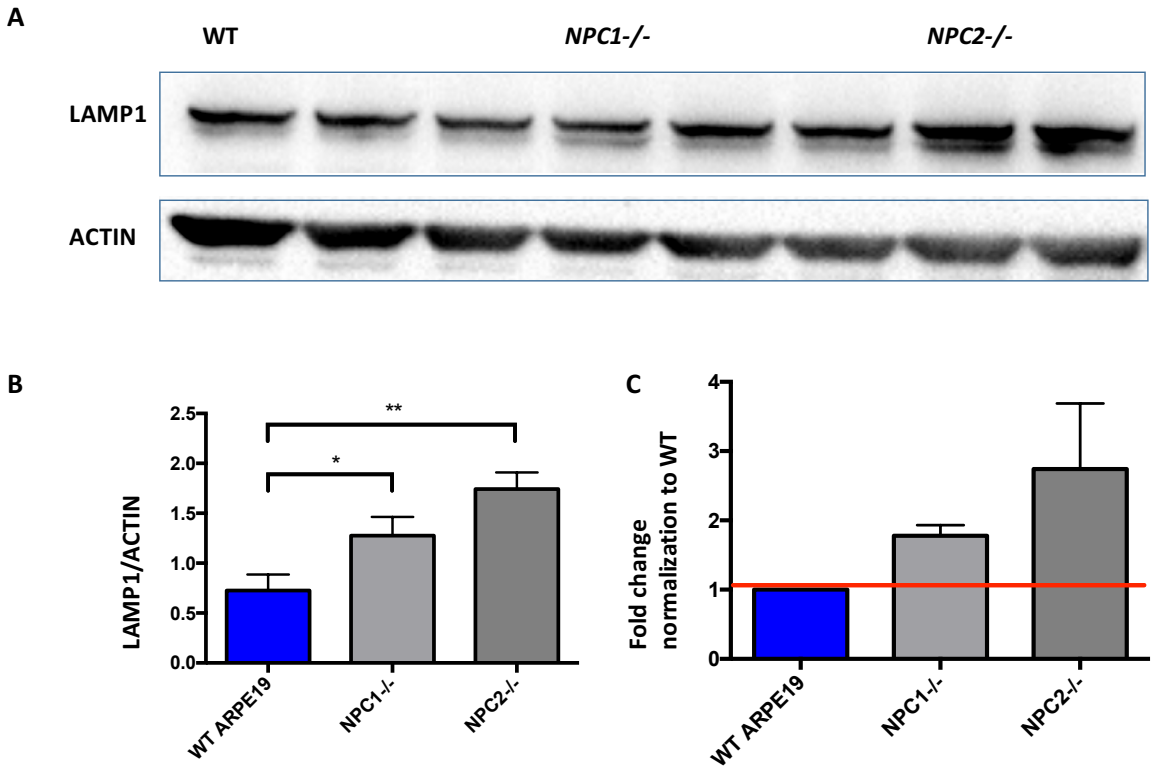

Fig. 4.4 Western blot analysis of LAMP1 expression in WT, *NPC1*$^{-/-}$ and *NPC2*$^{-/-}$. Total cell lysates were immunoblotted with antibodies to LAMP1 and to ACTIN. The intensities of the bands shown in panel A were quantified as LAMP1/ACTIN signals and are reported in panel B. Error bars indicate standard deviation (SD). * and ** indicate $p < 0.05$ and $p < 0.01$ respectively, calculated with the Dunett's multiple comparisons test. Each sample was compared to WT. Panel C depicts the fold change of panel B data normalised to WT. Representative experiment.

The enlargement of LE/LY in *NPC1*$^{-/-}$ and *NPC2*$^{-/-}$ was also demonstrated by LysoTracker FACS experiments in which mutant cells showed a three to four-fold rise of LysoTracker fluorescence with respect to control (Fig. 4.5). This difference between WT and knockout cells was statistically significant for both *NPC1*$^{-/-}$ ($p < 0.001$) and *NPC2*$^{-/-}$ ($p < 0.01$).

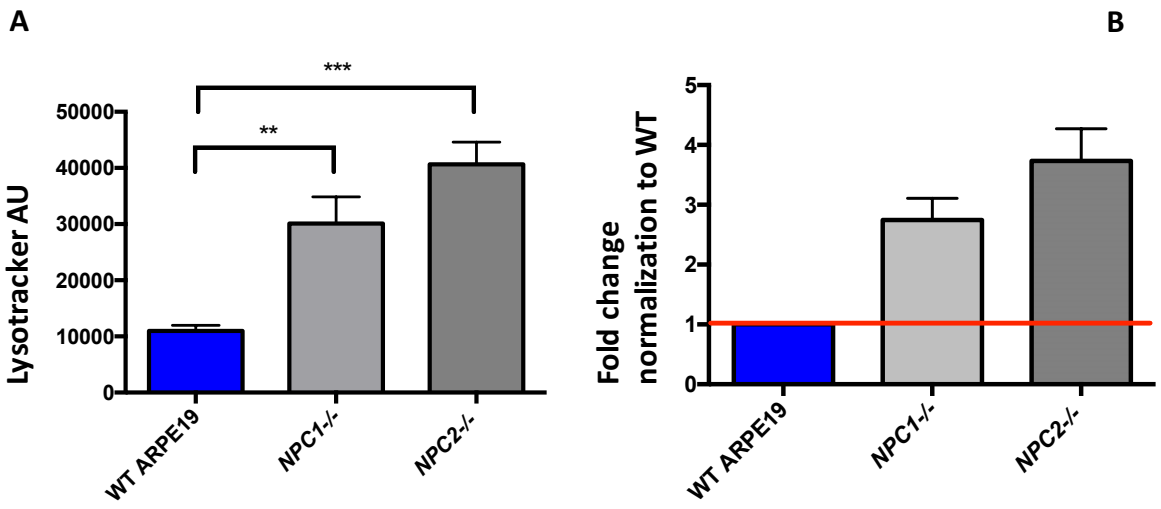

Fig. 4.5. Volume of the acidic organelles in *NPC1*$^{-/-}$ and *NPC2*$^{-/-}$ increased relative to WT. Panels A depicts LysoTracker-green fluorescence in WT, *NPC1*$^{-/-}$ and *NPC2*$^{-/-}$ detected by flow cytometry (10000 LysoTracker positive events). AU= Arbitrary units. Panel B reports the fold change of panel A data normalised to WT. Error bars = SD. ***p value < 0.001 **p < 0.01 calculated with the Dunett's multiple comparisons test in which each sample was compared to WT. Representative experiment.

Electron microscopy examination of the endolysosomal compartments of WT, *NPC1*$^{-/-}$ and *NPC2*$^{-/-}$ confirmed what has been reported so far. The electron micrograph of *NPC1*$^{-/-}$ and *NPC2*$^{-/-}$ cells shows late endosomes/lysosomes that are swollen and full of undigested material, with the latter depicted as a dark area within LE/LY that tends to be geometrically organized in multilamellar concentric circles. In addition, among the late endosomal/ lysosomal population, several acidic organelles of *NPC1*$^{-/-}$ and *NPC2*$^{-/-}$ appear to have lost their physiological outline with their limiting membranes fused with with each other in the formation of vacuoles (Fig 4.6). By contrast, LE/LY of WT cells look healthy, with well-shaped organellar membranes and bright inner compartments. Even multivesicular bodies (MVBs) and their intraluminal vesicles can be identified in the electron micrograph of the WT cell line (Fig 4.6). The EM experiment was performed by the Microscopy Core at Tigem.

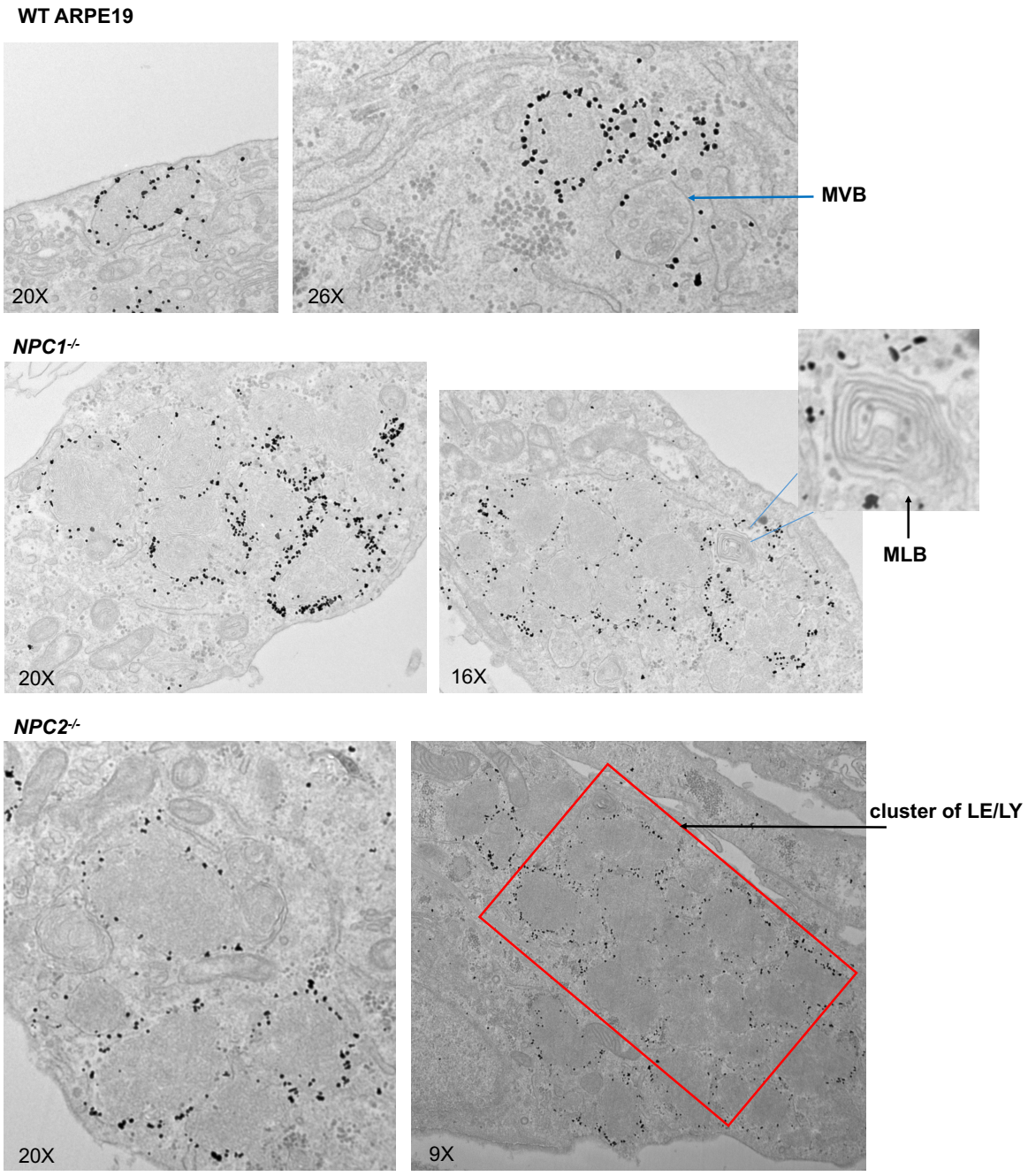

Fig. 4.6. Electron micrograph of WT ARPE19, *NPC1*$^{-/-}$ and *NPC2*$^{-/-}$ immunolabelled with LAMP1 (black dots). Images illustrate the interior of LE/LY at different magnifications. A multivesicular body (MVB), a multilamellar body (MLB) and clustered LE/LY are indicated by arrows.

4.3 No variations in the autophagic pathway of *NPC1*$^{-/-}$ and *NPC2*$^{-/-}$

Since IF, LysoTracker and EM experiments had shown a pathological late endosomal/ lysosomal phenotype in *NPC1*$^{-/-}$ and *NPC2*$^{-/-}$, I decided to investigate whether the autophagic pathway of *NPC1*$^{-/-}$ and *NPC2*$^{-/-}$ had also been altered. To this end, I probed the autophagic marker LC3 by western blot to visualize LC3 I and its lipidated form LC3 II, in WT and knockout cells. As reported in Fig. 4.7, a quantitative analysis of the western blot experiments with an antibody to LC3 revealed that there was no significant difference in the basal levels of LC3 II among WT, *NPC1*$^{-/-}$ and *NPC2*$^{-/-}$.

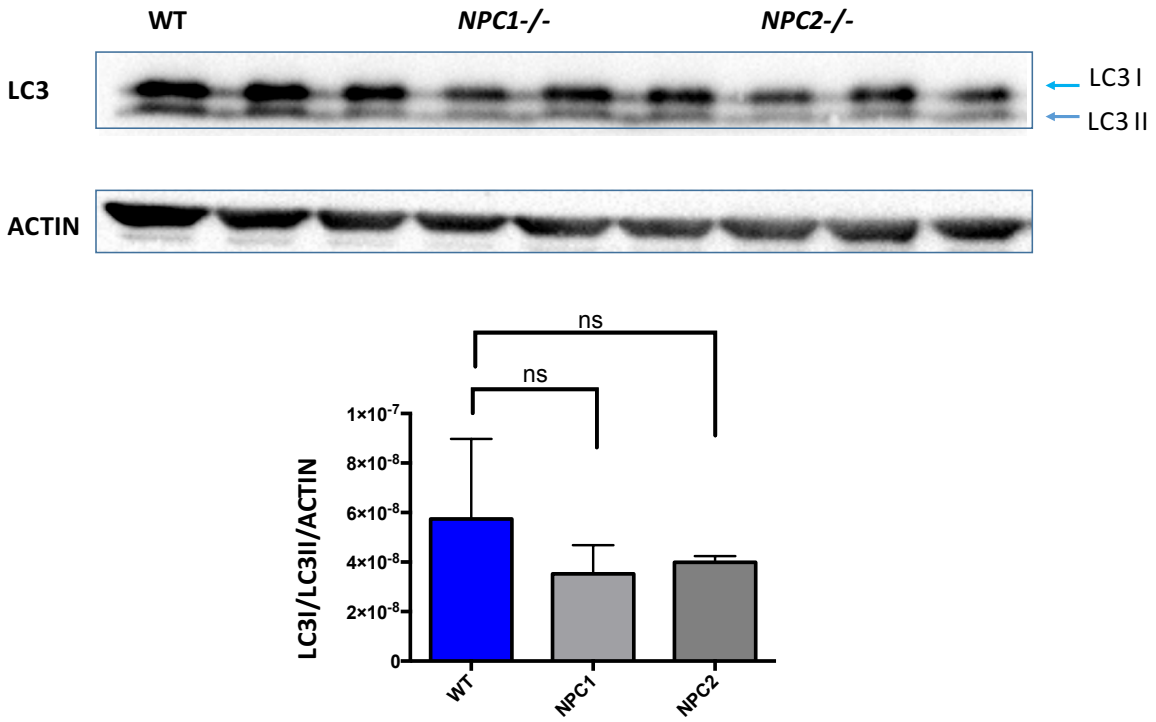

Fig. 4.7 Western blot analysis of LC3 I and LC3 II expression in WT, *NPC1*$^{-/-}$ and *NPC2*$^{-/-}$. Total cell lysates were immunoblotted with antibodies to LC3 II and to ACTIN. The intensities of the bands are reported in the histogram as LC3 I/LC3 II/ACTIN. Error bars indicate standard deviation (SD), ns= non statistically significant. Representative experiment.

4.4 Sphingosine and sphinganine accumulate within *NPC1*$^{-/-}$ and *NPC2*$^{-/-}$

I continued the characterization of *NPC1*$^{-/-}$ and *NPC2*$^{-/-}$ evaluating whether sphingolipids accumulate in these cell lines. For this purpose, the levels of the sphingolipid precursors sphingosine and sphinganine within WT, *NPC1*$^{-/-}$ and *NPC2*$^{-/-}$ were measured through a three-stage method. Sphingoid bases were extracted through SPE (solid-phase-extraction), derivatized with OPA and analysed by HPLC. Finally, OPA-linked substrates were quantified by detection of their fluorescence intensity at a given retention time. Concentrations of sphingosine and sphinganine in *NPC1*$^{-/-}$ *and NPC2*$^{-/-}$ were found to be significantly elevated with respect to WT ($p < 0.0001$ for *NPC1*$^{-/-}$ and $p < 0.001$ for *NPC2*$^{-/-}$). In particular, a three to four-fold rise in sphingosine and sphinganine concentrations in *NPC1*$^{-/-}$ *and NPC2*$^{-/-}$ compared to WT, was determined (Fig. 4.8). Furthermore, both sphinganine and sphingosine displayed the same trend in the two knockout cell lines.

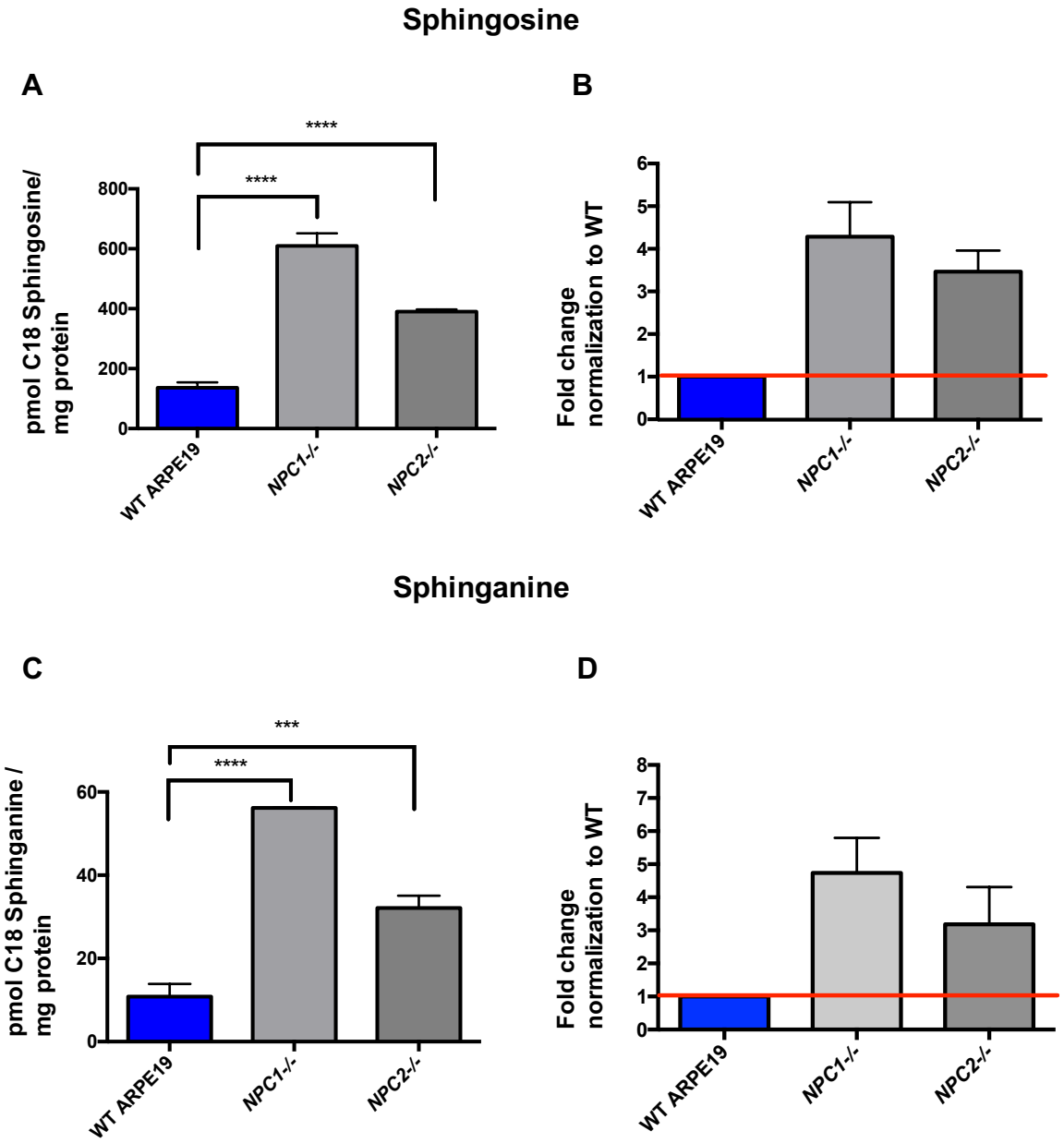

Fig. 4.8. HPLC measurement of sphingosine and sphinganine concentrations in WT, *NPC1-/-* and *NPC2*$^{-/-}$. Error bars= SD. * indicate $p < 0.001$; **** $p < 0.0001$ calculated with the Dunett's multiple comparisons test in which each sample was compared to WT. Concentration is expressed as pmol C18 sphingosine (panel A) or C18 sphinganine (panel B) / mg of protein. Histograms of panels B and D display the fold change of the data of panels A and C respectively, normalised to WT.**

4.5 Glycosphingolipids

As part of the assessment of the class of sphingolipids, the pattern of the complex glycosphingolipids including lactosylceramide, GM3, Gb3, Gb4 and glucosylceramide in control and NPC cells, was analysed. GSLs' carbohydrate headgroups were hydrolized from ceramide, derivatized with the fluorescent compound anthranilic acid (2AA), separated with HPLC on the basis of their retention time and detected by fluorescence.

Unlike what observed for the other parameters studied so far, all showing a very similar trends in *NPC1*$^{-/-}$ and *NPC2*$^{-/-}$, the pattern of glycosphingolipids in *NPC1*$^{-/-}$ and *NPC2*$^{-/-}$ varied on the basis of the specific glycosphingolipid. In fact, in comparison to WT, lactosylcermide concentration in *NPC1*$^{-/-}$ was significantly increased ($p < 0.0001$) while it decreased in *NPC2*$^{-/-}$ ($p < 0.001$). On the contrary, GM3 and Gb4 levels were both more elevated in *NPC2*$^{-/-}$ ($p < 0.01$ for GM3 and $p < 0.001$ for Gb3) than in WT and *NPC1*$^{-/-}$ while between the latter two cell lines no differences in GM3 and Gb4 concentrations were found. Values for Gb3 and glucosylceramide did not show any significant change among WT, *NPC1*$^{-/-}$ and *NPC2*$^{-/-}$. (Fig. 4.9).

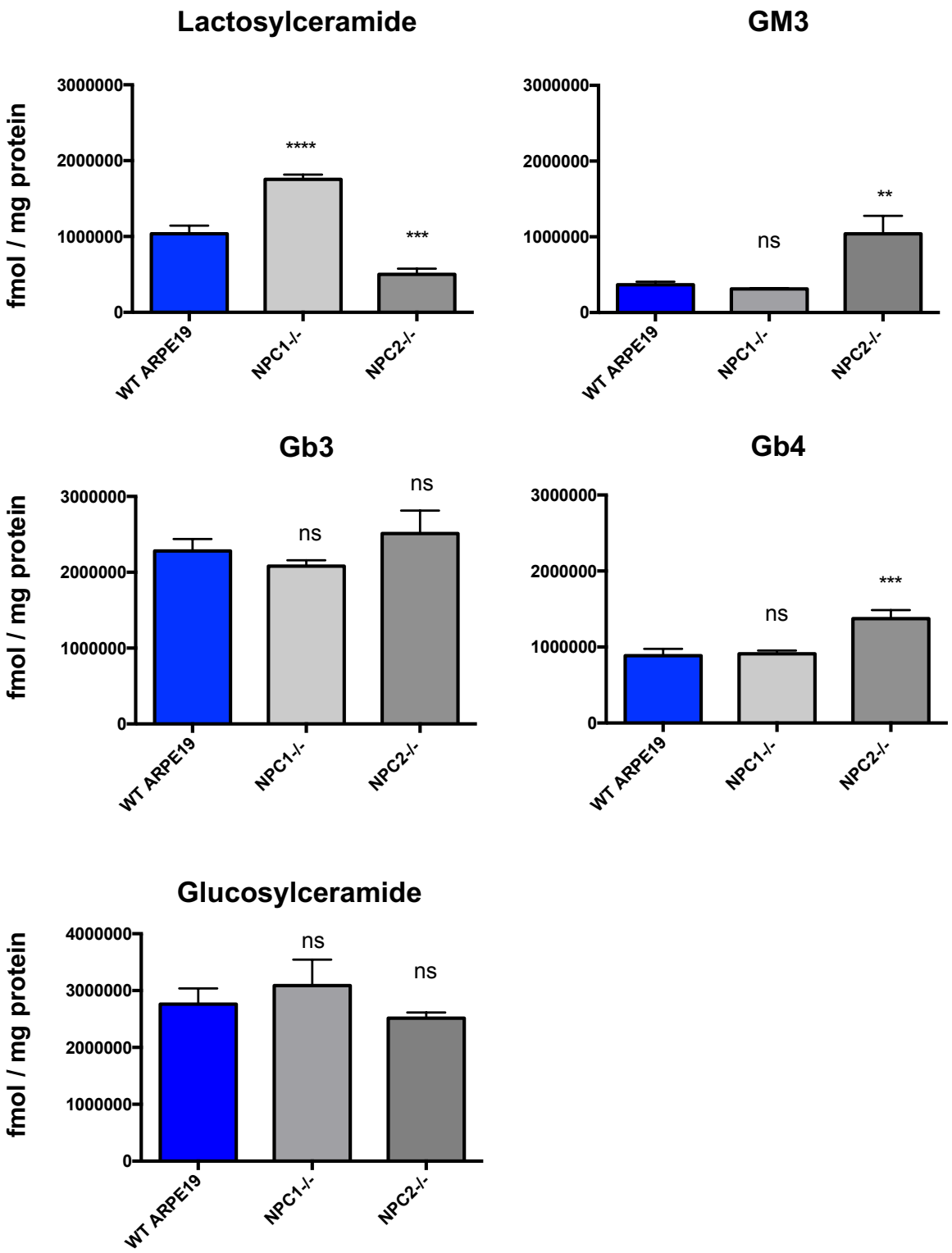

Fig. 4.9. HPLC measurement of the concentrations of the GSLs lactosylceramide, GM3, Gb3, Gb4 and glucosylceramide in WT, *NPC1*$^{-/-}$ and *NPC2*$^{-/-}$. Error bars = SD. ns= non significant, **$p < 0.01$ ***$p < 0.001$ ****$p < 0.001$ calculated with the Dunett's multiple comparisons test in which each sample was compared to WT. Concentration of the GSLs is expressed as fmol/mg protein.

4.6 No permeabilization of Lysosomal membranes

The Galactin-3 assay developed by Jaattela's lab was carried out on *NPC1*$^{-/-}$ and *NPC2*$^{-/-}$ to investigate whether their late endosomal/lysosomal population presented any damage at the late endosomal/lysosomal membrane (Aits et al. 2015). Firstly, WT, *NPC1*$^{-/-}$ and *NPC2*$^{-/-}$ were treated with LLOMe (L-leucyl-L-leucine methyl ester) 1mM for 1.5h to generate an experimental control consisting of cells with damaged late endosomes/ lysosomes. Then, both untreated and LLOMe treated cells were fixed, stained with an antibody to Galectin3 and analysed by confocal microscopy. As shown in Fig 4.10, LLOMe damaged cells present large round puncta of Galectin3 which are indicative of lysosomal membrane permeabilization. In contrast, the untreated cells showed tiny dots of Galectin-3 that are spread throughout the cytoplasm (Fig. 4.10). None of the untreated cells resembled the respective LLOMe control and therefore I could conclude that despite their morphological alteration, there is no membrane damage in the LE/LY of *NPC1*$^{-/-}$ and *NPC2*$^{-/-}$.

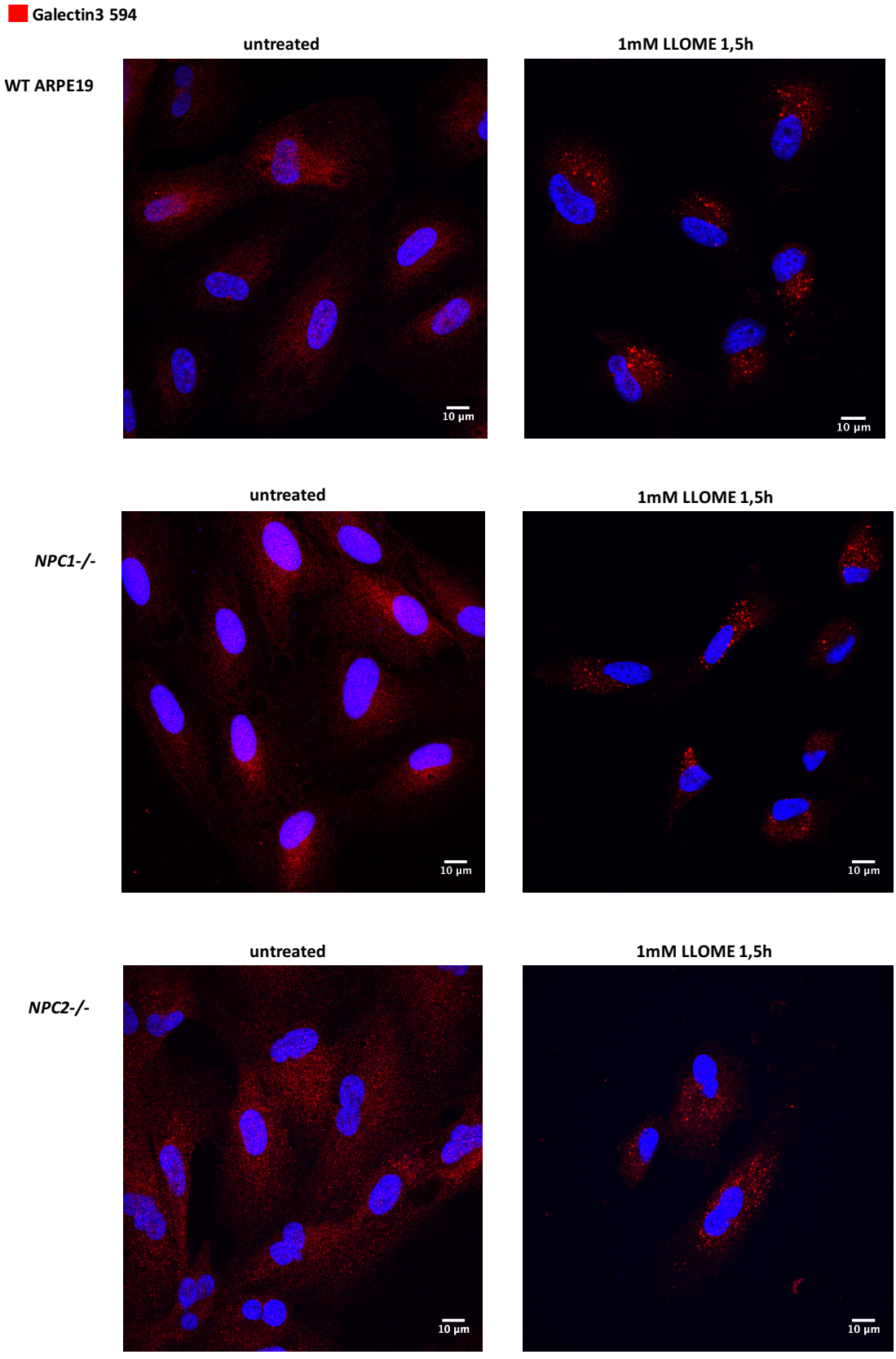

Fig. 4.10. Galectin-3 assay. The confocal microscopy images depict untreated and LLOMe treated WT, *NPC1*$^{-/-}$ and *NPC2*$^{-/-}$. Cells were immunostained with an antibody against Galectin-3 that was conjugated to Alexa Fluor-594. Nuclei were stained with DAPI. Scale bar =10um. Representative experiment.

4.7 No off-targets in *NPC1*$^{-/-}$

A possible drawback in the use of the CRISPR/Cas9 system is the generation of off-target effects. These are unwanted mutations that may occur when the 20 bp gRNA binds to the wrong DNA sequences, in different genes, because of their similarity with the desired target site (Kuscu et al 2014). Hence, to exclude the possibility that the NPC phenotype described so far in *NPC1*$^{-/-}$ and *NPC2*$^{-/-}$ was due to off-target effects, I reconstituted, by heterologous expression, the missing proteins NPC1 in *NPC1*$^{-/-}$. By doing so, some of the pathological features previously detected in *NPC1*$^{-/-}$ were almost completely rescued.

Reconstitution of NPC1 was achieved by transduction of the knockout cells with lentiviral vectors encoding NPC1. The actual expression of this heterologous NPC1 was then verified by immunofluorescence. Confocal microscopy images of Fig. 4.11 show that the rNPC1 protein is expressed in transduced *NPC1*$^{-/-}$ (*rNPC1-NPC1*$^{-/-}$) and it is also correctly delivered to late endosomes/ lysosomes (NPC1-LAMP1 co-localization). Rescue of the NPC phenotype in rNPC1-*NPC1*$^{-/-}$ was demonstrated by reduction in the intracellular concentrations of sphingosine (here reported as fold change with respect to WT) and total cholesterol ($p < 0.0001$) as well as by a decreased LysoTracker fluorescence ($p < 0.0001$) measured in rNPC1-*NPC1*$^{-/-}$ with respect to *NPC1*$^{-/-}$. Besides, for all these experiments, the parameters considered above displayed similar values in rNPC1-*NPC1*$^{-/-}$ and WT cells (Fig. 4.12). However, there was not a full recovery of the NPC phenotype in rNPC1-*NPC1*$^{-/-}$ cells. This outcome may be explained by the heterogeneity of the rNPC1-*NPC1*$^{-/-}$ population which was composed of *NPC1*$^{-/-}$ cells that had integrated the lentiviral vector encoding rNPC1 and of *NPC1*$^{-/-}$ cells that had not been transduced. As for the *NPC2*$^{-/-}$, the reconstitution of the NPC2 recombinant protein to exclude the presence of relevant off-targets will be performed in the near future.

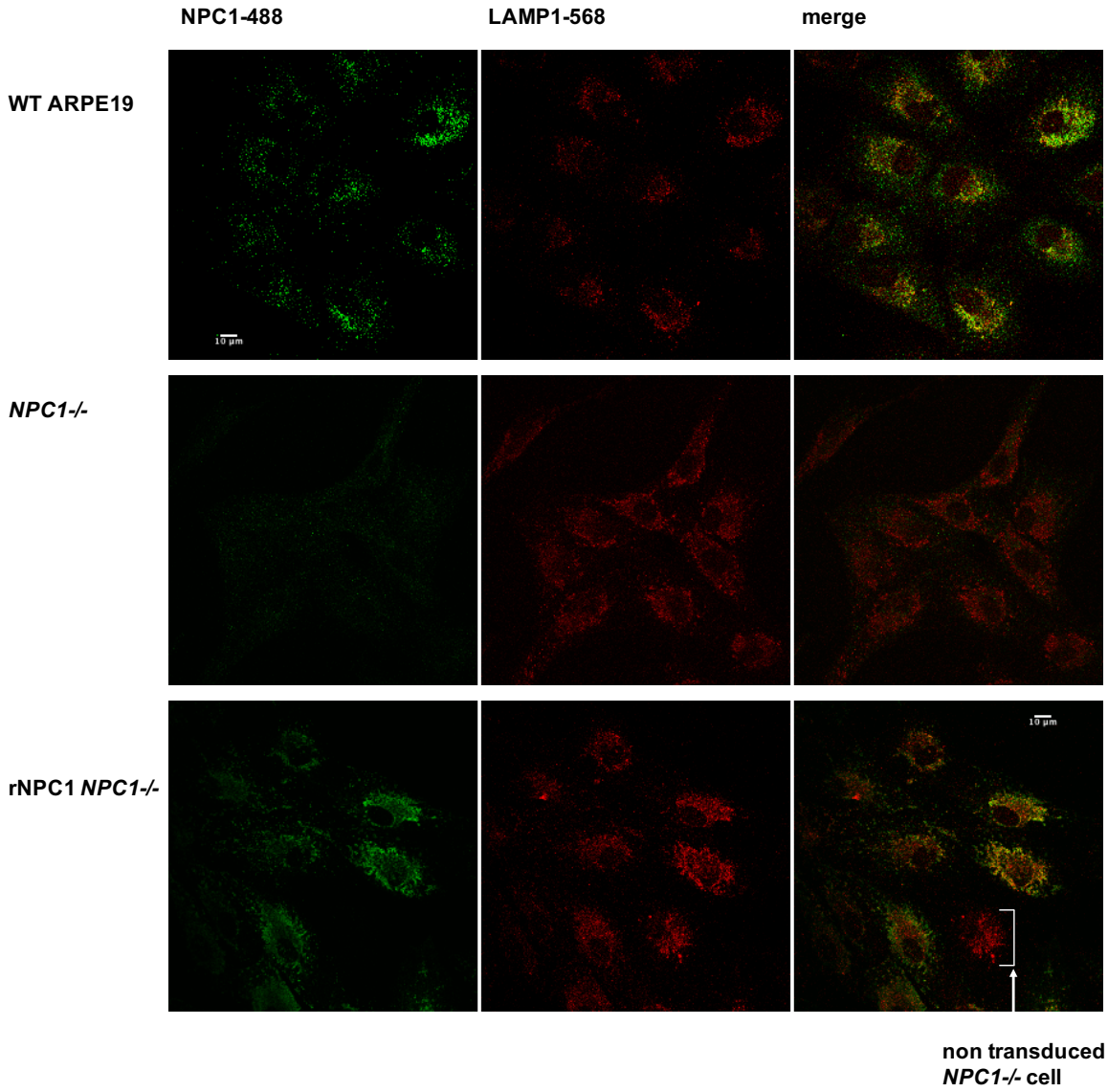

Fig. 4.11. Confocal images of the LE/LY localization of NPC1 in WT and *NPC1*$^{-/-}$ and of rNPC1-*NPC1*$^{-/-}$. The three cell lines were labelled with antibodies to NPC1 (Alexa fluor 488) and to LAMP1 (Alexa fluor 568). rNPC1= recombinant protein NPC1. The presence of non-transduced cells within the rNPC1-*NPC1*$^{-/-}$ population is indicative of the heterogeneity of the rNPC1-*NPC1*$^{-/-}$ cell line. Representative experiment.

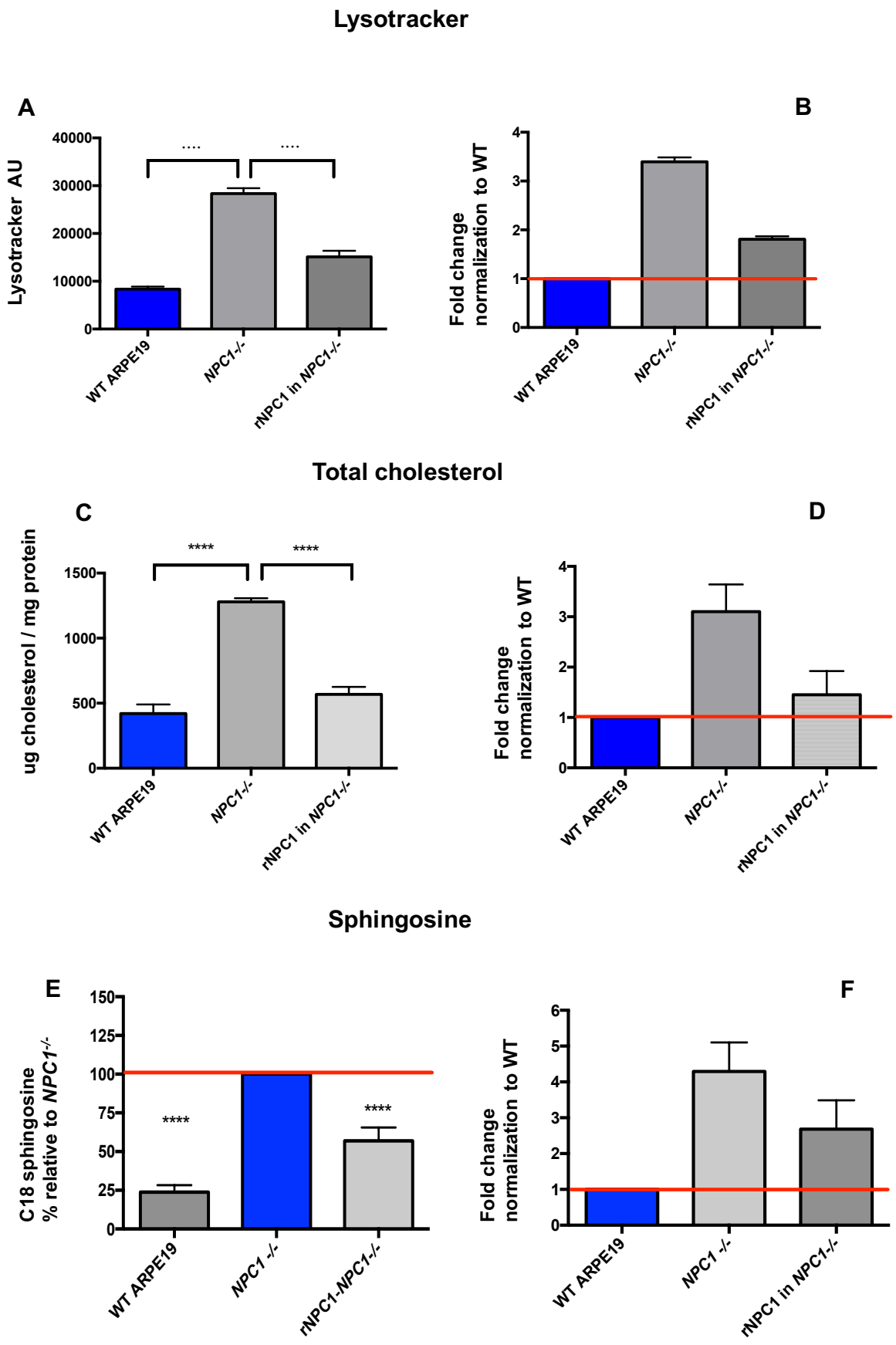

Fig. 4.12. Correction of the NPC phenotype.

Histograms of LysoTracker, total cholesterol and sphingosine assays in WT, *NPC1*$^{-/-}$ and rNPC1 in *NPC1*$^{-/-}$ show that the reconstituted NPC1 protein is functional and able to rescue the pathological

phenotype of *NPC1*$^{-/-}$. Panel A and C depict the LysoTracker fluorescence detected by flow cytometry and the total cholesterol concentration (ug cholesterol/ mg protein), respectively. AU= Arbitrary units. Error bars indicate SD. ****$p < 0.001$ was calculated with the Dunett's multiple comparisons test in which each sample was compared to *NPC1*$^{-/-}$. Panels B and D display the fold change of the data of A and C normalized to WT. Panel E illustrates the levels of sphingosine in WT, *NPC1*$^{-/-}$ and rNPC1-*NPC1*$^{-/-}$ expressed as % relative to the concentration (pmol C18 Sphingosine/mg protein) of untreated *NPC1*$^{-/-}$. Panel F displays the fold change of the data of panel E normalised to WT. Representative experiments.

5.0 High Content FDA-approved drug screening on *NPC2*$^{-/-}$ ARPE19 cell line

For the purpose of identifying one or more small molecules able to revert the pathological phenotype of NPC affected cells, I performed a High Content screen of the Prestwick library on the *NPC2*$^{-/-}$ cell line. In a second stage of the study I used the active compounds (or hits) obtained from the screening to carry out secondary assays on both *NPC1*$^{-/-}$ and *NPC2*$^{-/-}$ cell lines, so as to examine their effects on several hallmarks of the NPC disease. The workflow of the High-Content drug screening is illustrated in Fig. 5.1.

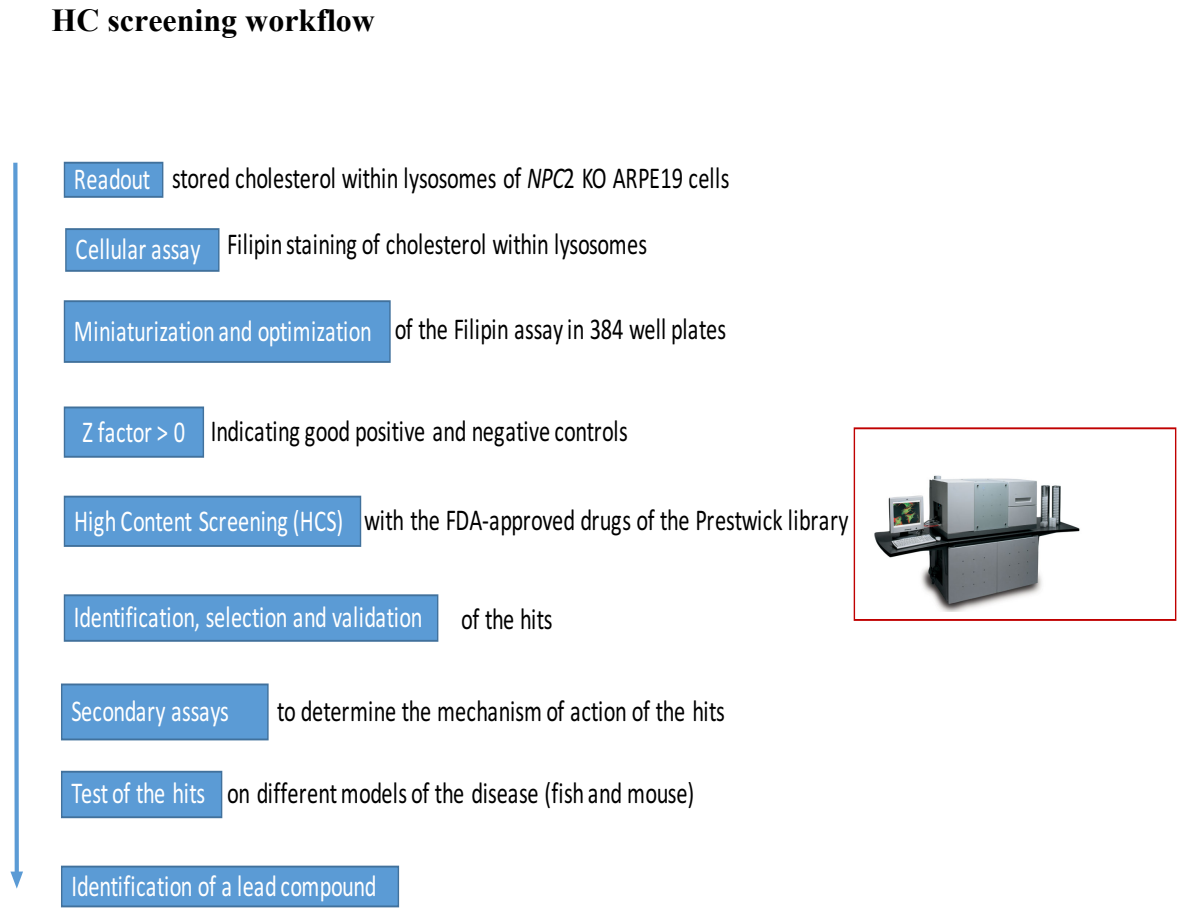

Fig. 5.1. Workflow of the Prestwick library drug screening.

5.1 Development of a HC microscopy assay: filipin-LAMP1-568 co-staining of LE/LY free-cholesterol

Since *NPC1*$^{-/-}$ and *NPC2*$^{-/-}$ cells have been demonstrated to accumulate un-esterified cholesterol within their LE/LY (Chapter 4.1), I decided to set this cellular feature as the readout of the high-content drug screening. To this end, in collaboration with Medina's lab I developed a cell-based microscopy assay to probe the un-esterified cholesterol accumulated within LE/LY of *NPC1*$^{-/-}$ and *NPC2*$^{-/-}$. In particular, this assay was used to monitor the effect of the FDA-approved drugs on the stored LE/LY free-cholesterol.

Hence, un-esterified cholesterol was labelled with the fluorescent probe Filipin, while LE/LY were stained with an antibody to LAMP1 excited at a wavelength of 568 nm (Fig. 5.2). Since filipin-LAMP1-568 co-staining allows a very good visualization of the free-cholesterol contained within LE/LY of *NPC1*$^{-/-}$ and *NPC2*$^{-/-}$ using both normal and high content confocal microscopes, filipin-LAMP1-568 co-staining was adopted as the microscopy assay to perform the Prestwick drug screening.

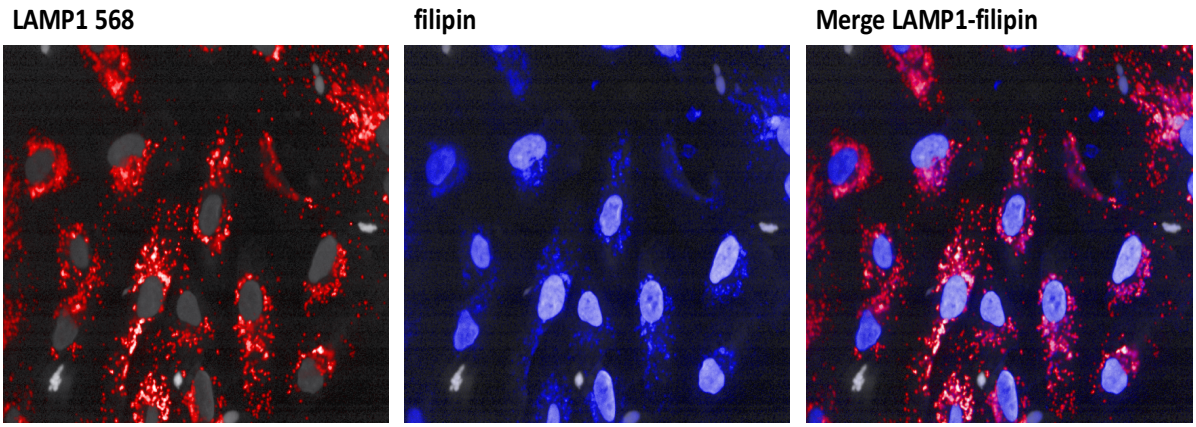

Fig. 5.2. Representative image of *NPC2*$^{-/-}$ cells stained with filipin and an antibody to LAMP1. Images were acquired with the Opera High Content device.

5.2 Miniaturization of the Filipin-LAMP1-568 assay in 384 well plates

Due to the High content nature of the experiment, the screening was carried out in 384 well plates. Therefore, as first step we set up a miniaturization of the cell based (Filipin-LAMP1-568) microscopy assay in 384-well black plates.

To optimize cell density per well, *NPC1*$^{-/-}$ and *NPC2*$^{-/-}$ cells were plated separately and at different seeding numbers in 384 well plates. Seeding was carried out with 500, 1000, 1500, 2000, 2500 and 3000 cells per well, cultured at 37°C for 72h and then fixed with PFA 4% (Fig. 5.3). Nuclei were then stained with Draq5 to count the number of cells per well so as to assess cell viability and cell confluence within the wells. I could find that 2500 cells/well is the appropriate plating density which allows the seeded cells to achieve the optimal confluence after 72h in culture. Overall, the outcome of the miniaturization stage led us to opt for employing *NPC2*$^{-/-}$ rather than *NPC1*$^{-/-}$ cells to perform the High Content drug screening because this cell line showed a better resistance to pipetting operations. The miniaturization of the microscopy assay of the screening did not require any modification of the staining procedure (un-esterified cholesterol, filipin and LE/Lys, LAMP1) previously used in the normal confocal microscope analysis (Chapter 4.1).

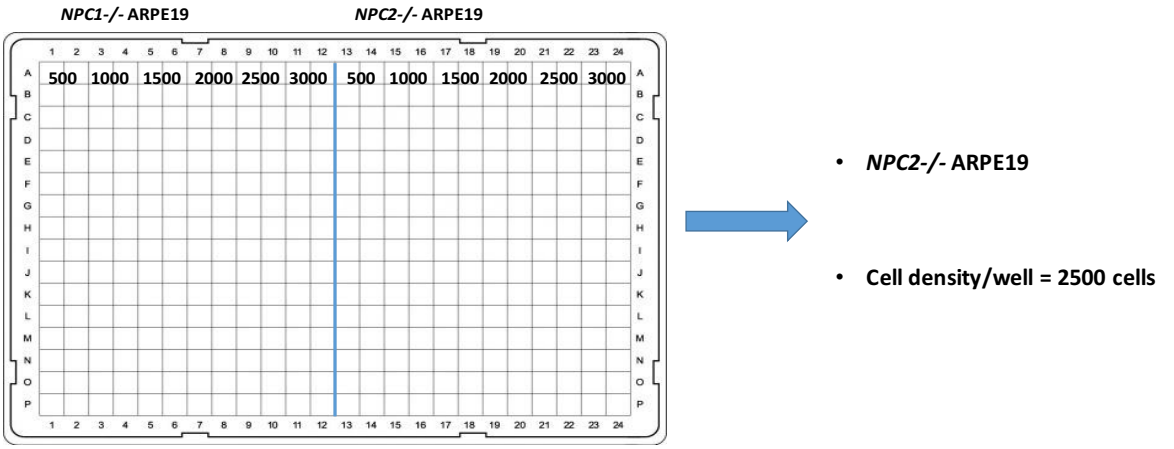

Fig. 5.3. Miniaturization of the Filipin-LAMP1-568 microscopy assay into 384-well black plates. ***NPC2*$^{-/-}$ cells resulted more suitable than *NPC1-/-* to perform experiments in 384-well black plates over a time of 72h.**

5.3 Quality validation of the filipin-LAMP1-568 microscopy assay

Since the identification of the hits occurs among thousands of compounds, the assay of an HC screening has to be sensitive, reproducible and accurate (Zhang et al. 1999).

Therefore, before carrying out the actual screening of the library, we had to validate the quality and robustness of the chosen microscopy assay by calculating the Z' index for the filipin-LAMP1-568 assay. The Z' index is a dimensionless statistical parameter commonly used to determine whether the difference in the signal of an HT (or HC) assay between positive and negative controls, is statistically significant (Zhan et al. 1999) (Fig. 5.4).

$$Z' = 1 - \frac{(3\sigma_{c+} + 3\sigma_{c-})}{|\mu_{c+} - \mu_{c-}|}$$

Fig. 5.4. Equation of the Z' index. μ_{c+} = mean of the assay signal of the positive control (C+)
μ_{c-} = mean of the assay signal of the negative control (C-)
σ_{c+}= standard deviation of the (C+) from the μ_{c+} σ_{c-}= standard deviation of the (C-) from the μ_{c-}

To this end, the filipin-LAMP1-568 co-staining assay was run on several plates of *NPC2*$^{-/-}$ cells, with half of each plate treated with DMSO 0.05% v/v (negative control) and the other half with ß-cyclodextrin 10uM (positive control), for 48h (Fig. 5.5; Fig. 5.6). As a result, we obtained a Z' factor > 0 which confirmed the high reproducibility of the filipin-LAMP1-568 assay as it excluded the presence of any significant variation among the signals of each of the two controls (Fig. 5.4).

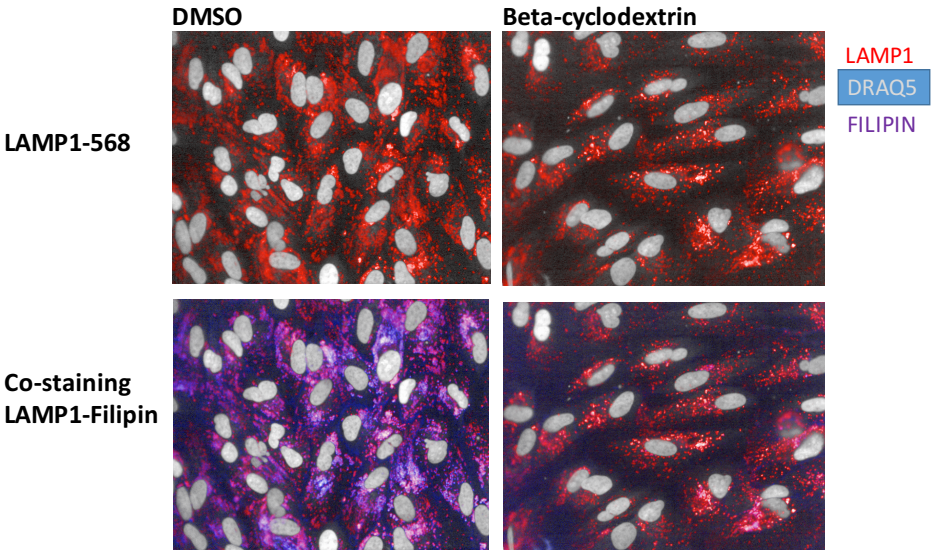

Fig. 5.5. Opera High-Content confocal images of *NPC2*$^{-/-}$ stained with Filipin, Draq5 (nuclei) and antibodies to LAMP1 (Alexa fluor-568). Panels of column A display cells cultured in DMSO 0.05% (negative control) whereas panels of column B represent cells treated with ß-cyclodextrin 10uM (positive control) for 48h.

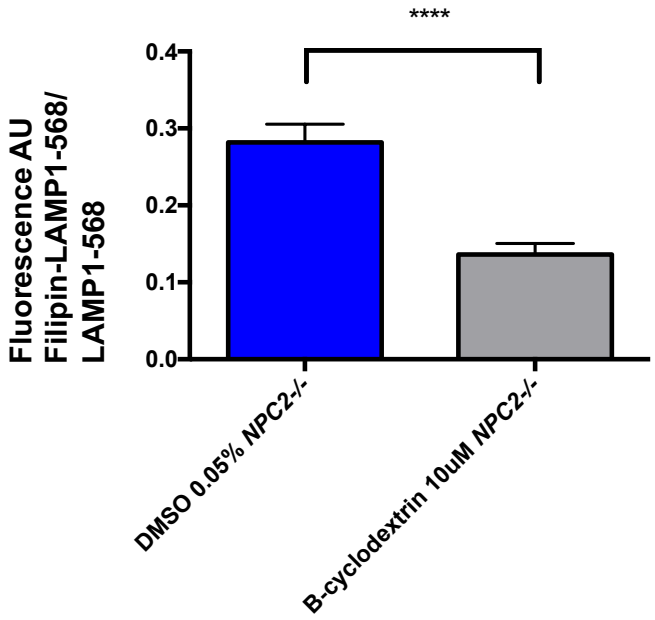

Fig. 5.6. Histogram illustrating a highly significant difference between LE/LY filipin fluorescence of negative (DMSO 0.05% v/v) and positive (ß-cyclodextrin 10uM, 48h) controls used in the HC drug-screening. AU= Arbitrary units ** *p* value < 0.0001 t-student's test.**

5.4 Design of the Prestwick screen and Columbus software data analysis

Our screening was designed to test all the compounds of the Prestwick library at the same concentration and for the same period of time.

In fact, *NPC2*$^{-/-}$ cells were cultured with the Prestwick drugs for 48h at a concentration of 10uM. The compounds of the library were added to the 384-well plates alongside positive and negative controls. The first two columns of the plates were filled with ß-cyclodextrin 10uM (positive control) while the last two contained DMSO 0.05% v/v (negative control). Each other well of the plate was dispensed with a single different drug from the library, for a total of 332 drugs per plate (Fig. 5.7).

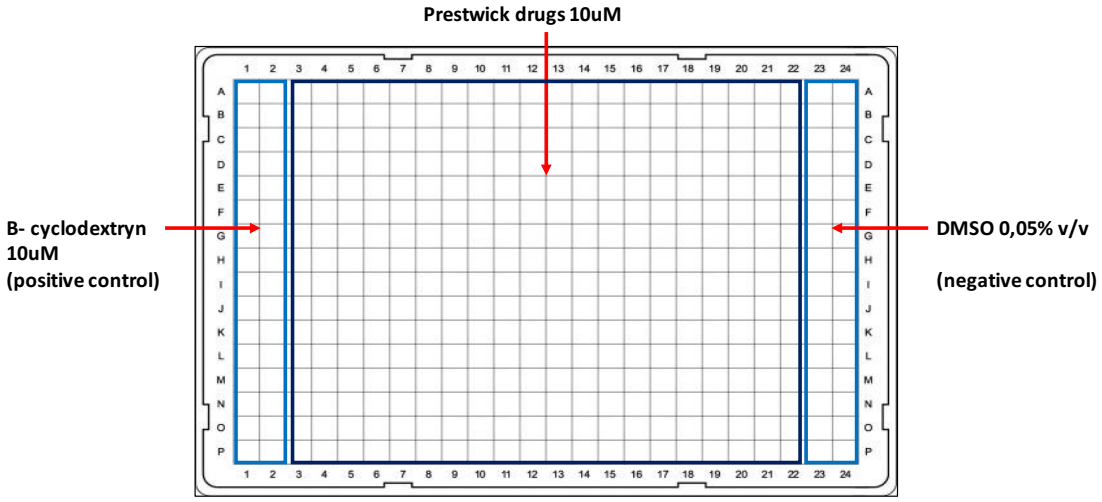

Fig. 5.7. Outline of the 384-well black plates employed in the Prestwick library HC drug screening. On the left and right edges of the plate (columns 1-2 and 23-24) there are positive and negative controls, while the Prestwick drugs are located in the middle (columns 3-22).

Images were acquired by the Opera HC microscope and processed automatically by a software named Columbus. The latter, was able to distinguish each cell singularly and quantify the intensity of the fluorescence of the marked components of the cells.

The Columbus software reported the filipin-LAMP1-568 signal as data per single well and these data points were calculated as: Fluorescence of filipin overlapping LAMP1-568, normalized to the fluorescence emitted by the LAMP1-568 detected in the specific well.

We analysed and interpreted the HC data with the Columbus software by taking advantage of its very intuitive graphical interface. In fact, Columbus reports the outcome of the HC experiments through the representation of a 384-well plate with coloured wells. The colours of the plate are a guide to signal the *NPC2*$^{-/-}$ cells' LE/LY filipin fluorescence intensities. Darker colours indicate lower intensities of LE/LY filipin while lighter colours indicate higher levels of LE/LY filipin intensity (Fig 5.8).

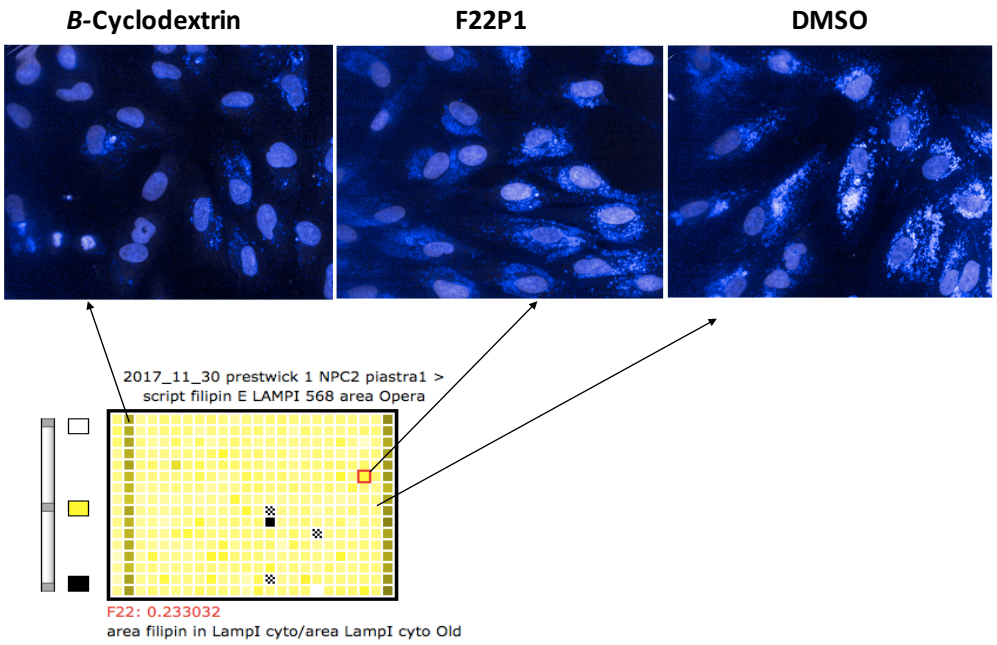

Fig. 5.8. Graphical interface of the Columbus software. The lower image depicts a classical 384-well plate employed in the Prestwick-library screening. The three panels in the upper section of the figure instead, show the filipin staining of *NPC2*$^{-/-}$ cells in different wells that were cultured with one of the following drugs: ß-cyclodextrin 10uM (positive control), fendiline (F22P1) 10uM or DMSO 0.05% (negative control).

5.5 Filters applied for active-compound selection: hit-threshold (DMSO) and cell-viability 60%

In order to identify active compounds among the Prestwick library drugs, we defined criteria for the selection of the hits.

Data were thus sorted for hit detection on the basis of hit-threshold and cell viability.

DMSO was set up as negative-control, hit-threshold and reference control for cell-viability.

In our study, the hit-threshold was represented by DMSO LE/LY filipin fluorescence intensity whereas cell viability was calculated by assigning a value of 100% to the number of cells counted in the DMSO wells after 48h of incubation.

In order to be selected as active compounds, the drugs of the library had to meet the following criteria: their LE/LY filipin fluorescence intensity had to fall within the range of the fluorescence intensities that were below the hit-threshold (DMSO 0.05% v/v), and the percentage of viability associated with drug treatments had to be above 60% (Fig. 5.9).

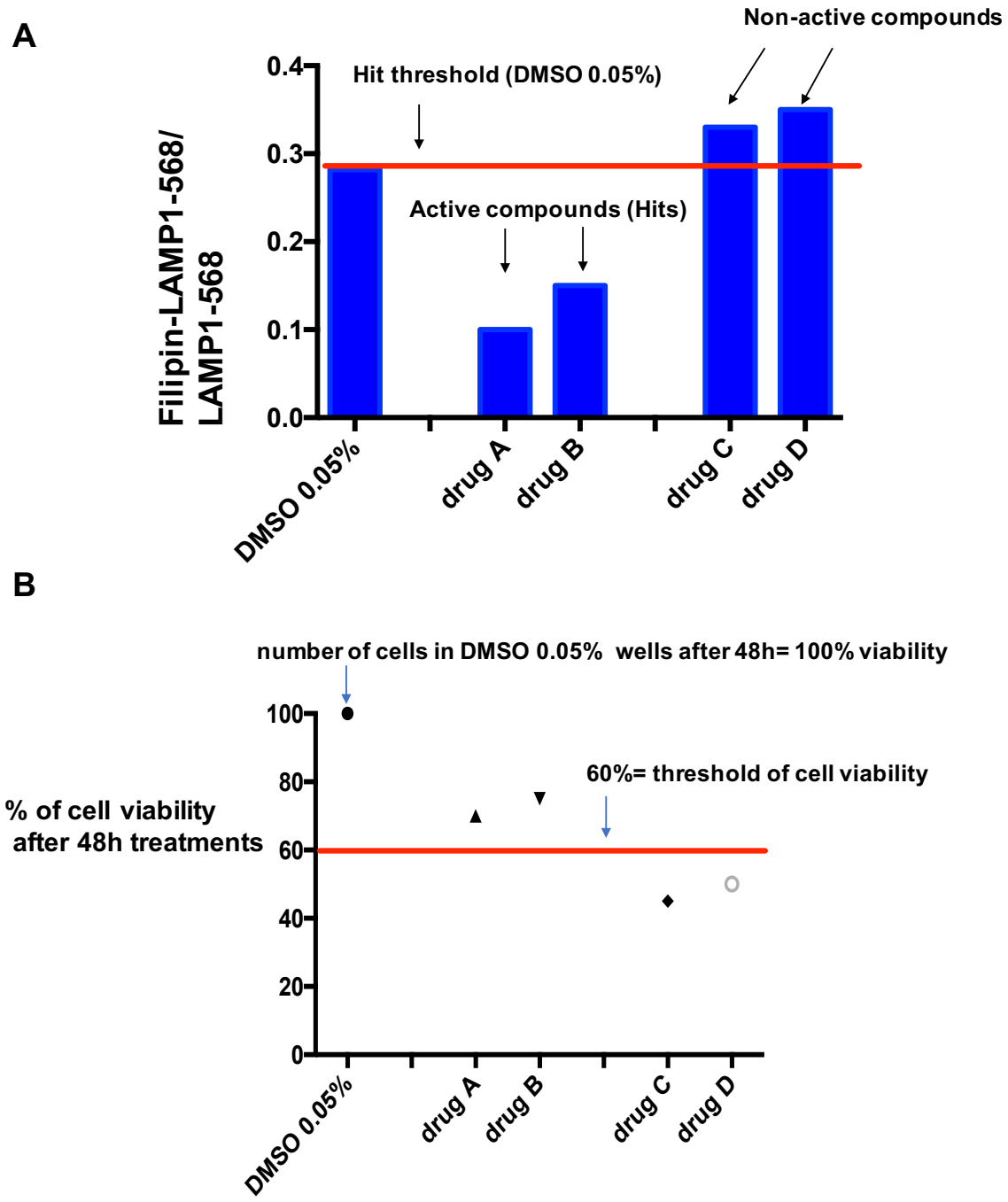

Fig. 5.9 Criteria for the selection of hit-compounds in the Prestwick-library screening. Imaginary data are reported on the Y axes of panels A and B.

Panel A: hit-threshold for filipin-LAMP1/LAMP1 = LE/LY filipin fluorescence of DMSO 0.05% v/v treated cells. Active compounds= Drugs with LE/LY filipin fluorescence lower than the hit-threshold. Non-active compounds= Drugs with a LE/LY filipin fluorescence higher than the hit-threshold.

Panel B: assessment of drug toxicity in the Prestwick screening. Cell viability is defined as the number of cells in DMSO 0.05% wells after 48h incubation. Non- toxic drugs (A and B) show cell viability > 60%.

5.6 Primary screen among 1200 drugs of the Prestwick library: ten active compounds selected

From this primary screen, we found that 10 compounds out of 1200 FDA-approved drugs met the criteria previously set for the hit selection, namely LE/LY filipin fluorescence intensities lower than the hit-threshold (DMSO) and cell viability > 60% (Fig. 5.9 A; B). These hit compounds belonged to different classes of drugs: antidepressants, antipsychotics, calcium-channel blockers and histamine antagonists. All these molecules have a common cyclical chemical structure and, more specifically, with the exception of fendiline, all the hits have a tricyclic nucleus. Furthermore, these drugs target the H1 histamine receptor and almost all of them are inhibitors of the lysosomal enzyme ASM (Acid sphingomyelinase) (Beckmann, 2014).

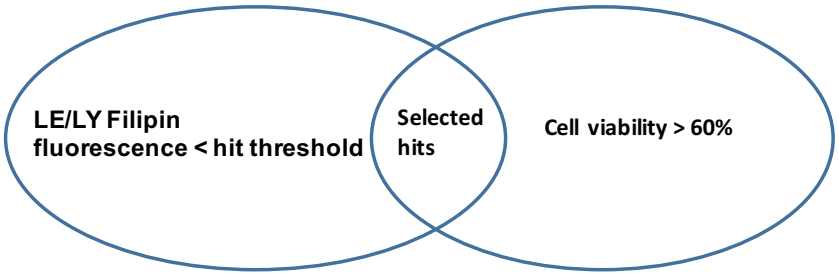

Fig. 5.10. Venn diagram showing that only those compounds with LE/LY filipin fluorescence intensity < hit-threshold and with cell viability > 60% are considered beneficial for *NPC2*$^{-/-}$ cells and are therefore selected as hits.

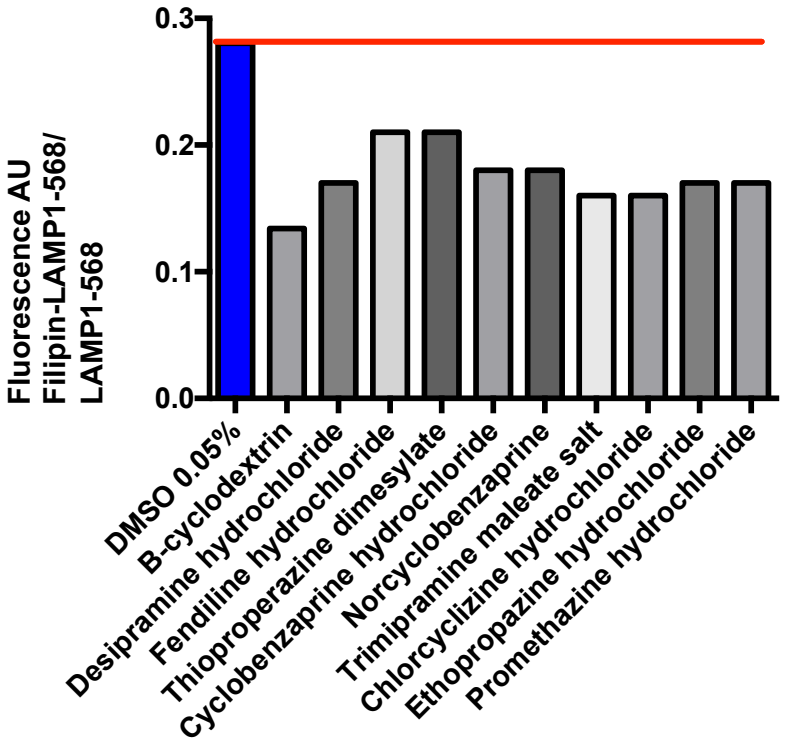

Fig 5.11. FDA-approved drugs that were selected from the primary screening of the Prestwick library. AU= Arbitrary units. On the Y axis the LE/LY filipin fluorescence is reported.

5.7 Validation of the primary sorting

In order to confirm the activity of the selected drugs all the wells of a 384-well plate were treated with the same type of drug and then a filipin-LAMP1 assay was performed. The procedure was carried out on both *NPC1*$^{-/-}$ and *NPC2*$^{-/-}$ cells (Fig. 5.12).

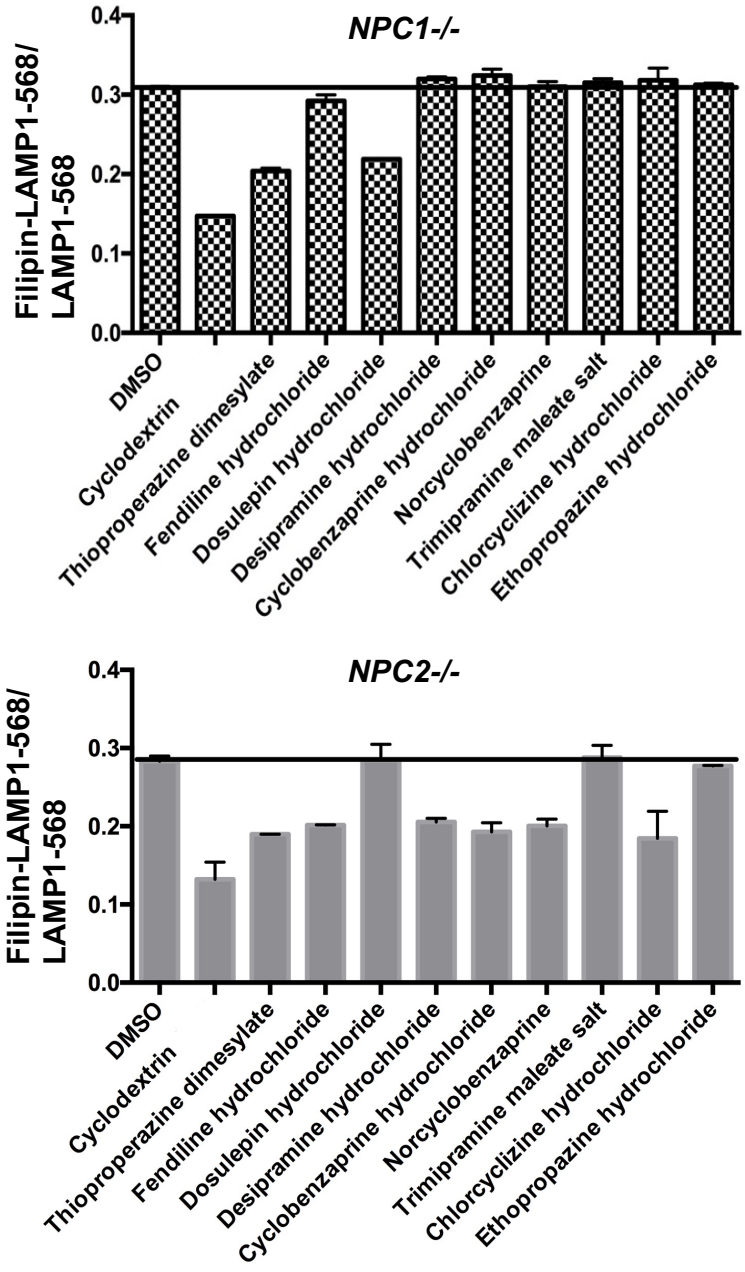

Fig. 5.12. Validation of the ten hits selected from the primary screening of the Prestwick library. Confirmation was carried out treating *NPC1*$^{-/-}$ and *NPC2*$^{-/-}$ with each hit-compound singularly at a concentration of 10uM for 48h. DMSO 0.05%= negative control and cyclodextrin= ß-cyclodextrin 10uM (positive control). On the Y axis, filipin-LAMP1-568/LAMP1-568 fluorescence is reported. This experiment was performed by C. Soldati at Tigem.

As a result of the validation stage, three drugs, desipramine, fendiline and thioproperazine were selected as candidate drugs (Fig 5.13).

Of these, desipramine was seen to be effective in reducing the levels of LE/LY free-cholesterol only in *NPC2*$^{-/-}$ cells, while thioproperazine and fendiline proved to be active on both *NPC2*$^{-/-}$ and *NPC1*$^{-/-}$ cells. More specifically, fendiline appeared to be more effective in *NPC2*$^{-/-}$ than *NPC1*$^{-/-}$.

Visual observation of the levels of LE/LY free-cholesterol of the HC images is in agreement with the outcome of the Columbus software analysis (Fig. 5.10).

5.8.0 Selected hits: desipramine, fendiline and thioproperazine

Desipramine hydrochloride

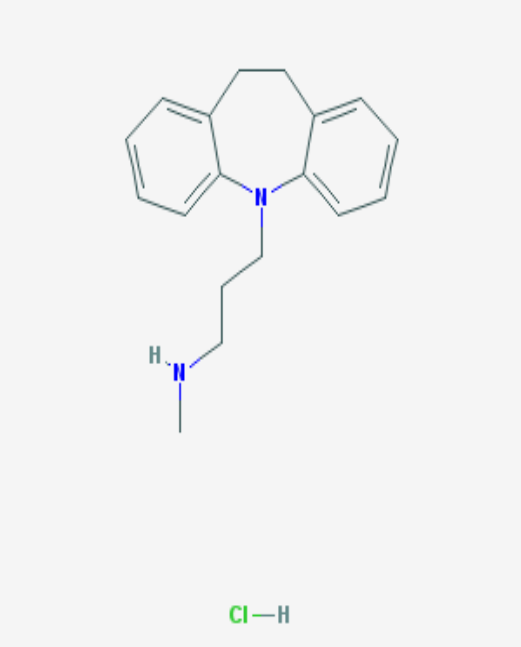

Fendiline hydrochloride

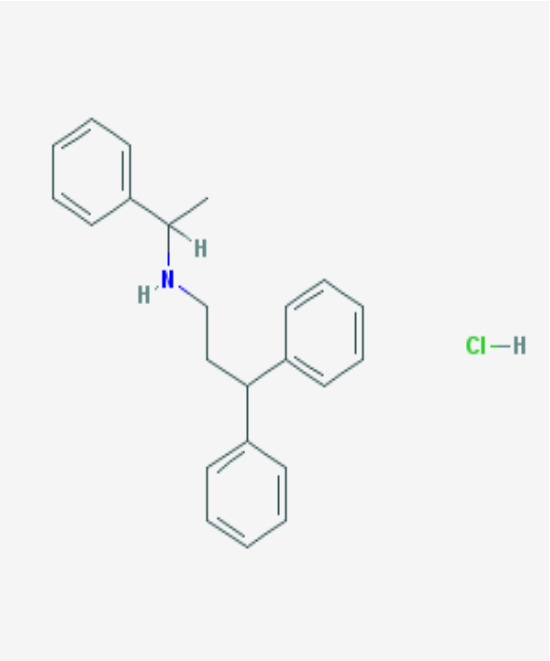

Thioproperazine dimesylate

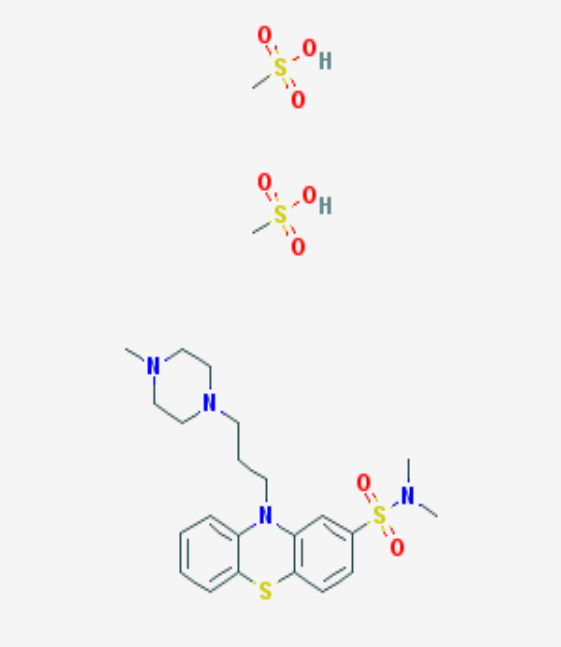

Fig. 5.13. 2D structures of desipramine hydrochloride, fendiline hydrochloride and thioproperazine dimesylate. Images were taken from PUBCHEM.

5.8.1 Secondary readouts to test the activity of the hits

Once the Prestwick drugs had been sorted, I decided to assess the impact that the hit-compounds might have on other features of the NPC disease. To do so, I carried out secondary assays such as LysoTracker FACS analysis, sphingosine assay and total cholesterol analysis on the *NPC1*$^{-/-}$ and *NPC2*$^{-/-}$ cell lines that I had previously generated and characterized in the lab (chapters 3 and 4).

5.8.2 Desipramine and thioproperazine reduce the concentration of sphingosine in *NPC1*$^{-/-}$

In order to measure the effect of the selected hits on the levels of sphingosine in NPC affected cells, I carried out a sphingosine assay on *NPC1*$^{-/-}$ cells grown for 48h with desipramine, fendiline or thioproperazine at a concentration of 10uM. As positive control of the experiment I used the *NPC1*$^{-/-}$ cell line that overexpresses the recombinant protein rNPC1, whereas as negative control I employed untreated *NPC1*$^{-/-}$ cells. As shown by the histograms of Fig. 5.14, desipramine and thioproperazine reduced the amount of the sphingoid bases sphingosine and sphinganine in *NPC1*$^{-/-}$ to about 50% ($p < 0.05$ and $p < 0.001$, respectively, for the sphingosine levels). The levels of sphingosine (Fig. 5.14 A) are expressed as percentage of the samples' concentrations (pmol C18 sphingosine/mg protein) with respect to untreated *NPC1*$^{-/-}$. By contrast, fendiline did not have any effect on the *NPC1*$^{-/-}$ sphingosine storage but it induced a dramatic increase in the levels of sphinganine (Fig 5.14 B). The latter evidence can be interpreted as a sign of toxicity of fendiline when added to the *NPC1*$^{-/-}$ cells at 10uM for 48h.

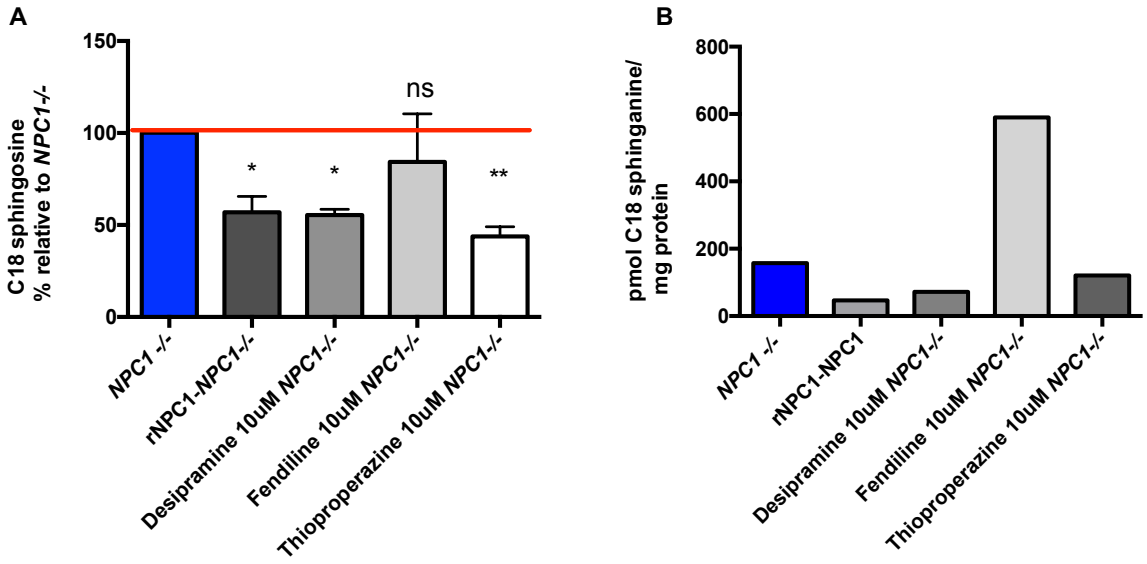

Fig 5.14. Desipramine and thioproperazine, but not fendiline decreased the levels of sphingosine and sphinganine in *NPC1*$^{-/-}$. Cells were treated with the drugs for 48h at a concentration of 10uM. Panel A reports the levels sphingosine in rNPC1-*NPC1*$^{-/-}$ (positive control) and treated *NPC1*$^{-/-}$ expressed as % relative to the concentration (pmol/mg protein) of untreated *NPC1*$^{-/-}$ (negative control). In fact, sphingosine concentration of *NPC1*$^{-/-}$ was set as 100%. Error bars indicate the SD; ns=non significant. * $p < 0.05$ and ** $p < 0.01$ were calculated with the Dunnet's multiple comparisons test in which samples were compared to untreated *NPC1*$^{-/-}$. Panel B depicts the relative comparison of the sphinganine concentration (pmol/mg) among untreated *NPC1*$^{-/-}$, rNPC1-*NPC1*$^{-/-}$ and treated *NPC1*$^{-/-}$. Representative experiments.

5.8.3 Desipramine, fendiline and thioproperazine reduced total (esterified and free) cholesterol in *NPC1*$^{-/-}$ cells

As part of the validation process of desipramine, fendiline and thioproperazine, I investigated whether these selected hits were able to lower the total cholesterol that I had demonstrated to accumulate within *NPC1*$^{-/-}$ and *NPC2*$^{-/-}$ cells. Therefore, desipramine, fendiline and thioproperazine were applied to *NPC1*$^{-/-}$ cells at 10uM for 48h. As a result, the levels of total (esterified and unesterified) cholesterol were reduced (5.15). In particular, in comparison to untreated *NPC1*$^{-/-}$, desipramine and thioproperazine induced a 20% decrement of cholesterol concentration ($p < 0.05$) whereas fendiline determined over a 50% reduction of the accumulated cholesterol ($p < 0.0001$). Surprisingly, fendiline appeared to be even more effective than the positive control ß-cyclodextrin. Although the ability of fendiline to mobilize the esterified cholesterol from the plasma membrane is reported in literature (Cho et al. 2016), such a net breakdown of the amount of total cholesterol is suspicious and therefore needs to be further analysed.

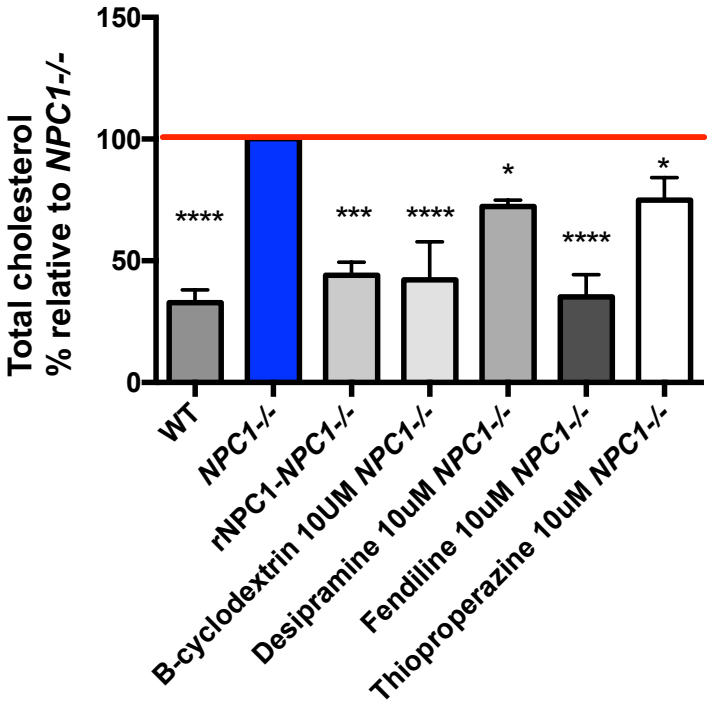

Fig. 5.15. Desipramine, fendiline and thioproperazine decreased the levels of total cholesterol in *NPC1*$^{-/-}$. Cells were treated with the drugs for 48h at a concentration of 10uM and then assayed for total cholesterol. Positive controls= ß-cyclodextrin and rNPC1-*NPC1*$^{-/-}$. Negative control= *NPC1*$^{-/-}$. The histogram reports the levels of total cholesterol in WT, rNPC1-*NPC1*$^{-/-}$, and treated *NPC1*$^{-/-}$ expressed as % relative to the concentration (ug cholesterol/ mg protein) of untreated *NPC1*$^{-/-}$. Error bars indicate SD. * $p < 0.05$; ** $p < 0.01$; ***$p < 0.001$ and $p < 0.0001$ were calculated with the Dunnet's multiple comparisons test in which samples were compared to untreated *NPC1*$^{-/-}$. Representative experiment.

5.8.4 Desipramine, fendiline and thioproperazine 10uM did not reduce LE/LY volume in *NPC1*$^{-/-}$ and *NPC2*$^{-/-}$

Since *NPC1*$^{-/-}$ and *NPC2*$^{-/-}$ present a pathological enlargement of their acidic compartments (chapter 3), I decided to monitor, by LysoTracker FACS analysis, the effect of desipramine, thioproperazine and fendiline on the LE/LY volume of *NPC1*$^{-/-}$ and *NPC2*$^{-/-}$. Treatment of *NPC2*$^{-/-}$ cells for 48h with either desipramine or thioproperazine at 1-5-10uM did not induce any significant variation in the volume of the acidic compartments (Fig. 5.16). On the contrary, *NPC2*$^{-/-}$ cells grown with fendiline 5uM for 48h showed a two-fold increase of their LE/LY volume ($p < 0.01$) (Fig. 5.17).

In addition, *NPC2*$^{-/-}$ cultured with either desipramine or fendiline 0.1 uM for 48h had a slight decrease in the LE/LY volume of *NPC2*$^{-/-}$ cells ($p < 0.05$ for desipramine;

$p < 0.01$ for fendiline) (Fig 5.18 A). Differently from *NPC2*$^{-/-}$, treatment of *NPC1*$^{-/-}$ with desipramine, fendiline or thioproperazine at a concentration of 0.1uM for 48h did not reduce the *NPC1*$^{-/-}$ LE/LY volume (Fig. 5.18 B).

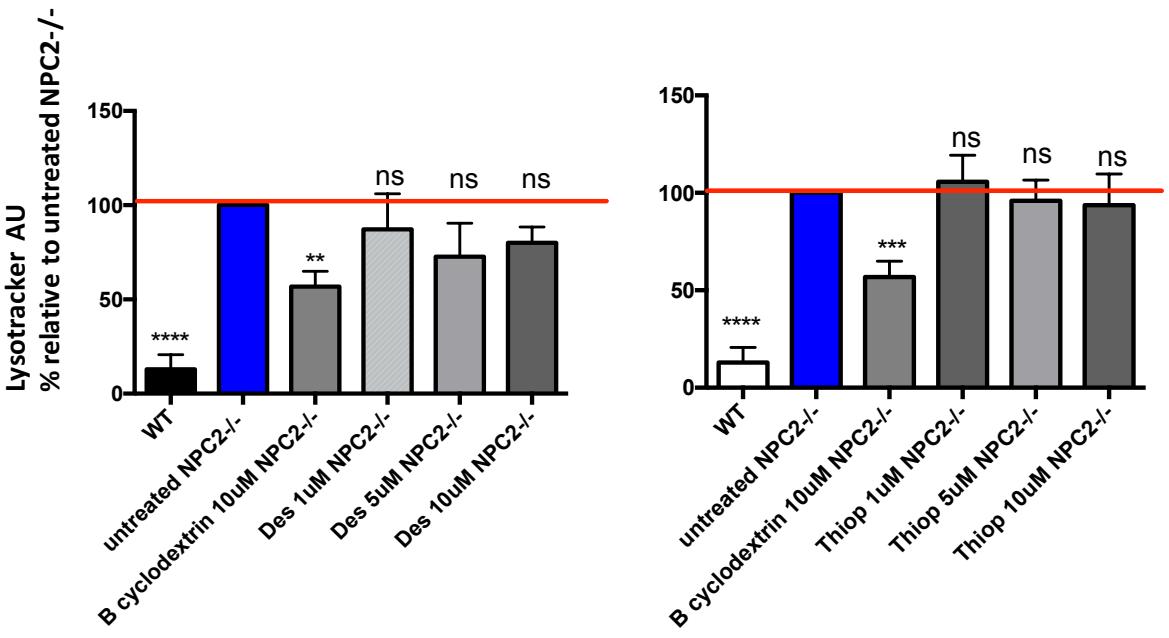

Fig 5.16 LysoTracker flow cytometry of *NPC2*$^{-/-}$ cells treated with desipramine or thioproperazine demonstrates that these drugs did not have any effect on LE/LY volume. Histograms depict the % LysoTracker-green fluorescence relative to *NPC2*$^{-/-}$ in WT and *NPC2*$^{-/-}$. The latter cell line was

either left untreated (negative control) or underwent single drug treatments with ß-cyclodextrin 10uM (positive control), desipramine 1-5-10uM or thioproperazine 1-5-10uM for 48h. AU= Arbitrary units. Error bars indicate the SD. ns= non significant. ** $p < 0.01$; ***$p < 0.001$ and **** $p < 0.0001$ were calculated with the Dunnet's multiple comparisons test in which samples were compared to untreated *NPC2*$^{-/-}$. Representative experiment.

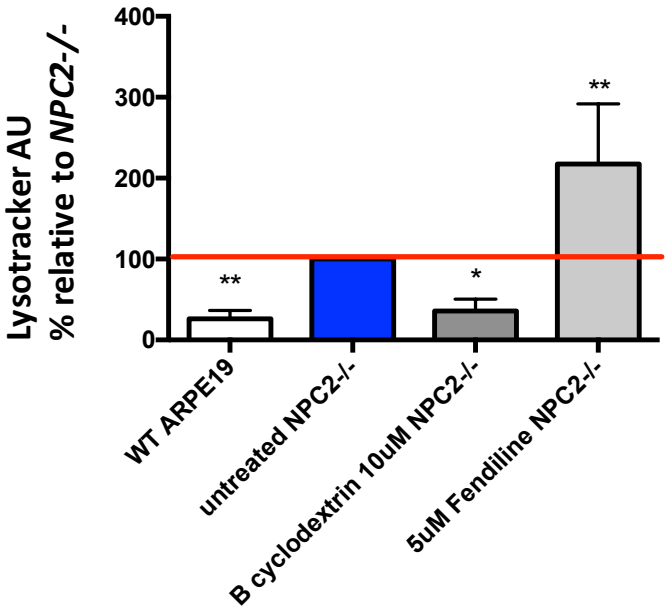

Fig 5.17 LysoTracker FACS analysis of *NPC2*$^{-/-}$ treated with Fendiline 5uM showed an increase of LysoTracker fluorescence relatively to WT. The histogram depicts the % LysoTracker-green fluorescence relative to *NPC2*$^{-/-}$ in WT and *NPC2*$^{-/-}$. The latter cell line was either left untreated (negative control) or underwent single drug treatments with ß-cyclodextrin 10uM (positive control) or fendiline 5 uM for 48h. AU= Arbitrary units Error bars= SD. * $p < 0.05$; **$p < 0.01$ were calculated with the Dunnet's multiple comparisons test in which samples were compared to untreated *NPC2*$^{-/-}$. Representative experiment.

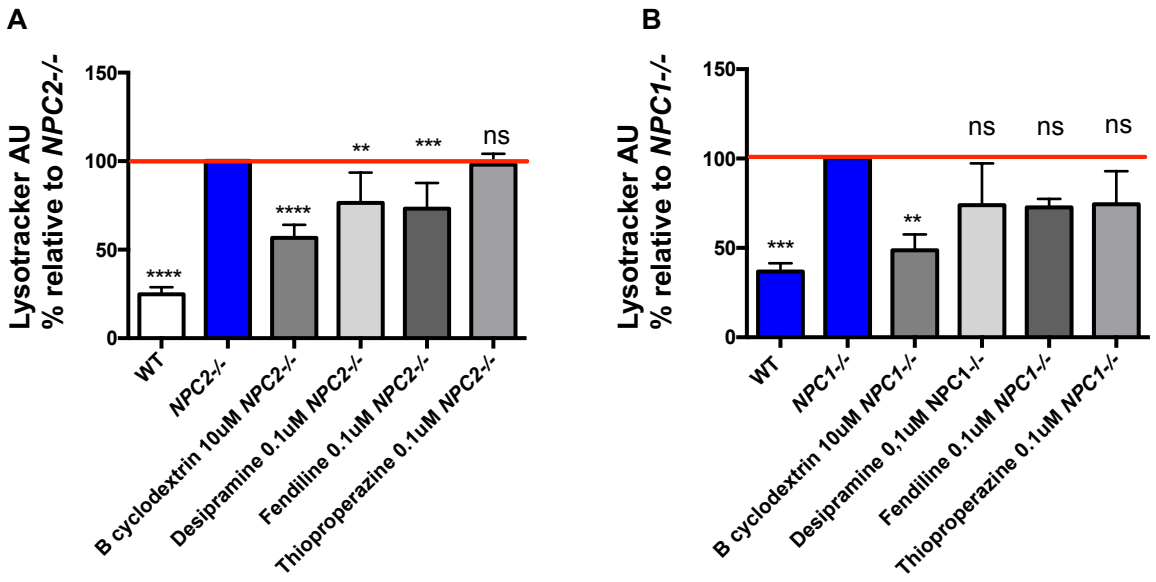

Fig 5.18 LysoTracker FACS analysis of *NPC2*$^{-/-}$ and *NPC1*$^{-/-}$ cells treated with desipramine, fendiline or thioproperazine at 0.1uM. The histogram depicts the % LysoTracker-green fluorescence relative to *NPC2*$^{-/-}$ (panel A) or *NPC1*$^{-/-}$ (panel B), in WT, *NPC2*$^{-/-}$ and *NPC1*$^{-/-}$. The latter two cell lines were either left untreated (negative control) or underwent single drug treatments with ß-cyclodextrin 10uM (positive control), desipramine 0.1uM, fendiline 0.1uM or thioproperazine 0.1uM for 48h. AU=Arbitrary units. Error bars= SD. * $p < 0.05$; ** $p < 0.01$ were calculated with the Dunnet's multiple comparisons test in which samples were compared to untreated *NPC2*$^{-/-}$ (panel A) or *NPC1*$^{-/-}$ (panel B). Representative experiments.

6.0 Discussion

In this study I used CRISPR/Cas9 technology to generate two isogenic cell lines in which the expression of either the *NPC1* or the *NPC2* gene was knocked out in ARPE19 cells. The choice of the ARPE19 cell line was based on its being a human cell line with a normal karyology, not transformed and very easy to handle in comparison to primary and iPS cells (Samuel et al. 2017). In addition, *NPC1*$^{-/-}$ and *NPC2*$^{-/-}$ ARPE19 have the same genetic background, a characteristic that allows thorough comparative studies of the two diseases.

Generation of the *NPC1*$^{-/-}$ and *NPC2*$^{-/-}$ isogenic cell lines

The *NPC1*$^{-/-}$ and *NPC2*$^{-/-}$ ARPE19 cells showed complete absence of the NPC1 and NPC2 proteins, respectively. Interestingly, by western blotting experiments, the NPC2 expression in *NPC1*$^{-/-}$ as well as the NPC1 expression in *NPC2*$^{-/-}$ appeared increased, suggesting an attempt of the modified cells to compensate for the lack of NPC1 or NPC2. This phenomenon is in line with what observed in NPC fibroblasts in a previous study (Blom et al. 2003). *NPC1*$^{-/-}$ and *NPC2*$^{-/-}$ ARPE19 cell lines have been proven to be good cellular models for studying Niemann-Pick disease type C since they recapitulate the main hallmarks, LE/LY morphology alteration and lipid accumulation that characterize the disease. Furthermore, *NPC1*$^{-/-}$ and *NPC2*$^{-/-}$ present exactly the same pathological phenotype, that is observed in NPC1 and NPC2 patients, both clinically and biochemically (Vanier et al. 1996, Park et al 2003). Because the two cell lines have the same genetic background and differ only for the *NPC1* and *NPC2* genes, it can be asserted that compared to patient fibroblasts, NPC animal cells and their derived iPSCs, the *NPC1*$^{-/-}$ and *NPC2*$^{-/-}$ represent a better controlled disease model for NPC.

Phenotypic characterization of *NPC1*$^{-/-}$ and *NPC2*$^{-/-}$

Since cholesterol storage is the most characteristic feature of NPC, I began the characterization of *NPC1*$^{-/-}$ and *NPC2*$^{-/-}$ assessing the level of LE/LY unesterified-cholesterol. By co-staining of the knockout cells with filipin and antibodies to LAMP1 I verified, by confocal microscopy, that *NPC1*$^{-/-}$ and *NPC2*$^{-/-}$ have accumulation of free-cholesterol within their late endosomal/lysosomal compartments. This observation is indicative of hampered egress of free-cholesterol from LE/LY. In particular, the knockout cells showed a three-fold increase in the amount of accumulated free-cholesterol with respect to the WT. This difference was quantified applying the filipin-LAMP1 co-staining microscopy assay in an automated High Content approach. The HC technology allowed a very accurate analysis of the LE/LY filipin fluorescence offering the advantage of constant irradiation times of the cells. This technical aspect was very useful because this made it possible to measure subtle variations of filipin intensity despite the fact that this dye bleaches rapidly when exposed to fluorescent light. Furthermore, with the HC approach I was able to extract and analyse a huge amount of data because in each experiment thousands of cells were scanned.

NPC1$^{-/-}$ and *NPC2*$^{-/-}$ were thus demonstrated to be suitable for large scale high throughput analyses. However, despite being a diagnostic hallmark, cholesterol is not considered the primary offending metabolite of NPC and in fact, the etiology of the disease is still a matter of debate (Emyr-Lloyd et al. 2010). To date, the most accredited theory on the pathogenesis of Niemann-Pick type-C identifies the build-up of sphingosine as the initial causative event followed by storage of cholesterol and GSLs (Emyr-Lloyd et al. 2008). In chapter 4 it is reported that sphingosine accumulates in *NPC1*$^{-/-}$ and *NPC2*$^{-/-}$ and that sphingosine concentration in these knockout cells was three to four-fold higher than in WT cells. Therefore, *NPC1*$^{-/-}$ and *NPC2*$^{-/-}$ represent a valuable tool for investigating the pathology of Niemann-Pick type-C. On the contrary, *NPC1*$^{-/-}$ and *NPC2*$^{-/-}$ are not suitable for the study of GSLs because their glycosphingolipid profile is still not clear.

The accumulation of lipids within LE/LY determined an alteration in the morphology of these organelles. Confocal and electron microscopy images of WT and knockout cells labelled with antibodies to LAMP1 revealed that LE/LY of *NPC1*$^{-/-}$ and *NPC2*$^{-/-}$ were swollen, clustered and full of undegraded material. Moreover, some LE/LY presented the concentric lamellae typical of the multilamellar bodies that characterize sphingolipidoses (Rodriguez et al. 2014). A further confirmation of the perturbed LE/LY physiology of *NPC1*$^{-/-}$ and *NPC2*$^{-/-}$ was seen in the increase of LAMP1 expression and LysoTracker intensity registered in these cells with respect to WT. The latter observation, once again demonstrates the resemblance of *NPC1*$^{-/-}$ and *NPC2*$^{-/-}$ to patient fibroblasts (Xu et al. 2014; te Vruchte et al. 2014). In addition, the up-regulation of LAMP1 and the rise in LysoTracker intensity could reflect an enlargement of LE/LY and/or an increase in their number. The aforementioned LE/LY phenotype would suggest an impairment of the autophagic flux as previously found in Npc1$^{-/-}$ mice (Sarkar et al. 2013). Surprisingly, no alteration of the basal level of autophagy was detected in *NPC1*$^{-/-}$ and *NPC2*$^{-/-}$ relatively to WT. A possible explanation could be the phagocytic nature of the WT ARPE19 cells that gives them a high rate of autophagy. Therefore, it could be difficult to observe any variation of the autophagic clearance in the knockout cells in comparison to WT. Challenging the autophagic flux with short starvation or low dose bafilomycin-A1 treatment might trigger a higher rate of autophagy in *NPC1*$^{-/-}$ and *NPC2*$^{-/-}$, thus unmasking any autophagic flux problem. This approach was proven in the case of a variant form of NPC1 fibroblasts. At the basal level, the latter did not show, by filipin staining, any accumulation of free-cholesterol. By contrast, after LDL-treatment, variant-NPC1 cells appeared to accumulate a large quantity of free-cholesterol with respect to WT, acquiring a classical NPC cholesterol phenotype (Sun et al. 2001). Furthermore, the alteration of the endosomal/lysosomal pathway did not impact the limiting membrane of the acidic compartments in *NPC1*$^{-/-}$ and *NPC2*$^{-/-}$. In fact, a Galectin-3 assay demonstrated that LE/LY membranes are not damaged in the knockout cells. This means that both NPC models could be used to test strategies to revert their pathological

phenotype back to normal.

However, before employing *NPC1*$^{-/-}$ and *NPC2*$^{-/-}$ as tools for the study of the Niemann Pick disease it was important to ensure that the NPC features hitherto observed were actually due to ablation of either *NPC1* or *NPC2* genes and not caused by Cas9 off-target mutations. To this end, NPC1 and NPC2 recombinant proteins were reintroduced within *NPC1*$^{-/-}$, to verify that the NPC phenotype in these cells was corrected. In fact, LysoTracker intensity, total cholesterol and sphingosine concentrations in *NPC1*$^{-/-}$ were nearly normalized by heterologous expression of rNPC1 in *NPC1*$^{-/-}$.

Prestwick library HC screening

At the moment, the miglutat GSLs substrate reduction therapy is the only treatment approved for Niemann Pick type C (Williamson 2014; EMA 2018). Although miglustat induces an amelioration in the neurological symptoms of the disease, it is not curative. Therefore, more effective therapeutic approaches are needed.

Since the mechanism underlying NPC has not yet been fully defined, I thought that screening FDA-approved drugs for NPC would be a good approach to tackle the disease unbiasedly, without targeting any specific protein.

In collaboration with Medina's lab, I used the *NPC2*$^{-/-}$ cell line to screen the 1200 FDA-approved drugs of the Prestwick library. LE/LY free-cholesterol probed by filipin-LAMP1 co-staining was the readout chosen to monitor the effect of the drugs on *NPC2*$^{-/-}$. To this end, the automated high content filipin-LAMP1 assay previously developed to quantify differences in LE/LY free-cholesterol between WT and knockout cells (chapter-4) was miniaturized to 384-well plates. The ability of the drugs to decrease the LE/LY filipin intensity values was measured by the Opera HC device, a sensitive detector of filipin fluorescence.

Each drug of the Prestwick library was applied alone to a single well of a 384-well plate.

To provide a correction for differences of cell numbers in the wells of the plate at the time of measurement, the LE/LY filipin-LAMP1 fluorescence of each well was divided by the LAMP1 fluorescence detected in the well. ß-cyclodextrin and DMSO were set as positive and negative controls, respectively. In point of fact, ß-cyclodextrin rapidly removes the accumulated free cholesterol from NPC cells while DMSO is the vehicle in which the drugs of the library were dissolved (Chen et al. 2010). In order to be selected as effective-compounds (hits), drugs of the library had to meet two criteria: their cell viability per well had to be higher than or equal to 60% of the DMSO (negative control) cell-viability and the LE/LY filipin intensity after drug treatment had to be lower than the intensity measured in the negative control (chapter-4). As a result, three potential hits, desipramine, fendiline and thioproperazine were selected. Fendiline is an old calcium antagonist whereas desipramine and fendiline are tricyclic antidepressants. These three drugs are weak bases with lysosomotropic properties, therefore they tend to be retained within the acidic compartments of cells (Nadanaciva et al. 2011, Muehlbacher et al. 2012).

It is known that lysosomotropism of fendiline and tricyclic antidepressants is manifested through indirect inhibition of acid sphingomyelinase (ASM), a LE/LY enzyme that hydrolyses sphingomyeline into ceramide (Beckmann et al. 2014; Kornhuber et al. 2008). Perturbation of this enzymatic pathway could thus explain some of the effects that desipramine, fendiline or thioproperazine induced in the levels of total cholesterol, sphingoid bases and LysoTracker fluorescence of treated *NPC1*$^{-/-}$ and/or *NPC2*$^{-/-}$ (Chapter-4).

Previous published work reports that fendiline and tricyclic antidepressants deplete cholesterol from the plasma membrane of mammalian cells similarly to ß-cyclodextrin (Cho et al. 2016; van der Hoeven et al. 2018). This observation is in line with the finding of a reduction in the concentration of total cholesterol in *NPC1*$^{-/-}$ after treatment with desipramine, fendiline or thioproperazine (Chapter-4). In this respect, it could be inferred

that the decrease of the free-cholesterol detected in the Prestwick screening was mediated by the hits through a mechanism similar to the one used by ß-cyclodextrin.

In agreement with the hypothesis that the selected drugs block ASM functionality, it was found that desipramine and thioproperazine reduced the accumulation of sphingosine in *NPC1*$^{-/-}$ (Chapter-4). In fact, most likely, upon ASM inhibition, the late endosomal/lysosomal level of ceramide decreases determining a slowdown of the conversion-rate of ceramide into LE/LY sphingosine. As a consequence, an overall decrease in the cellular level of sphingosine occurs (van der Hoeven et al. 2018). As for the LysoTracker staining, *NPC1*$^{-/-}$ and *NPC2*$^{-/-}$ treated with desipramine and thioproperzine did not show any variation in dose-response (1-5-10uM) experiments in comparison to untreated *NPC1*$^{-/-}$ and *NPC2*$^{-/-}$ (chapter-4). Also this result could be assigned to ASM-malfunction. In particular, the LE/LY accumulation of sphingomyelin that occurs subsequent to ASM-inhibition would be responsible for trapping LysoTracker dye within LE/LY. The latter hypothesis will be tested in the near future assessing the LE/LY levels of sphingomyelin in desipramine, fendiline and thioproperazine-treated *NPC1*$^{-/-}$ and *NPC2*$^{-/-}$. However, the hypothesised inhibition of ASM by the candidate drugs does not clarify their ability to reduce the levels of free cholesterol in *NPC1*$^{-/-}$ and *NPC2*$^{-/-}$. The latter phenomenon would be explained hypothesising an opposite mechanism of action for desipramine, fendiline and thioproperazine, in which the activity of ASM in *NPC1*$^{-/-}$ and *NPC2*$^{-/-}$ would be increased by the drugs. In fact, overexpression of the acid SMase enzyme in NPC1 patient fibroblasts has been shown to reduce LE/LY free cholesterol (Devlin et al. 2010). Therefore, further experiments are needed to develop a robust hypothesis for describing the effects of desipramine, fendiline and thioproperazine on LE/LY cholesterol and sphingosine in *NPC1*$^{-/-}$ and *NPC2*$^{-/-}$.

Variability of drug effects is dependent on drug concentration

The hypothesis that desipramine, fendiline and thioproperazine inhibit ASM would theoretically imply that cells treated with these drugs develop an NP-A like phenotype thus accumulating sphingomyelin and cholesterol as primary and secondary substrates, respectively (Gabandè-Rodriguez et al. 2014). As demonstrated in chapter-4 this is not the case for the NPC knockout cells treated with the aforementioned compounds (10uM for 48h) because their total cholesterol appeared to be diminished. Hence, it can be deduced that the extent of ASM dysfunction determined by the three drugs is lower than that caused by the ASM genetic mutation that occurs in NP-A (Gabandè-Rodriguez et al. 2014).

Drug dosage is an important issue that can be a source of high variability in their effects. In fact, preliminary data of chapter-4 show that 100 nM concentrations of desipramine and fendiline slightly but significantly reduce LysoTracker intensity in *NPC2*$^{-/-}$. This data is in complete contrast with the increase of LysoTracker intensity shown by *NPC2*$^{-/-}$ that had been treated with fendiline 5uM for the same period of time.

In addition, unlike what was observed with desipramine and thioproperazine, no variation of sphingosine concentration was detected in *NPC1*$^{-/-}$ cells that were treated with fendiline. Instead, interestingly, it was the concentration of another sphingoid base, sphinganine, that notably increased upon treatment of *NPC1*$^{-/-}$ with fendiline. Since the level of sphinganine in all the other treatments had not shown any relevant variation in comparison to the untreated controls, this sphinganine accumulation might be interpreted as a sign of toxicity of fendiline at the given concentration. In fact, in literature, a similar situation is reported in the case of cells treated with fumonisin B1 (Yoo et al. 1996). However, before excluding fendiline from the Prestwick hits it would be worth testing its effect at concentrations ranging in the order of nM rather uM.

Overall, the study of desipramine, fendiline and thioproperazine as drug candidates for the treatment of NPC is still very preliminary. Before drawing any conclusion on the efficacy of these compounds, the same experiments of chapter-4 would need to be performed on *NPC1*$^{-}$

$^{-/-}$ and *NPC2*$^{-/-}$ as well as in other NPC cellular models, at lower drug dosages and with prolonged incubation times. Different NPC cell lines such as patient fibroblasts would give the possibility of testing the drugs in *in vitro* models that are not full knockout for either NPC1 or NPC2. This would allow monitoring whether the presence of mutant proteins makes a difference in the drugs' activity. In fact, there is a line of research that identifies chaperones of mutant NPC1 as potential effective compounds for rescuing the NPC phenotype (Ohgane et al. 2013).

Conclusion

The research illustrated in this thesis has demonstrated that *NPC1*$^{-/-}$ and *NPC2*$^{-/-}$ are indeed very useful cellular models for the study of Niemann Pick type-C because they recapitulate three important pathological phenotypes of the disease: accumulation of free-cholesterol and sphingosine as well as increase of LysoTracker intensity. These features are so pronounced in *NPC1*$^{-/-}$ and *NPC2*$^{-/-}$ that they represent valuable alternatives to substitute free-cholesterol as the primary readout in *in vitro* drug-screening studies. In this study, a drug-repurposing screening monitoring LE/LY free-cholesterol in *NPC1*$^{-/-}$ and *NPC2*$^{-/-}$ has led to the selection of three drugs, desipramine, fendiline and thioproperazine as potential candidates for the treatment of NPC. In fact, these drugs seem to be effective also in rescuing other phenotypes of the disease (chapter 5). Nevertheless, to obtain a clear picture of the efficacy of the hits, further experiments to test their effect on secondary readouts such as sphingosine storage and LE/LY enlargement, are needed. In this respect, to date, three high-throughput drug-screenings monitoring free-cholesterol have been published and none of them has led to the discovery of a lead compound for the treatment of NPC (Liscum et al. 2002, Pipalia et al

2006; Pugach et al. 2018). Furthermore, results of the first clinical trial with VTS-270 (2-hydroxypropyl- ß-cyclodextrin) report that patients administered with the drug have not shown any improvement with respect to the patients that were given a placebo (Science Press release 9 Nov 2018, data not yet published). Hence, on the basis of the pathogenic cascade of NPC, in a future perspective, it would be worth employing *NPC1*$^{-/-}$ and *NPC2*$^{-/-}$ to screen manually small groups of compounds monitoring their effects on sphingosine accumulation. Alternatively, *NPC1*$^{-/-}$ and *NPC2*$^{-/-}$ could be employed in an automated high content screening of drug-libraries using LysoTracker staining as the primary readout.

Bibliography

Aits, S., Jäättelä, M. and Nylandsted, J. (2015) 'Methods for the quantification of lysosomal membrane permeabilization: A hallmark of lysosomal cell death', *Methods in Cell Biology*.

Auburger, M. J. (2012) 'Primary Skin Fibroblasts as a Model of Parkinson s Disease'.

Babalola, J. O. *et al.* (2007) *Development of an assay for the intermembrane transfer of cholesterol by Niemann-Pick C2 protein*.

Barrangou, R. *et al.* (2007) 'Against Viruses in Prokaryotes', *Science*, 315(March).

Beckmann, N. *et al.* (2014) *Inhibition of acid sphingomyelinase by tricyclic antidepressants and analogons*.

Bergamin, N. *et al.* (2013) 'A human neuronal model of Niemann Pick C disease developed from stem cells isolated from patient's skin', *Orphanet Journal of Rare Diseases*.

Blom et al. (2003) *Defective endocytic trafficking of NPC1 and NPC2 underlying infantile Niemann–Pick type C disease*

Brown, M. S. and Goldstein, J. L. (1986) ''A receptor-mediated pathway for cholesterol homeostasis,' *Science*.

Carstea, E. D. *et al.* (1997) 'Niemann-Pick C1 disease gene: Homology to mediators of cholesterol homeostasis', *Science*.

Chen et al. (2010) *Cyclodextrin Induces Calcium-Dependent Lysosomal Exocytosis*

Cho, K. *et al.* (2016) *Inhibition of Acid Sphingomyelinase Depletes Cellular Phosphatidylserine and Mislocalizes K-Ras from the Plasma*.

Davies et al. (2000) *Transmembrane Molecular Pump Activity of Niemann-Pick C1 Protein*

Davies, J. P. and Ioannou, Y. A. (2000) 'Topological analysis of Niemann-Pick C1 protein reveals that the membrane orientation of the putative sterol-sensing domain is identical to those of 3-hydroxy-3-methylglutaryl-CoA reductase and sterol regulatory element binding protein cleavage-activating', *Journal of Biological Chemistry*.

Deffieu, M. S. and Pfeffer, S. R. (2011) 'Niemann-Pick type C 1 function requires lumenal domain residues that mediate cholesterol-dependent NPC2 binding', *Proceedings of the National Academy of Sciences*.

Devlin C. et al. 2010, *Improvement in Lipid and Protein Trafficking in Niemann-Pick C1 Cells by Correction of a Secondary Enzyme Defect*

Dunn K. C. et al. (1996) *ARPE-19, A Human Retinal Pigment Epithelial Cell Line with Differentiated Properties.*

Efthymiou, A. G. *et al.* (2015) 'Rescue of an In Vitro Neuron Phenotype Identified in Niemann-Pick Disease, Type C1 Induced Pluripotent Stem Cell-Derived Neurons by

Modulating the WNT Pathway and Calcium Signaling', *STEM CELLS Translational Medicine*.

EMA European Medicine Agency Zavesca 2018

Gabandé-Rodríguez, E. *et al.* (2014) 'High sphingomyelin levels induce lysosomal damage and autophagy dysfunction in Niemann Pick disease type A', *Cell Death and Differentiation*.

Greer, W. *et al.* (1999) 'Mutations in NPC1 Highlight a Conserved NPC1-Specific Cysteine-Rich Domain', *The American Journal of Human Genetics*.

Heler, R. *et al.* (2015) 'Cas9 specifies functional viral targets during CRISPR-Cas adaptation', *Nature*. Nature Publishing Group, 519(7542).

Higgins, M. E. *et al.* (1999) 'Niemann-pick C1 is a late endosome-resident protein that transiently associates with lysosomes and the trans-Golgi network', *Molecular Genetics and Metabolism*.

Hoeglinger doris *et al.* (2015) *Intracellular sphingosine releases calcium from lysosomes*.

Hoeven, D. *et al.* (2018) 'Sphingomyelin metabolism is a regulator of KRAS function', *Molecular and Cellular Biology*.

Hughes, M. P. *et al.* (2018) *AAV9 intracerebroventricular gene therapy improves lifespan , locomotor function and pathology in a mouse model of Niemann – Pick type C1 disease*.

Horton, Goldstein, B. (2002) 'SREBP activators of the complete program of cholesterol and fatty acid synthesis in the liver'.

Jiang, F. and Doudna, J. A. (2017) *CRISPR – Cas9 Structures and Mechanisms*.

Jinek, M. *et al.* (2012) 'A Programmable Dual-RNA – Guided', *Science*, 337(August).

Jinek, M. *et al.* (2013) 'RNA-programmed genome editing in human cells', *eLife*, 2013.

Kirchhoff, C. (1996) 'Molecular cloning and characterization of HE1, a major secretory protein of the human epididymis', *Biology of Reproduction*.

Kornhuber, J. *et al.* (2008) *Identification of New Functional Inhibitors of Acid Sphingomyelinase Using a Structure - Property - Activity Relation Model*.

Kuscu, C. *et al.* (2014) 'Genome-wide analysis reveals characteristics of off-target sites bound by the Cas9 endonuclease', *Nature Biotechnology*. Nature Publishing Group.

Kwon, H. J. *et al.* (2009) 'Structure of N-Terminal Domain of NPC1 Reveals Distinct Subdomains for Binding and Transfer of Cholesterol', *Cell*. Elsevier Ltd.

Li *et al.* a (2016) *Clues to the mechanism of cholesterol transfer from the structure of NPC1 middle lumenal domain bound to NPC2*.

Li *et al.* b (2016) 'Structure of human Niemann–Pick C1 protein', *Proceedings of the National Academy of Sciences*, 113(29).

Liebers, M. (2011) 'NIH Public Access', *Annual Review of Biochemistry*.

Liscum, L. *et al.* (2002) *Identification of a pharmaceutical compound that partially corrects the Niemann-Pick C phenotype in cultured cells*.

Lloyd-Evans, E. *et al.* (2008) 'Niemann-Pick disease type C1 is a sphingosine storage disease that causes deregulation of lysosomal calcium', *Nature Medicine*.

Lloyd-evans, E. and Platt, F. M. (2010) *Lipids on Trial : The Search for the Offending Metabolite in Niemann-Pick type C Disease*.

Lyseng-Williamson, K. A. (2014) 'Miglustat: A review of its use in Niemann-Pick disease type C', *Drugs*.

Maetzel, D. *et al.* (2014) *Genetic and Chemical Correction of Cholesterol Accumulation and Impaired Autophagy in Hepatic and Neural Cells Derived from Niemann-Pick Type C Patient-Specific iPS Cells*, *Stem Cell Reports*. The Authors.

Malnar et al. *Bidirectional links between Alzheimer's disease and Niemann–Pick type C disease*

Medina, D. L. *et al.* (2015) 'Lysosomal calcium signalling regulates autophagy through calcineurin and TFEB', *Nature Cell Biology*.

Merrill, B. A. H., Caligan, T. B. and Wang, E. (2000) *[l] Analysis of Sphingoid Bases and Sphingoid Liquid Chromatography*, *Sphingolipid Metabolism and Cell Signaling*. Elsevier Masson SAS.

Millat, G. *et al.* (2001) 'Niemann-Pick C1 Disease: Correlations between NPC1 Mutations, Levels of NPC1 Protein, and Phenotypes Emphasize the Functional Significance of the Putative Sterol-Sensing Domain and of the Cysteine-Rich Luminal Loop', *The American Journal of Human Genetics*.

Moskot, M. *et al.* (2014) 'The phytoestrogen genistein modulates lysosomal metabolism and Transcription Factor EB (TFEB) activation', *Journal of Biological Chemistry*.

Muehlbacher, M. *et al.* (2012) 'Identification of Drugs Inducing Phospholipidosis by Novel in vitro Data', *ChemMedChem*.

Nadanaciva, S. *et al.* (2011) 'A high content screening assay for identifying lysosomotropic compounds', *Toxicology in Vitro*. Elsevier Ltd.

Narita, K. *et al.* (2005) 'Protein transduction of Rab9 in Niemann-Pick C cells reduces cholesterol storage.', *FASEB journal : official publication of the Federation of American Societies for Experimental Biology*.

Naureckiene, S. *et al.* (2000) *Identification of HE1 as the Second Gene of Niemann-Pick C Disease*.

Ohgane, K. *et al.* (2013) 'Discovery of oxysterol-derived pharmacological chaperones for

NPC1: Implication for the existence of second sterol-binding site', *Chemistry and Biology*. Elsevier Ltd.

Palmieri, M. *et al.* (2011) 'Characterization of the CLEAR network reveals an integrated control of cellular clearance pathways', *Human Molecular Genetics*.

Park, W. D. *et al.* (2003) 'Identification of 58 novel mutations in Niemann-Pick disease type C: Correlation with biochemical phenotype and importance of PTC1-like domains in NPC1', *Human Mutation*.

Patterson M. C. et al. (2012) *Recommendations for the diagnosis and management of Niemann–Pick disease type C: An update*

Pipalia, N. H. *et al.* (2006) *Automated microscopy screening for compounds that partially revert cholesterol accumulation in Niemann-Pick C cells*.

Platt, F. M., Boland, B. and van der Spoel, A. C. (2012) 'Lysosomal storage disorders: The cellular impact of lysosomal dysfunction', *Journal of Cell Biology*.

Platt, F. M., Ferreira, C. R. and Gahl, W. A. (2018) 'Lysosomal storage diseases', *Metabolic Diseases: Foundations of Clinical Management, Genetics, and Pathology*.

Poirier Steve and Seidah (2013) 'NIH Public Access'.

Pu, J. *et al.* (2015) *Article BORC , a Multisubunit Complex that Regulates Lysosome Positioning Article BORC , a Multisubunit Complex that Regulates Lysosome Positioning*, *Developmental Cell*. Elsevier Inc.

Pu, J. *et al.* (2016) 'Mechanisms and functions of lysosome positioning', *Journal of Cell Science*.

Pugach, E. K. *et al.* (2018) *High-content screen for modifiers of Niemann-Pick type C disease in patient cells*.

Reinhard Jahn and Richard H. Sheller (2006) 'SNAREs-engines for membrane fusion', pp. 631–643.

Riccardi, C. and Nicoletti, I. (2006) 'Analysis of apoptosis by propidium iodide staining and flow cytometry', *Nature Protocols*.

Rodriguez-Lafrasse (1994) *Free sphingoid bases in tissues from patients with type C Niemann-Pick disease and other lysosomal storage disorders*.

Samuel, W. *et al.* (2017) *Appropriately differentiated ARPE-19 cells regain phenotype and gene expression profiles similar to those of native RPE cells*.

Sander, J. D. and Joung, J. K. (2014) 'Targeting', *Nature Biotechnology*.

Sardiello, M. et al. (2009) *A Gene Network Regulating Lysosomal Biogenesis and Function*.

Sarkar, S. *et al.* (2013) *Article Impaired Autophagy in the Lipid-Storage Disorder Niemann-Pick Type C1 Disease*, *CellReports*. The Authors.

Scott, C. *et al.* (2004) 'Targeting of NPC1 to late endosomes involves multiple signals, including one residing within the putative sterol-sensing domain', *Journal of Biological Chemistry*.

Settembre, C. *et al.* (2012) *A lysosome-to-nucleus signalling mechanism senses and regulates the lysosome via mTOR and TFEB open*, *The EMBO Journal*. Nature Publishing Group.

Settembre, C. *et al.* (2013) 'Signals from the lysosome : a control centre for cellular clearance and energy metabolism', *Nature Publishing Group*. Nature Publishing Group.

Spampanato, C. *et al.* (2013) 'Transcription factor EB (TFEB) is a new therapeutic target for Pompe disease', *EMBO Molecular Medicine*.

Sternberg, S. H. *et al.* (2014) 'DNA interrogation by the CRISPR RNA-guided endonuclease Cas9', *Nature*. Nature Publishing Group.

Sturley, S. L. (2011) 'Niemann-Pick type C pathogenesis and treatment: from statins to sugars'.

Sun, X. *et al.* (2001) 'Niemann-Pick C Variant Detection by Altered Sphingolipid Trafficking and Correlation with Mutations within a Specific Domain of NPC1', *The American Journal of Human Genetics*.

Trilck, M. *et al.* (2013) 'Niemann-Pick type C1 patient-specific induced pluripotent stem cells display disease specific hallmarks', *Orphanet Journal of Rare Diseases*.

Vanier, M. T. *et al.* (1996) 'Genetic heterogeneity in Niemann-Pick C disease: a study using somatic cell hybridization and linkage analysis.', *American journal of human genetics*.

Vanier, M. T. (2010) 'Niemann-Pick disease type C Review'.

Vanier, M. T. and Latour, P. (2015) *Laboratory diagnosis of Niemann-Pick disease type C: The filipin staining test*, *Methods in Cell Biology*. Elsevier Ltd.

Vanier and Niemann, M. G. (2003) *Niemann – Pick disease type C*.

Vanier T. (1983) *Biochemical studies in niemann-pick disease i. major sphingolipids*.

Vanier M. T. et al. (1988) *Niemann-Pick disease group C: clinical variability and diagnosis based on defective cholesterol esterification.*

Vruchte, D. *et al.* (2004) *Accumulation of Glycosphingolipids in Niemann-Pick C Disease Disrupts Endosomal Transport*.

Te Vruchte, D. *et al.* (2014) 'Relative acidic compartment volume as a lysosomal storage disorder-associated biomarker', *Journal of Clinical Investigation*.

Wang, H. *et al.* (2016) *Ebola Viral Glycoprotein Bound to Its Endosomal Article Ebola Viral Glycoprotein Bound to Its Endosomal Receptor Niemann-Pick C1*. Elsevier Inc.

Wassif, C. A. *et al.* (2016) *Original Research Article High incidence of unrecognized visceral / neurological late-onset Niemann-Pick disease , type C1 , predicted by analysis of massively parallel sequencing data sets*.

Willenborg, M. *et al.* (2005) 'Mannose 6-phosphate receptors, Niemann-Pick C2 protein, and lysosomal cholesterol accumulation', *Journal of Lipid Research*.

Xu, M. *et al.* (2014) *A phenotypic compound screening assay for lysosomal storage diseases*, *Journal of Biomolecular Screening*.

Xu, S. *et al.* (2007) 'Structural basis of sterol binding by NPC2, a lysosomal protein deficient in Niemann Pick type C2 disease', *J Biol Chem*.

Yoo, H. S. *et al.* (1996) 'Elevated sphingoid bases and complex sphingolipid depletion as contributing factors in fumonisin-induced cytotoxicity', *Toxicology and Applied Pharmacology*.

Yu, D. *et al.* (2014) 'Niemann-pick disease type C: Induced pluripotent stem cell-derived neuronal cells for modeling neural disease and evaluating drug efficacy', *Journal of Biomolecular Screening*.

Zerial, M. and McBride, H. (2001) 'Rab Proteins As Membrane', *Nature Reviews Molecular Cell Biology*, 2(February).

Zhang, J.-H., Chung, T. D. Y. and Oldenburg, K. R. (1999) 'A Simple Statistical Parameter for Use in Evaluation and Validation of High Throughput Screening Assays, *Journal of Biomolecular Screening*.